UNIVERSITY OF CRETE
DEPARTMENT OF BIOLOGY AND CHEMISTRY
JOINT MSC. PROGRAM IN PROTEIN BIOTECHNOLOGY

Deciphering tumor-nerve interactions: combining *in silico* and *in vivo* approaches

DIPLOMA THESIS

MARIA-ANNA SOTIROPOULOU

Supervisor: Maria Vamvakaki
Professor, UOC

Herakleion, February 2024

UNIVERSITY OF CRETE
DEPARTMENT OF BIOLOGY AND CHEMISTRY
JOINT MSC. PROGRAM IN PROTEIN BIOTECHNOLOGY

Deciphering tumor-nerve interactions: combining *in silico* and *in vivo* approaches

DIPLOMA THESIS

MARIA-ANNA SOTIROPOULOU

Supervisor: Maria Vamvakaki
Professor, UOC

Approved by the three-member graduation committee on

Maria Vamvakaki Professor, University of Crete	Georgios Lolas Coordinator of Systems Medicine-Biology Group at Oncology Unit, Sotiria General Hospital	Lasse Jensen Associate Professor, Linkoping University

Herakleion, February 2024

.....
Maria-Anna Sotiropoulou

Acknowledgements

Maria-Anna Sotiropoulou
February 2024

I extend my sincere gratitude to Professor Maria Vamvakaki for providing me the chance to gain experience and knowledge in polymer research at her laboratory, as well as allowing me to engage in collaborations with exceptional scientists like Dr. Georgios Lolas, Dr. Arianna Bianchi, Professor Lasse Jensen, and Dr. Maria Psarrou, that has significantly contributed to my academic and research journey. I am particularly grateful to Dr. Georgios Lolas and Dr. Arianna Bianchi for originating the project idea and that gave me courage for beginning to work on such a complicated research field as Mathematical Modelling. Their guidance, support, and mentoring during the project, as well as their insightful modeling classes, were invaluable. This collaborative endeavor would not have been possible without them and I truly appreciate the opportunity they provided me. I also want to thank Professor Lasse Jensen for providing me with hands-on experience in zebrafish and cancer cell management through our collaborative project in his laboratories. Special thanks to Dr. Maria Psarrou for her invaluable guidance and support in the polymer lab, her thorough instruction on protocols and impactful mentorship.

Special thanks to Professor Konstantinos Syrigos and Dr. Maximos Anagnostakis and acknowledgment is due to the Hellenic Society of Medical Oncology (HeSMO) for their funding support, enabling me to conduct experiments in Linkoping, Sweden. I extend my thanks to Zaheer Ali, Decky Tandiono and Gabriela Vazquez Rodriguez who work in Bioreperia and prepared zebrafish embryos for my experiments. My gratitude extends to Jesper Palm, my fellow researcher in the zebrafish laboratory, for providing valuable guidance on experimental protocols.

Finally, I express my heartfelt thanks to all my friends, fellow researchers and laboratory partners in the polymer laboratory for their assistance in fundamental chemical principles and equipment operation. Special acknowledgments go to Myrto Vrentzou, Dimitris Fergadis, George Karchilakis, Anna Papaioannou, Rania Chamalaki, Dimitra Gaitanou, Vasillis Tsampallas, George Papas, Sophia Panagiotidou, Dr. Eva Vasilaki, and Dr. Maria Kalyva for their genuine support. Last but not least, I am grateful to my life partner for their emotional encouragement and insights and also for the unwavering emotional and financial backing from my family during my time pursuing a Master's degree. Their contributions have been truly invaluable to my academic and personal journey.

Abstract

Recent studies show that nerves play a major role in tumor initiation, growth, as well as dissemination, leaving aside the long-lasting perception of nerves as passive bystanders of the tumor microenvironment. It was the work by Magnon [1] that back in 2013, highlighted the process of tumor induced neurogenesis, where cancer cells secrete neurotrophic factors that could trigger the genesis of a new neural network in the tumor vicinity, in a similar manner that new blood and lymphatic vessels generate. The investigation of the dynamic interplay between nerves and tumor generated a new field in cancer research called *"cancer neuroscience"* or *"exoneural cancer biology"*. The aforementioned neural cancer processes are controlled by both deterministic and stochastic phenomena. In the current thesis, we will construct an agent-based model of neuron-cancer interactions in order to incorporate both aspects (stochastic and deterministic). Agent-based model, an in silico approach, simulates the interactions of decision-making entities (or agents) over time based on a set of rules. In addition, we will experimentally validate as well as calibrate our model with experiments utilizing zebrafish larvae and biodegradable (mPEG-*b*-PLLA diblock) polymeric nanocarriers (nanoparticles) controlling drug release. Lastly, we will also explore the effect of chronic stress, through the activation of the neuronal system, on tumor growth and dissemination.

Key Words

Nerve-Cancer, Neurogenesis, Chronic Stress, Tumor Microenvironment, Agent-Based Model, Zebrafish Larvae, Polymeric Nanocarriers, Nanoparticles, Drug Release

Περίληψη

Πρόσφατες μελέτες έχουν δείξει ότι τα νεύρα παίζουν σημαντικό ρόλο στην έναρξη και την ανάπτυξη του καρκινικού όγκου, καθώς και τη διασπορά, εξαιρώντας τη μακροχρόνια αντίληψη πως τα νεύρα συνυπήρχαν παθητικά στο μικροπεριβάλλον του όγκου. Το έργο της Magnon το 2013 [1] ήταν εκείνο που ανέδειξε τη διαδικασία νευρογένεσης επαγόμενης από όγκο, καθώς βρέθηκε πως τα καρκινικά κύτταρα εκκρίνουν νευροτροφικούς παράγοντες που θα μπορούσαν να πυροδοτήσουν τη γένεση ενός νέου νευρικού δικτύου στην περιοχή του όγκου, με τρόπο παρόμοιο με εκείνο που προάγει το νέο αίμα και τα λεμφικά αγγεία. Η διερεύνηση της δυναμικής αλληλεπίδρασης μεταξύ νεύρων και καρκινικού όγκου δημιούργησε ένα νέο πεδίο στην έρευνα για τον καρκίνο που ονομάζεται *«νευροεπιστήμη του καρκίνου»* ή *«βιολογία εξωνευρικού καρκίνου»*. Οι προαναφερθείσες αλληλεπιδράσεις καρκίνου και νευρικού συστήματος ελέγχονται και από φαινόμενα ντετερμινιστικά και στοχαστικά. Στην παρούσα διπλωματική εργασία, θα κατασκευάσουμε ένα Agent-based μοντέλο αλληλεπιδράσεων νευρώνων-καρκίνου προκειμένου να ενσωματωθούν και οι δύο πτυχές (στοχαστική και ντετερμινιστική). Το Agent-based μοντέλο βασίζεται σε agents (οντότητες), είναι μια προσέγγιση μέσω προσομοίωσης σε υπολογιστή και προσομοιώνει τις αλληλεπιδράσεις λήψης αποφάσεων των agents (οντοτήτων) σε κάποιο επιθυμητό χρόνο, βασισμένο σε ένα σύνολο κανόνων. Επιπλέον, θα επικυρώσουμε και θα βαθμονομήσουμε πειραματικά το μοντέλο μας με πειράματα σε έμβρυα ζεβρόψαρα και με βιοαποικοδομήσιμους (mPEG-*b*-PLLA diblock) πολυμερικούς νανοφορείς (νανοσωματίδια) τα οποία θα χρησιμοποιηθούν για ελεγχόμενη απελευθέρωση φαρμάκου. Τέλος, θα διερευνήσουμε την επίδραση του χρόνιου στρες, μέσω της ενεργοποίησης του νευρωνικού συστήματος, στην ανάπτυξη και τη διασπορά του όγκου.

Λέξεις κλειδιά

Νεύρα-Καρκίνος, Νευρογένεση, Χρόνιο Στρες, Μικροπεριβάλλον Όγκου, Agent-Based Model, Έμβρυα ζεβρόψαρα, Πολυμερικοί Νανοφορείς, Νανοσωματίδια, Απελευθέρωση Φαρμάκου

Contents

List of Figures

List of Tables

Chapter 1

Thesis Plan

In this dissertation, we explore the complex and reciprocal relationship between neurons and cancer, a phenomenon that has recently emerged as a critical factor influencing both metastasis and the development of new neural structures, known as neurogenesis or neoneurogenesis. The emergence of new neurons in the tumor microenvironment has been identified as a hallmark of cancer, raising questions about its correlation with tumor proliferation.

Our primary objective is to develop a discrete computational model using Agent-Based Modelling (ABM) to thoroughly examine the dynamic interaction between neurons and cancer. Additionally, we aim to investigate the influence of chronic stress transmitted through the peripheral nervous system on tumor growth dynamics by creating another ABM specifically for analyzing this impact. In ABM, treating individual cells discretely and considering their interactions with neighboring cells/agents proves essential for modeling the complexity of cancer systems. By simulating events like cell proliferation, neurogenesis, and apoptosis as probabilities, our ABM methods capture the stochastic evolution of tumor dynamics, allowing us to explore both spatial and phenotypic heterogeneity - which are known to be two major obstacles in tumor therapeutics.

Furthermore, we investigate the effect of chronic stress on cancer growth. Our experiments focused on zebrafish larvae, a commonly utilized model organism. Specifically, we triggered molecular stress in these organisms by exposing them to stress-inducing substances such as epinephrine, dexamethasone and norepinephrine. This approach effectively replicated conditions of chronic stress. These studies were designed to bridge the gap between theoretical modeling and experimental evidence, offering insights into the influence of stress on cancer progression within a biological system.

We also synthesized loaded mPEG-*b*-PLLA micelles (nanoparticles) encapsulating the beta-blocker DL-Propranolol, which we utilized for targeted treatment in our zebrafish experiments. This novel drug delivery method aims to mitigate the effects of chronic stress on tumor growth, providing a tangible link between our computational models and practical interventions.

Chapter 2

Cancer and Nerves

2.1 Cancer

The word "cancer" refers to a group of diseases characterized by the uncontrolled growth of cells within the body [2]. Cancer can accumulate and form masses of tissue called tumors. If left untreated, cancerous cells can invade surrounding tissues (e.g., blood, lymph, or nerves) and even spread to other parts of the body through a process known as metastasis [3].

Cancer arises from genetic mutations or alterations in the DNA of cells, disrupting the normal regulatory mechanisms that control cell growth and division. Mutations, defined as abnormalities in DNA of various kinds, are believed to build up and endure in inactive sites of the genome due to a lack of mechanisms that eliminate, prevent, or repair them [4], [5]. These mutations can be caused by a combination of genetic predisposition, environmental factors (such as exposure to carcinogens like tobacco smoke or ultraviolet radiation), and lifestyle choices (such as diet, physical activity, and alcohol consumption) [6]–[8].

Cancer can occur in virtually any tissue or organ of the body and is classified into various types based on its origin. Common types of cancer include carcinoma (originating in epithelial tissues), sarcoma (originating in connective tissues), lymphoma (originating in the lymphatic system), leukemia (originating in blood-forming cells), melanoma (originating in melanocytes), and others [2], [3].

2.1.1 Melanoma Cancer

Melanoma is a cancer originating from melanocytes, which are pigment-producing cells derived from the neuroectoderm and distributed throughout the body, including the skin, iris, and rectum. The cutaneous variant of this cancer is prevalent in Western countries and is responsible for the majority (75%) of fatalities associated with skin cancer [9]. Its worldwide occurrence is estimated to be between 15 to 25 cases per 100,000 individuals [9], [10]. Among all types of cancer, melanoma is experiencing a more rapid rise in incidence among men than any other malignancy. For women, it is increasing at a pace greater than all other cancers except for lung cancer [11]. The median age at which diagnosis occurs is 59 years [11]. Exposure to sunlight, particularly Ultraviolet (UV) radiation, represents the primary risk element for cutaneous melanoma. This exposure results in a genetic pattern that is distinctive for melanoma [12].

2.2 The nervous system

The nervous system can be described as an intricate web of specialized cells, tissues, and organs that collaborate to convey and interpret information across the body and regulates the functions of most organs. It is the primary communication and regulatory system of the body, responsible for receiving sensory inputs from the environment, processing them, and coordinating appropriate responses [13].

The nervous system is divided into two main components: the Central Nervous System (CNS) and the Peripheral Nervous System (PNS) [13], [14].

2.2.1 Central Nervous System (CNS)

The CNS consists of the brain and spinal cord (Figure 2.1). It serves as the central processing unit of the body, responsible for interpreting sensory input, generating thoughts and emotions, and initiating motor responses. The brain's significance extends to advanced cognitive functions, memory retention, decision-making, and awareness. Meanwhile, the spinal cord serves as a channel, relaying signals between the brain and the rest of the body [15], [16].

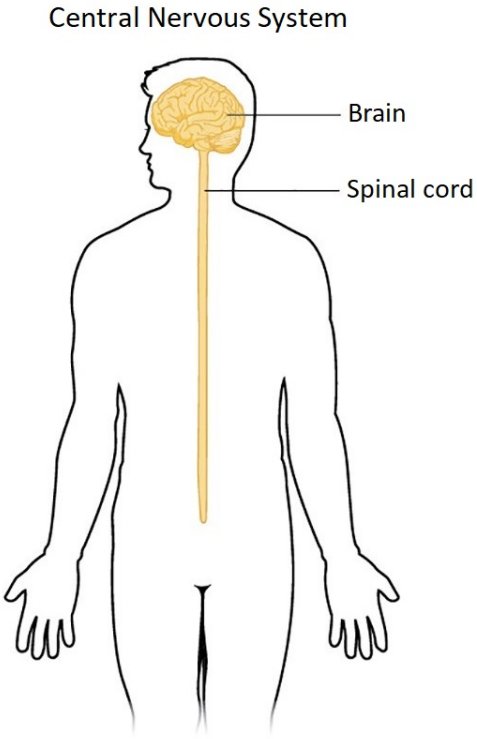

Figure 2.1: CNS, *Image by CNX Openstax*.

2.2.2 Peripheral Nervous System (PNS)

The PNS includes all the nerves and ganglia (clusters of nerve cell bodies) outside the CNS (Figure 2.2). It is subdivided into the Somatic Nervous System (SoNS) and the Autonomic Nervous System (ANS) [16]. The SoNS controls voluntary movements

and transfers sensory information to the CNS. In contrast, the ANS regulates involuntary bodily functions, including those that occur automatically without conscious control, including heart rate, digestion, and respiration. It plays a critical role in maintaining internal homeostasis and responding to stressors [13].

Moreover, the ANS is further divided into two main branches: the Sympathetic Nervous System (SyNS) and the Parasympathetic Nervous System (PaNS). The SyNS is often associated with the "fight or flight" response. It becomes active during situations that require increased alertness and energy expenditure. It can lead to increased heart rate, dilated pupils, and the release of stress hormones like adrenaline. In contrast, the PaNS is often called the "rest and digest" system. It promotes relaxation and recovery. It is active during periods of rest and helps to conserve energy. It slows down heart rate, constricts pupils, and facilitates processes like digestion and repair [13], [14], [16].

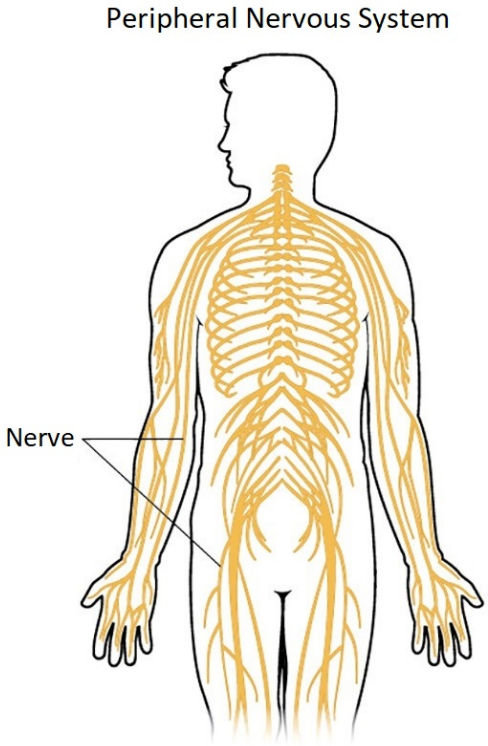

Figure 2.2: PaNS, *Image by CNX Openstax*.

2.2.3 Neurotransmitters

Certain diverse chemical substances, known as Neurotransmitters (NTR), transform the electrical signals that are traveling through a neuron (nerve cell) into signals that are communicated to another neuron via a synapses [17]. NTR are responsible for transmitting these signals between neurons or from neurons to target cells, such as muscle cells, within the nervous system. [18]. These molecules play a critical role in communication within the nervous system and are essential for the proper functioning of the brain and body [18]. NTR bind to receptors called Neurotransmitters receptors (NTR receptors). NTR receptors are specialized proteins located on the surface of neurons or other target cells. In 1926, Otto Loewi made a groundbreaking discovery by demonstrating that acetylcholine served as the first

known NTR, transmitting a chemical signal from the vagus nerve to the heart, resulting in a slowed heart rate. Since then, researchers have identified over one hundred different substances and a considerably larger number of NTR receptors involved in the process of synaptic transmission [19].

NTR originate from precursor molecules abundant within the cell and fall into various classes, such as amino acids, monoamines, and peptides. Monoamines are created by modifying a single amino acid, for example serotonin's precursor being the amino acid tryptophan. Peptide transmitters, known as neuropeptides, are protein-based and are often released alongside other transmitters, exerting a modulatory influence [20]. Purine NTR, such as ATP, stem from nucleic acids, while other NTR consist of metabolic byproducts like nitric oxide and carbon monoxide [21].

NTR can be categorized into several classes based on their chemical structures and functions [22]. The major classes of NTR include:

1. Amino Acids [23]: The most common NTR.
   (a) Glutamate: The primary excitatory neurotransmitter in the brain.
   (b) GABA (Gamma-Aminobutyric Acid): The primary inhibitory neurotransmitter.
   (c) Glycine: Another inhibitory neurotransmitter, mainly found in the spinal cord.
2. Biogenic Amines: Synthesized from amino acids.
   (a) Dopamine: Involved in reward, motivation, and motor control.
   (b) Serotonin: Regulates mood, appetite, and sleep.
   (c) Norepinephrine (Noradrenaline): Influences stress response and mood.
   (d) Epinephrine (Adrenaline): Associated with the "fight or flight" response.
   (e) Histamine: Plays a role in allergic reactions and wakefulness.
3. Acetylcholine: It is the primary neurotransmitter at neuromuscular junctions and is also found in the central nervous system. It's involved in muscle control and various cognitive functions.
4. Neuropeptides: These are larger molecules involved in a wide range of functions, including pain modulation, stress response, and regulation of appetite. Examples include substance P, enkephalins, and endorphins.
5. Purines: These include adenosine and ATP. They have various functions, including neuromodulation and as signaling molecules.
6. Gasotransmitters: These are gases that serve as NTR. Examples include nitric oxide (NO) and carbon monoxide (CO). They play roles in blood vessel dilation and neuronal signaling.
7. Endocannabinoids: These are lipid-based NTR involved in processes such as pain regulation, mood, and appetite.

2.2.3.1 Neurotransmitters' role in cancer

G protein-coupled receptors (GPCRs) are a large family of cell surface receptors that play a crucial role in signal transduction. They are involved in the transmission of signals from the extracellular environment to the inside of the cell. Adrenergic receptors are a class of GPCRs that respond to the binding of the NTR epinephrine and norepinephrine. These receptors play a crucial role in the physiological responses to

stress and the "fight or flight" response. NTR play a role on stromal cells, common components of the tumor microenvironment, actively contribute to the carcinogenic process through the activation of adrenergic receptors. In a groundbreaking study, Magnon et al. [1] demonstrated that the activation of β2- and β3-adrenergic receptors expressed on stromal cells enhances the survival of prostate cancer cells and initiates tumor formation. This underscores the direct impact of NTR (that are primarily produced in neurons) on tumor growth and metastasis, extending beyond cancer and stromal cells to influence endothelial cells and immune cells. This multifaceted influence promotes processes like angiogenesis, lymphangiogenesis, and inflammatory responses in the context of tumor development and progression [24].

Extensive documentation supports the critical role of angiogenesis, or neovascularization (form new blood vessels), in the growth and metastasis of malignant cancers and NTR role for that. There is evidence that supports the notion that endothelial cells express NTR and can be stimulated by exogenous NTR to form new blood vessels [25] [24]. As an example, dopamine has the capacity to mobilize endothelial progenitor cells from the bone marrow. Their subsequent involvement contributes significantly to neovascularization and the growth of tumors [24].

2.2.4 Neurogenic factors

The process of neurogenesis, or the creation of new neurons, is stimulated or influenced by elements known as neurogenic factors [26], [27]. Neurogenesis primarily occurs in certain regions of the brain, such as the hippocampus and the subventricular zone. Their functions include supporting the production of new neurons from progenitor or neural stem cells.

Some of the main neurogenic factors are:

1. Nerve Growth Factor (NGF): NGF is a neurotrophin that supports the growth, maintenance, and survival of certain neurons. While it is primarily known for its role in the peripheral nervous system, there is evidence that it might also influence neurogenesis in specific brain regions [28].
2. Vascular Endothelial Growth Factor (VEGF): VEGF known for its role in angiogenesis, has also been implicated in promoting neurogenesis and enhancing cognitive function [29].
3. Brain-Derived Neurotrophic Factor (BDNF): BDNF is a neurotrophic factor that plays a crucial role in promoting the survival and growth of neurons. It is also involved in neurogenesis, particularly in the hippocampus, which is important for learning and memory [30].
4. Insulin-Like Growth Factor (IGF): IGF is a peptide that plays a role in cell growth and development. It has been implicated in promoting neurogenesis in the adult brain [31].
5. Fibroblast Growth Factor 2 (FGF-2): FGF-2 is a growth factor that has been shown to stimulate neurogenesis, particularly in the hippocampus [32].

2.2.4.1 Neurogenic factors' role in neurogenesis

The production of neurogenic factors and their corresponding receptors affects nerve-cancer cross-talk [33]. Nerve Growth Factor receptor (NGFR), the receptor for NGF,

is expressed in a variety of cancer forms. For instance, it has been observed that basal-like cells resistant to antiestrogens express NGF in luminal breast cancer [33]. Across a variety of tumor types, NGFR creates a negative feedback loop that decreases p53 activation within tumor cells. Both the in vitro proliferation of melanoma stem cells and the in vivo formation of melanoma depend on this process [34]. Via this mechanism, NGF signaling from nerves via NGFR expression on cancer stem cells may drive cancer stem cell proliferation and renewal [35].

2.3 Nerve-Cancer Cross-talk

Interactions between a tumor and the nervous system are complex and bilateral [36]. Tumors can influence the nervous system through various mechanisms, including secretion of factors that initiate the development of a neural network, resulting neoneurogenesis or neurogenesis [26], [27], and the release of signaling molecules that stimulate nerve growth and activation. The latter can result in the infiltration of nerves within the tumor, a phenomenon known as Perineural invasion (PNI), and the promotion of tumor growth and spread along nerve pathways [37]. On the other hand, the nervous system can also impact tumors, when nerves release NTR that affect tumour growth and migration [38]. Also, stress and other neurological factors can influence the tumor microenvironment, affecting factors like inflammation and immune response, which can, in turn, impact tumor progression [39].

2.3.1 Cancer influences the Nervous System

In 2008, Ayala et al. discovered and validated the connection between prostate cancer and axonogenesis (growth and elongation of nerve axons). Their research revealed for the first time that known neurogenic factors, like NGF, that can promote axonogenesis are produced by cancer cells [40]. The deregulation of NGF, crucial for the survival, differentiation, and neurite outgrowth of neurons, has been implicated in various cancer types expressing Tyrosine-receptor kinases (Trks) like TrkA, TrkB, and TrkC, along with the p75 neurotrophin receptor [41]. While cancer cells increase secretion of neurogenic factors, nerves increase expression of the previously mentioned complementary receptors confirming a bilateral cancer-nerve interaction [35], [41].

In addition to researching the role of cancer in axonogenesis, Ayala et al. and Magnon et al. argued that cancer may also promote neurogenesis (an increase in the number of neurons), with the growth of neural progenitors into the tumor [35]. Magnon et al. have shown that prostate tumor autonomic nerve sprouting is critical to prostate cancer advancement [1]. Ayala et al. presented data on increased nerve density in cancer areas and preneoplastic lesions of the human prostate suggesting cancer-related axonogenesis and neurogenesis. Their study also identifies a putative regulatory mechanism involving Semaphorin 4F (S4F), which is overexpressed in cancer cells and induces neurogenesis [40].

Mauffrey et al. addressed the earlier theory, demonstrating that neural progenitor cells expressing the neural stem cell marker Doublecortin (DCX+) migrate through

the bloodstream from neurogenic areas of the brain's subventricular zone to tumorous and metastatic niches, where they differentiate into mature, noradrenergic neuronal phenotypes. However, further investigations aimed at elucidating the mechanisms underlying the migration of DCX+ progenitor cells will be crucial in validating the findings of this study and advancing our understanding of cancer-related neurogenesis [35], [42].

2.3.2 The Nervous System influences cancer

The intricate interactions between nerves and the tumor microenvironment significantly influence the progression of cancer, shaping a complex landscape that demands closer examination.

Indeed, nerves play a significant role in the development and progression of cancer, particularly through PNI in which cancer cells have the ability to surround and eventually penetrate nerves [37]. During PNI, cancer cells invade and spread along the nerves, using them as a pathway to infiltrate nearby tissues and potentially reach distant organs [37]. PNI is a common characteristic observed in visceral and soft tissue cancers, providing an illustrative example of the pivotal role nerves can play in cancer progression [43], [44]. Emerging evidence indicates that the prognosis of cancer is closely linked to the infiltration of nerves within the tumor. This phenomenon is particularly prevalent in cancers that originate in highly innervated organs, such as nearly all pancreatic cancers, 80% of head and neck cancers, 75% of prostate cancers, and 33% of colorectal cancers [35], [45].

However, it is important to highlight that nerves are passive during PNI because they essentially act as a pathway for the proliferation of cancer cells [46].

The nervous system also exerts another indirect impact on cancer progression by controlling hormone release, including epinephrine and cortisol, through the Hypothalamic-Pituitary-Adrenal (HPA) axis. Thus, there have been documented instances of sensory neurons playing a role in tumorigenesis and the progression of cancer [47]. In recent findings, it has become evident that neurons and nerve fibers play essential roles within the tumor microenvironment, promoting the onset and advancement of numerous solid tumors [48]–[50].

Likewise, preclinical studies have shown that before the onset of tumor formation, individual neoplastic cells invade neural tissue [47]. This implies that nerves might be exploited as a pathway for the dissemination and metastasis of cancer cells.

Interestingly, tumors seem to adopt neural programs to facilitate their growth and progression, much like how healthy tissues recruit and maintain innervation through the PNS [1], [51]–[53]. The PNS consists of autonomic and sensory nerves in the periphery, forming a network that plays a crucial role in coordinating molecular-level, cellular-level, and organ-level processes, which are essential for the body to maintain homeostatic control. These coordinated systems continuously make adjustments to internal variables, such as blood pressure, pH, and metabolism, to adapt to both internal and external pressures. In a similar manner, tumors must also regulate these processes to ensure their survival [39], [54].

Research findings have indicated that the ANS has significant roles in the develop-

ment of tumors and the advancement of cancer [52], [55].

Furthermore, as it was stated in the previous section, cancer cells enhance the release of neurogenic factors, like NGF, promoting axonogenesis, while nerves increase the expression of the complementary receptors. One of them, the p75 neurotrophin receptor, is also expressed on nerves, and it has recently been shown that the p75 neurotrophin receptor acts as a chemoattractant for cancer cells, because the chemotaxis ability of p75-transfected pancreatic cancer cells to NGF was significantly stronger than non-transfected cells [56]. This finding states as a neurons' direct impact on cancer cells.

Consistently, the existence of nerve fibers stands as an autonomous prognostic determinant for overall survival in cases of pancreatic ductal adenocarcinoma [45], [57]–[59], gastric carcinoma [60], [61], biliary tract tumors [62], head and neck cancer [63]–[65], and cervical cancer [66], [67]. Additionally, it serves as an indicator of recurrence risk in instances of pancreatic cancer [68], prostate cancer [66], [69], gastric cancer [70], and colorectal cancer [35], [46], [71]–[75].

2.4 Cancer and Stress

Stress activates the body's "fight or flight" response, which is controlled by the SyNS, one of the branches of the ANS. When faced with a stress-inducing situation, like a challenging event, human body releases stress hormones. These hormones prepare the body to react to the stressor by boosting your heart rate, widening air passages, and redirecting blood flow toward essential organs [76], [77].

Stress can be categorized into two main types: acute stress and chronic stress. Acute stress typically arises during emergency situations, like situations that require quick action or escape. During acute stress, alterations occur in the configuration and operation of specific molecules and brain tissues, prompting the activation of the emotional and cognitive systems. As a result, individuals make decisions regarding strategies to cope with the stress [78]. Simultaneously, the body undergoes a temporary surge in catecholamines and corticosteroids to enhance mobility and alertness during acute stress, rendering it generally advantageous for the body. However, chronic stress is closely associated with adverse health effects and is now recognized to encompass factors like occupational stress and unusual adversities. Its potential negative effects encompass a wide range of psychosomatic symptoms [79], [80] and an high risk of developing cancer [76].

The relationship between chronic stress and cancers has aroused growing attention and concern within the medical field. Numerous researchers have conducted investigations into the links between stress and various types of cancer, including prostate [81], breast [82]–[86], gastric [87], [88], lung [74], [89], and skin cancer [90], [91]. Their findings have provided evidence suggesting that chronic stress has the potential to initiate tumorigenesis and facilitate the progression of cancer [76].

It's important to note that the relationship between stress and cancer is complex and not fully understood. Not everyone who experiences stress will develop cancer, and not all cancers are influenced by stress in the same way. Additionally, the impact of stress on cancer may vary depending on an individual's genetic predisposition

and overall health.

2.5 Zebrafish

The zebrafish, a tropical freshwater species, is primarily found in the rivers of the Himalayan region in South Asia. This habitat encompasses countries such as India, Nepal, Bhutan, Pakistan, Bangladesh, and Myanmar. Classified as a bony fish or teleost, it falls under the family Cyprinidae within the class Actinopterygii, which includes ray-finned fishes [92].

In 1981, George Streisinger from the University of Oregon introduced the zebrafish as a biological model [93]. It gained popularity due to its simplicity compared to mice and its genetic manipulability [94]. Model organisms play a crucial role in monitoring the environmental well-being of our planet. These non-human animal species serve as invaluable tools for delving into specific biological processes and obtain information that can shed light on the functioning of various organisms. Among these model organisms, the zebrafish (Danio rerio) stands out as one of the best models for exploring developmental biology, cancer, toxicology, drug discovery, molecular genetics, and evolution [95]–[100]. This tiny fish shows remarkable versatility as a model organism across diverse research fields. Its appeal lies in its easy maintenance, ease of breeding, and the transparency of its body during early development [101].

Remarkably, zebrafish shares numerous physiological and genetic resemblances with humans, spanning areas such as the brain, digestive system, musculature, vasculature, and innate immune system [95], [102]–[107]. Notably, approximately 70% of human disease genes exhibit functional similarities with those found in zebrafish [108].

2.6 PDX zebrafish model

Patient-derived xenografts (PDX) are cancer models created by implanting and successfully growing human tumor samples within animal hosts [109]–[111]. A PDX model grows in a 3D microenvironment containing blood vessels for in vivo nutrient and oxygen supply, along with host stromal cells that engage in interactions and communication with the tumor cells [112], [113]. In contrast to xenograft models derived from cell lines, PDX models better recapitulate the heterogeneity found in primary tumors and preserve their gene expression and mutation profiles, leading to better understanding tumor's behavior, response to treatments, and potential therapeutic strategies [114]–[117]. In summary, a PDX represents a highly promising preclinical model within the realm of personalized medicine. It holds the potential for predicting individualized responses to drugs and offering valuable insights to tailor patient treatments [118]. A zebrafish PDX model representation is shown in Figure 2.3.

Most PDX models are generated using mice which are costly and time consuming. Conversely, a zebrafish (Danio rerio) model offers significant advantages over

a mouse model when it comes to evaluating drug effectiveness. It demands considerably less material, enables efficient high-throughput screening, facilitates toxicity assessments, allows for convenient drug administration, and results in shorter experimental timelines [119], [120]. Moreover, zebrafish exhibit several features that make them an attractive model choice for studies related to human cancer research [95], [121], [122]. In zebrafish, the adaptive immune system doesn't fully develop until four weeks after fertilization. This unique feature enables the avoidance of graft rejection without immune suppression [112]. Zebrafish share a similar vertebrate anatomy and possess orthologs for 70% of human proteins, along with paralogs for 84% of all recognized disease-related genes [123]. Additionally, zebrafish embryos have the capability to absorb a range of small molecular weight compounds from their surrounding water. This, combined with the high degree of conservation of genes associated with cancer, has positioned zebrafish as a highly promising model organism for in vivo cancer research [110], [124].

Figure 2.3: Zebrafish PDX model representation, *Image by BioReperia*.

In this dissertation, we conducted experiments involving human melanoma cancer cells that were cultured within the laboratory setting. These cultured cells were subsequently microinjected into zebrafish larvae as part of a PDX zebrafish model. Subsequently, we induced stress in the zebrafish using three distinct stressors: epinephrine, norepinephrine, and dexamethasone. To investigate the potential stress-reducing effects, the zebrafish were subjected to treatment with propranolol. Detailed descriptions of both the stressors and the treatment can be found in the following sections.

2.7 Stressors

Stress can be defined as a situation where an organism perceives a threat, whether it's real or perceived, to its overall homeostasis and well-being. Within this definition, two broad and distinct categories of stressors become evident. The first category, known as 'systemic' or 'physiological' stress, represents an actual and immediate physical danger to the organism's health and well-being. Importantly, conscious awareness or recognition of the threat by the organism is not necessary for it to be classified as 'stress,' nor is it required for the initiation of a 'stress response.' The second category, termed 'processive' or 'psychogenic' stress, relies on

an individual's perception, cognitive processing, and interpretation of the stimulus to imbue it with a stressful quality [125]–[128].

Therefore, when it comes to stress induced by a stimulus, whether it's physiological or psychological in nature, certain chemicals (or "stressors") are generated within the organism. Many researchers have played a significant role in characterizing the mechanisms for the damage caused by stressors and the subsequent biological response known as the "stress response" [129]–[131]. In this dissertation, we administer stressors to zebrafish to artificially induce a state of stress [132]. The chosen stress-inducing agents for the zebrafish include epinephrine, norepinephrine, and dexamethasone.

1. **Norepinephrine (Noradrenaline)**

   Norepinephrine, also known as noradrenaline, acts as both a neurotransmitter (NTR) and a hormone [133]. In the central nervous system, it's involved in arousal, attention, and stress responses. In the peripheral nervous system, it functions as a hormone, preparing the body for the "fight or flight" response [134] by increasing heart rate, blood pressure, alertness and energy availability. Norepinephrine belongs to the catecholamine family which are a group of NTR and hormones that play significant roles in the nervous system and the body's stress response. Norepinephrine is released by the adrenal medullas (the inner core of the adrenal glands, which are located on top of each kidney) and sympathetic (SyNS) nerve endings in response to acute stress [135]–[137].

2. **Epinephrine (Adrenaline)**

   Epinephrine is primarily a hormone produced by the adrenal medullas [138]. It is released into the bloodstream during moments of acute stress or danger. It triggers the same "fight or flight" responses as norepinephrine, preparing the body to respond quickly to a perceived threat [139].

3. **Dexamethasone**

   Dexamethasone is a synthetic corticosteroid (steroid hormone), meaning it is a man-made drug (it is not naturally produced by the body). Dexamethasone is occasionally employed in laboratory environments as a pharmacological stressor, particularly in studies related to stress responses. It can induce a stress response by influencing the HPA axis, ultimately resulting in increased cortisol levels.

   Cortisol is a natural hormone produced by the adrenal glands [140]. It is released in response to stress and helps regulate various bodily functions, including metabolism, immune response, and blood pressure. Cortisol is less potent than dexamethasone, thus dexamethasone has a much stronger anti-inflammatory and immunosuppressive effect compared to cortisol. Moreover, cortisol exhibits a relatively brief duration of activity within the body. For this reason, we opted for dexamethasone due to its more prolonged presence in the body post-administration [141]–[143].

2.8 Treatment

Stress has the potential to induce immunosuppression (weakening of the immune system's activity) [144], which, in turn, can impact the prognosis of cancer patients [145], [146]. Moreover, stress hormones originating from the SyNS can potentially trigger the proliferation and invasive behavior of tumor cells. This effect might be facilitated through beta-adrenergic receptors present on tumor cells themselves [147], [148]. Consequently, chronic stress has the potential to exacerbate the prognosis of malignancies for various types of cancers. This situation underscores the beta-adrenergic system as a possible target for therapeutic interventions [145], [147], [149], [150].

Beta-adrenergic receptors are a type of receptor in the body that interact with NTR called beta-adrenergic agonists, such as epinephrine and norepinephrine. When these agonists bind to beta-adrenergic receptors, they trigger a "fight or flight" response, leading to increased heart rate, elevated blood pressure, and heightened alertness [151].

Beta-adrenergic receptor antagonists, commonly referred to as beta-blockers, are medications that block the action of beta-adrenergic agonists. By doing so, they reduce the effects of the "fight or flight" response, resulting in lowered heart rate and blood pressure, thus, they are primarily known for their use in the treatment of various cardiovascular conditions including hypertension, angina, and arrhythmiasand heart-related disorders [152], [153].

2.8.1 Propranolol

Propranolol (or DL-Propranolol), a beta-adrenergic receptor antagonist, was formulated over 50 years ago by the British scientist Sir James Black, with its primary application aimed at treating angina pectoris [154], [155]. It wasn't long before it became evident that propranolol's therapeutic benefits extended beyond angina treatment, proving effective in addressing various cardiovascular ailments like hypertension, myocardial infarction, and arrhythmias [153], [155]–[158]. Throughout the years, propranolol has also found its utility in numerous noncardiovascular conditions, encompassing migraine, essential tremors, anxiety, portal hypertension, hyperthyroidism, and pheochromocytoma [159]–[161].

Here, we utilize propranolol as a therapeutic agent (treatment) for melanoma cancer in zebrafish while simultaneously investigating its effects in combination with stressors.

Chapter 3

Cancer Cell and Zebrafish Larvaes' Materials and Protocols

3.1 Cancer Cell Materials

3.1.1 PBS 1X (Phosphate-buffered saline) buffer

In 1954, Dulbecco and Vogt detailed the formulation of Phosphate-buffered saline (PBS), often referred to as Dulbecco's PBS or PBS 1X, in the context of generating plaques on monkey tissue monolayer cultures [162]. Since then PBS is a type of buffer solution commonly used in biological and chemical research [163]. The Dulbecco's PBS solution, consists of the following components: sodium chloride (NaCl) (137 mM), disodium hydrogen phosphate (Na_2HPO_4) (8.1 mM), potassium chloride (KCl) (2.7 mM), and monopotassium dihydrogen phosphate (KH_2PO_4) (1.5 mM) [164]. NaCl provides the saline component of PBS, helping to maintain osmotic balance and the physiological salt concentration in cells and tissues and Na_2HPO_4's phosphate component acts as a buffer, helping to maintain a stable pH level, typically around 7.4, which is similar to the pH of biological systems.

PBS 1X is preferred in many biological applications because its ion composition and pH closely mimic the conditions found in biological systems, making it suitable for various research and laboratory purposes.

In our experiments, we utilize a 1X PBS buffer for both staining cancer cells and the process of cell splitting.

3.1.2 Cell Culture Materials

Cell Culture Media

1. **McCoy's 5A**

   Medium 5A described by Thomas McCoy in the 1950s [165], often abbreviated as McCoy's A5 medium or simply McCoy's medium, is a type of cell culture medium used for the in vitro cultivation of various cell lines. McCoy's 5A medium is commonly used in research and biotechnology for the maintenance and propagation of mammalian cells.

   This medium contains a balanced mixture of amino acids, vitamins, salts, and glucose, providing the essential nutrients necessary for human and animal cell

growth. The efficacy of this medium is probably due to its particular balance of the constituents [166] and it is particularly suitable for the cultivation of cells that require lower bicarbonate concentrations than those found in other commonly used media. Fetal bovine serum (FBS) or other serum alternatives are frequently added to it as supplements to provide extra growth hormones and nutrients tailored to the cells being cultured.

Researchers and laboratories use McCoy's 5A medium for various cell-based experiments, maintenance of cell lines, and other cell culture applications.

2. **RPMI 1640**

   RPMI 1640 (Roswell Park Memorial Institute 1640) is a widely used cell culture medium in biology and research laboratories. It was developed by Dr. George Gey at the Roswell Park Memorial Institute in Buffalo, New York, hence the name [166]. RPMI 1640 is a modification of the medium 5A described by McCoy [165], which is considered as the best general-purpose medium for in vitro cultivation of various kinds of mammalian cells on glass and in suspension cultures [166], [167].

   It contains essential nutrients, vitamins, amino acids, and minerals that support the survival, cell growth and proliferation of cancer cells. It can support the growth of a variety of mammalian cell types, including both adherent and suspension cells.

   RPMI 1640 is often supplemented with fetal bovine serum (FBS) or other serum substitutes to provide additional growth factors and nutrients specific to the cells being cultured. Researchers and laboratories use it for tasks such as maintaining cell lines, cell proliferation assays, and cell-based experiments.

In our experiments, we employed either McCoy's 5A or RPMI 1640 medium for cell culture, cell splitting and cell staining procedures. These media were sourced from Biowest and were supplemented with 10% fetal bovine serum and 1% streptomycin solution. This consistent approach ensured that our cells received the necessary nutrients and antibiotics for optimal growth (proliferation) and maintenance throughout the course of our research.

3.1.3 Cell Split Materials

Trypsin

Trypsin is an enzyme that is derived from the pancreas and belongs to a class of enzymes known as proteases. Its primary role in cell culture is the dissociation of adherent cells from both each other and the culture vessel's surface. Upon introduction into the culture, trypsin enzymatically degrades the proteins responsible for cell adhesion, allowing cells to be easily harvested for various experiments or for subculturing (passaging) into new culture vessels [168].

3.1.4 Cell Stain Media

DiL Cell Dye

1,1'-Dioctadecyl-3,3,3',3'-tetramethylindocarbocyanine perchlorate (DiL) is a lipophilic

fluorescent dye used in cell biology and microscopy to label cell membranes. It exhibits a red fluorescence and is particularly helpful for staining the lipid bilayer of cell membranes [169]–[171].

DiL displays low fluorescence in aqueous solutions but exhibits strong fluorescence and impressive photostability when integrated into membranes. Upon application to cells, these dyes spread laterally within the cell's plasma membrane, leading to the staining of the entire cell [172], [173]. In Figures 3.1 and 3.2, DiL staining is demonstrated in melanoma cancer cells observed under normal light and fluorecsent light microscope. Typically, there is minimal transfer of these probes between intact membranes. DiL and similar compounds generally show minimal cell toxicity [169]. This makes it a helpful tool for a variety of applications, including cell movement investigations, cell migration studies, and the visualization of cellular structures since it enables researchers to see and track cell membranes [170].

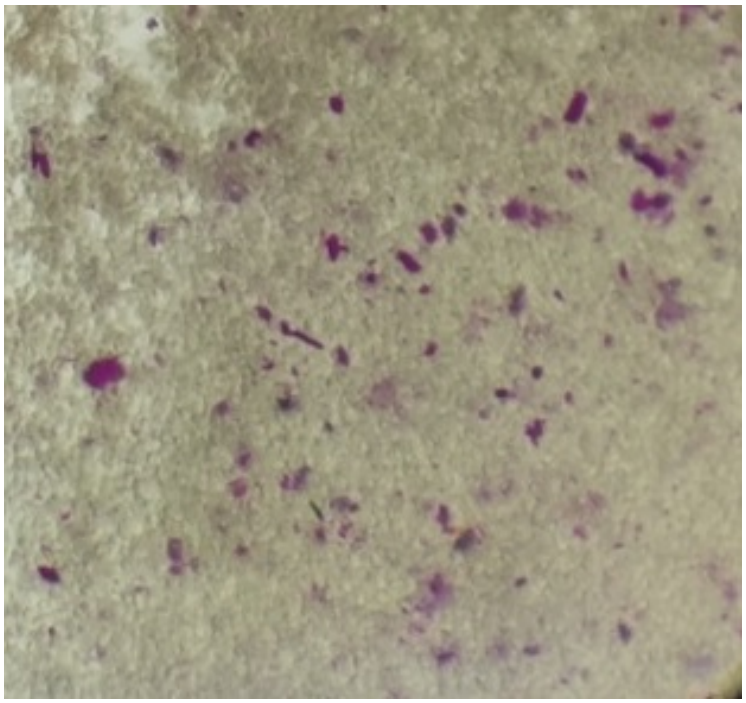

Figure 3.1: Melanoma Cancer cells dyed with DiL, under the microscope.

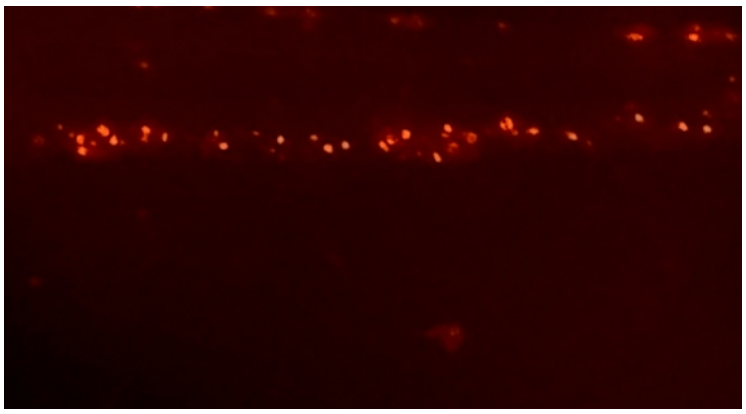

Figure 3.2: Melanoma Cancer cells dyed with DiL, under microscope's fluorescent light.

In our study, we employ DiL dye, in concentration 40mg/ml, diluted to 100% Ethanol, to monitor the growth and spread (metastasis) of melanoma cancer cells, with a focus on the primary tumor.

3.2 Cancer Cell Protocols

3.2.1 Cell Culture

Melanoma cancer cells have been cultured at 37°C with 5% CO_2 in a T-75 flask. Tissue culture technics have been described by Thomas McCoy [174]. The medium utilized was Biowest RPMI 1640 or MccoyA5, both with 10% fetal bovine serum and 1% streptomycin solution, as stated before. It is not possible to outline a routine feeding schedule since the requirements of the various cancer cells differed greatly. Hence, when medium's color began to change from red to more yellow than red, it signals the pH had altered and the medium had to be renewed [166]. When confluency reached 70%, the cells were split (chapter Cell Split) or stained with DiL red fluorescent dye (chapter Cell Stain) and injected with a microneedle to zebrafish larvae.

3.2.2 Cell Split

The flasks, which held adherent melanoma cells at approximately 70% confluence, needed to undergo a splitting process to provide these cells with fresh medium for proliferation. The protocol begins with the removal of media from the flask, followed by a subsequent rinsing of the flask with PBS. To separate the cell from the flask's surface, 2ml of trypsin was injected. We only keep the trypsin in for one minute because longer exposure to it can be toxic and damage the cells. After trypsin was withdrawn, 2 ml of medium was added. The flask was washed with the medium and gently tapped to make sure all cells were removed from the surface if the cells did not detach. The detached cells were given 2ml of media, removed, and placed in two brand-new flasks, each holding 1 ml. 10 ml of medium was supplied to each new flask so that the cells may continue to proliferate.

3.2.3 Cell Stain

Once the cell culture flasks reached an approximate confluence of 70% or more (shown in Figure 3.3), the staining process could be initiated. To prepare the dye, 10ml of PBS was added to a tube and left at room temperature for 1 minute. Subsequently, 3µl of the DiL cell dye was added, and the tube was gently shaken to ensure proper mixing.

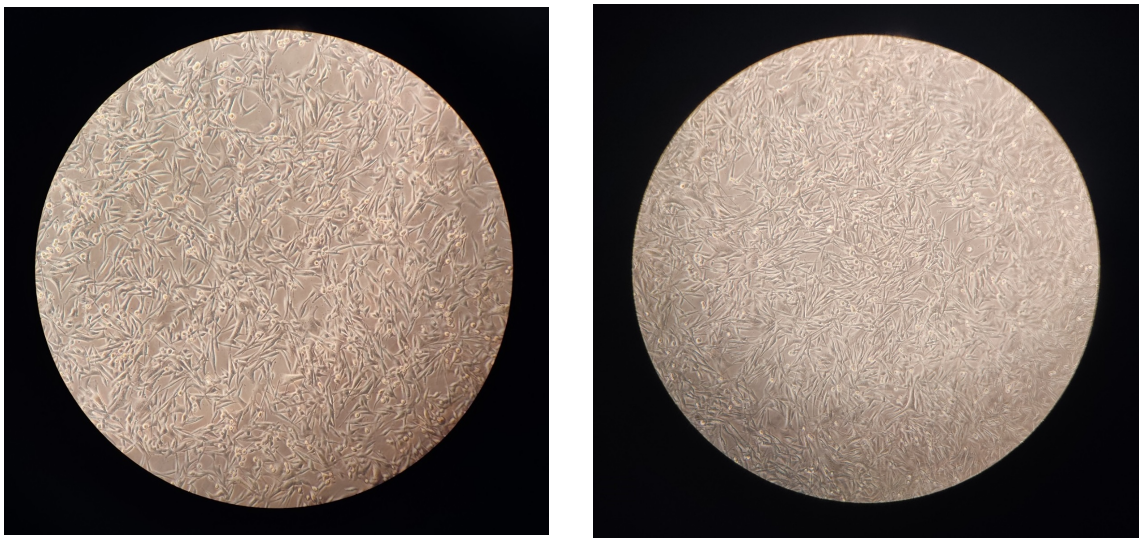

Figure 3.3: Melanoma cancer cells with an approximate confluence of 70% (left) or more (right).

Following this the culture medium was carefully poured out of the flasks, leaving only the melanoma cancer cells. The previously prepared dye liquid was then added to the flask, and the flask was incubated for 30 minutes. The cells were examined under a microscope to check if they were floating. In cases where they weren't, they were gently washed up and down using a pipette.

The stained cells were then passed through a 40 µm cell strainer to remove any residual dye crystals. Subsequently, the strained cells were transferred to a 15ml tube and centrifuged for 5 minutes at 2000g. The supernatant was discarded, and the cells were resuspended in 5ml of PBS.

Following this step, the cells were centrifuged once again for 5 minutes at 2000g. The supernatant was once more discarded. The cells were then resuspended in 1 ml of cell culture medium (either Biowest RPMI 1640 or MccoyA5) and transferred to a 2ml Eppendorf tube. This was followed by another centrifugation for 5 minutes at 10000 g.

Finally, the supernatant was discarded, and the stained melanoma cancer cells were diluted in 30µl of cell culture medium. At this point, the stained melanoma cancer cells were ready to be injected into the zebrafish for further experimentation.

3.3 Zebrafish laboratory facilities

The facilities of a university zebrafish laboratory are designed to support the care, maintenance, and research involving zebrafish, a widely used model organism in biological research. Here is a description of typical facilities found in such labs:

- Fish Housing: University zebrafish labs typically house zebrafish in specialized aquarium systems. These systems maintain optimal conditions for zebrafish, including temperature, pH, and water quality control. The fish are kept in tanks equipped with recirculating water systems to ensure a clean and stable environment.

- Breeding Facilities: Zebrafish labs have dedicated spaces for breeding zebrafish. These areas may include specialized tanks with dividers to separate male and female fish, as well as facilities for collecting and caring for embryos and larvae.
- Microinjection Laboratory: Micoinjections are often performed on zebrafish for various experimental purposes. Specialized suites equipped with microscopes and micromanipulators are available for these procedures.
- Microscopy and Imaging: Zebrafish labs typically have microscopy and imaging facilities equipped with confocal microscopes, fluorescence imaging systems, and other advanced imaging tools. These are essential for visualizing zebrafish at the cellular and subcellular levels.

3.4 Zebrafish Larvaes' Handling Materials

3.4.1 E3 medium

E3 medium is used to house and maintain zebrafish embryos and larvae during their early developmental stages. Zebrafish embryos are typically transparent and develop externally, making them well-suited for microscopic observation [175]. E3 medium provides a controlled and supportive environment for these embryos, ensuring they have access to the necessary ions and preventing fungal infections that can occur in other types of water [176].

E3 medium is a commonly used solution in zebrafish research. It is named after its primary components, which are water, salts, and methylene blue, and it is used to maintain and rear zebrafish embryos [176]. E3 medium is prepared with the following components:

1. Deionized Water: This serves as the base for the solution and is typically purified to remove impurities that might affect the development of zebrafish embryos.
2. Salts: E3 medium contains specific salts to provide essential ions and maintain osmotic balance. These salts often include sodium chloride (NaCl), potassium chloride (KCl), calcium chloride ($CaCl_2$), and magnesium chloride ($MgCl_2$).
3. Methylene Blue: Methylene blue is a dye that is added to E3 medium for its antifungal properties [177]. It helps prevent the growth of fungal and bacterial contaminants in the water, which can be detrimental to zebrafish embryos.

However, in the realm of zebrafish research, the inclusion of methylene blue in E3 medium is a common practice to prevent fungal and bacterial contamination during embryo development. However, there are situations where researchers may opt to omit methylene blue from their experimental setup. Experimental considerations come into play when researchers aim to avoid potential interactions or effects that methylene blue might have on the embryos. Given its nature as a dye, methylene blue can introduce unintended consequences into certain experimental outcomes. Moreover, specific research questions may demand zebrafish embryos to be raised in conditions closely resembling their natural habitat, prompting scientists to choose E3 medium without methylene blue to eliminate artificial factors that could influence the experiment's results. Lastly, while methylene blue is generally regarded as safe at the concentrations used in E3 medium, concerns about potential toxicity may

arise in specific experiments or when working with particularly sensitive strains of zebrafish, prompting researchers to explore alternative options.

In our experiments when preparing the E3 medium, we don't use Methylene Blue.

E3 medium preperation:

For ~1Lt E3 medium 60× stock solution, add:

- 17.4g NaCl
- 0.8g KCl
- 2.9 $CaCl_2 \cdot 2H_2O$
- 4.89g $MgCl_2 \cdot 6H_2O$

in 1Lt of nanopure H_2O and adjust the pH with NaOH and HCl until pH=7.2.

3.4.2 PTU

1-phenyl-2-thiourea (PTU), is a vital rate-limiting enzyme for melanogenesis, often used in zebrafish research labs as a treatment to prevent the development of pigmentation in zebrafish embryos [175]. Zebrafish embryos are naturally pigmented, which can make it challenging to visualize internal structures and cells, especially under a microscope. PTU treatment prevents the development of pigmentation, increasing their optical transparency for microscopic imaging and making it easier for researchers to observe and analyze various aspects of embryonic development, tissue differentiation, and organ formation [178]. Also, PTU treatment provides a standardized method for creating consistent experimental conditions. Thus, researchers can reduce variability and ensure that observations and measurements are not influenced by differences in pigmentation levels among individuals.

The chemical structure of PTU consists of a phenyl ring (a six-membered carbon ring with a benzene structure) attached to a thiourea group (a molecule containing a sulfur atom and two amino groups).

PTU medium preperation:

For ~50ml PTU medium 50X stock solution, add:

- 0.528gr PTU powder

to 50ml H_2O. Mix well with a stir bar until fully dissolved.

For ~1Lt PTU medium 1X, put:

- 20ml PTU medium 50X
- 16.5ml E3 medium 60X

in a bottle. Add nanopure H_2O so the final volume is reached up to 1Lt.

Zebrafish embryos are treated with 0.003% (w:v) (200 μM) PTU 1X before 24 hour-post-fertilization (hpf).

3.4.3 Tricaine or MS-222

The most common temporary laboratory anesthetic for zebrafish is ethyl 3-aminobenzoate methane-sulfonate (Tricaine) (commonly known as Tricaine or MS-222) that is reversible upon washout [179], [180] and it is used by 80% of research labs responding

to a survey carried out by Lidster et. al. [181]. It is the only Food and Drug Administration approved anesthetic for aquaculture to sedate and immobilize zebrafish during experimental manipulation and is widely used by the zebrafish research community [182]. For larvae, a stock solution of tricaine (working solution) can be diluted in E3 medium [179].

Tricaine stock solution preperation:

For ~100ml Tricaine stock solution, add:

- 400mg powder Ethyl 3-aminobenzoate methanesulfonate (Tricaine/MS222)

to 97.9ml deionized H_2O. Mix well until fully dissolved.
Adjust pH to 7.0-7.4 using 2.1ml 1 M Tris·Cl (pH 9).
Divide into 420µl aliquots and freeze.

Tricaine working solution preperation:

For ~10ml Tricaine solution for zebrafish larvae, add:

- 420µl of Tricaine stock solution

to 10ml deionized H_2O. Mix well.

In our experiments, we applied 2-3 drops of a Tricaine working solution to zebrafish larvae just before microinjection, while they were situated in an agarose gel petri dish.

3.5 Zebrafish's Handling Protocol

The protocol for handling zebrafish embryos, involves several crucial steps to ensure their health and rediness for the microinjection procedure.

Zebrafish are initially paired by licenced personnel who carefully choose appropriate partners. The containers are checked for successful matings before noon the following day. Mating containers in which eggs are visible on the bottom are labelled, the eggs are collected (by pouring the water from the outer container through a fine mesh sieve), and are transferred into a Petri dish in PTU medium [176].

Then, zebrafish larvae are incubated either at 28°C for two days or at room temperature for three days, depending on the experimental requirements.

A good clutch is believed to contain between 70 and 300 eggs, with a minimum of 80% being fertilized. During the incubation period, a daily regimen of maintenance is essential. Unfertilized eggs and feces can serve as a nutrient source for the growth of bacteria and mold, which can rapidly deteriorate the water quality [176]. This includes diligently removing any impurities, dead or unfertilized embryos, and feces from the petri dishes using a disposable plastic pipette to maintain optimal environmental conditions.

On the second or third day, corresponding to the incubation temperature, the embryos progress to the stage where decoronation is performed. Using fine forceps or microdissection scissors, we carefully grasp the chorion, which is typically located at one end of the embryo, near the tail. We are being gentle to avoid damaging the embryo itself. By applying a slight pressure, we cut or peel away the chorion from

the embryo. This process may require delicate handling to ensure the chorion is entirely removed without harming the developing embryo. In Figures 3.4 3.5 zebrafish larvae are observed before and after decoronation. After decoronation and before the microinjection of cancer cells, we select the embryos and gently transfer them to agarose gel-coated petri dishes.

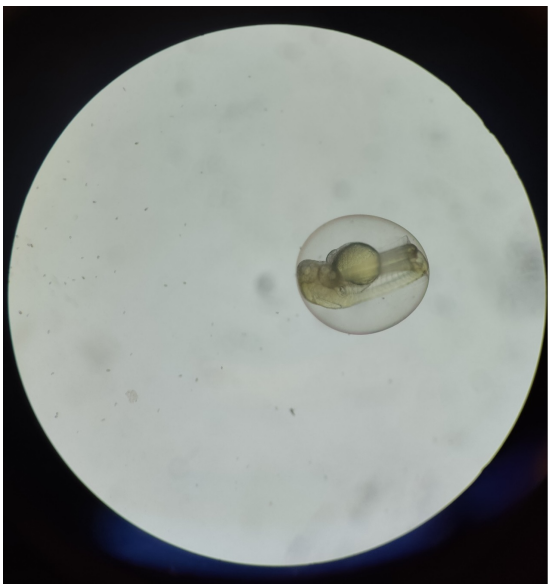

Figure 3.4: Zebrafish larvae before decoronation, under microscope.

Figure 3.5: Zebrafish larvae after decoronation, under microscope.

3.6 Zebrafish's Microinjection Protocol

For the microinjection, glass needles were meticulously crafted from borosilicate microcapillary tubes by heating and pulling the ends apart to create fine tips (Figure 3.7) with a needlepulling machine (Figure 3.6).

Figure 3.6: Needlepulling machine, image by Tritech Research.

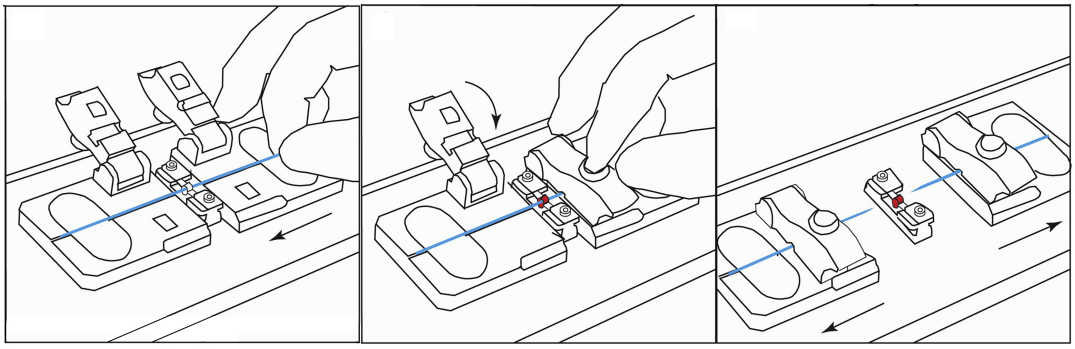

Figure 3.7: Needle-Pulling Process: A borosilicate capillary tube secured at both ends is heated in the middle by the machine, pulling one end to craft two needles with precise, fine tips, image by Star Protocols

Loading 5 µL of suspended stained cancer cells into the injection needle marks the initial step in the process of zebrafish microinjection. As the air source of the pneumatic picopump and microinjector are activated, the needle is inserted into the microinjector, ensuring a secure seal within the housing. Simultaneously, attention is directed towards the micromanipulator, ensuring its optimal positioning to allow a broad spectrum of movement and adjustments.

The needle tip is elevated high above the stage and brought into focus under the microscope, with an examination of the thinnest region the tip is delicately broken off using fine tweezers, achieving a tip opening diameter ranging from 5 to 10 µm (Figure 3.8).

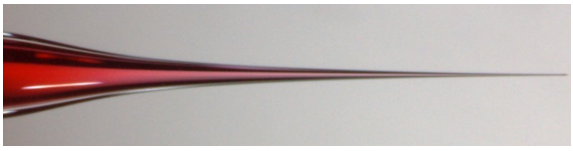

Figure 3.8: Tip of a filled microneedle, image adopted [183].

Adjustment of the injection pressure of the pneumatic picopump (Figure 3.9), synchronized with depressing the foot pedal, allows for careful monitoring of the bead

size. The quality of the needle tip and the injection pressure are crucial to both the quality and consistency of the injection.

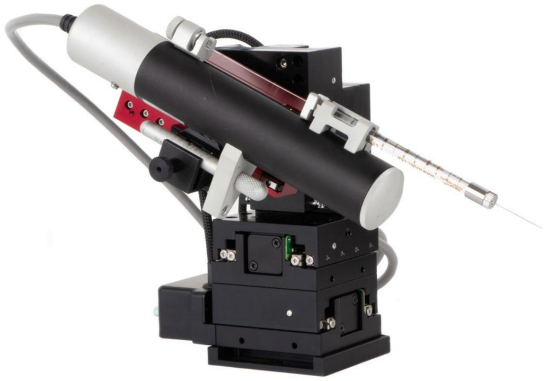

Figure 3.9: Micromanipulator siringe pump, image by AnimaLab.

Following the preparation of the injection material, decoronated zebrafish embryos (2-3 days post-fertilization) were carefully selected and gently transferred to agarose gel-coated 1% agarose injecting plates. To minimize movement during the microinjection process and make the procedure less stressful for them, the embryos were anesthetized by applying 2-3 drops of Tricaine solution. Orienting the injection plate by hand during the injections to place the embryos in the preferred position (i.e., diagonally) ensures the embryos are strategically positioned for needle insertion. Lowering the needle towards the agarose-coated petri dish containing the decoronated zebrafish larvae, the needle tip is precisely pointed at the injection site. A smooth insertion into the perivitelline space (Figure 3.10) between the yolk sac and periderm of the zebrafish embryo is executed, with vigilance against rupturing the yolk sac to avoid cancer cell implantation into it. Air bubbles or stretching the perivitelline space as either can be lethal to the embryo. Fine adjustments in pressure are made to maintain a consistent bead size throughout the microinjection process.

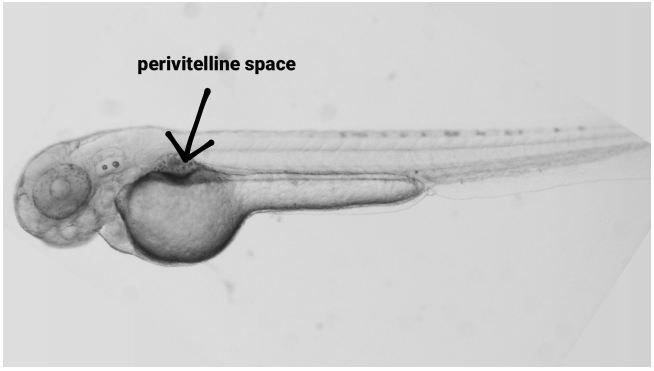

Figure 3.10: Zebrafish' perivitelline space.

Following the injection, the effective integration of cancer cells was visually confirmed by observing a subtle expansion of the injected area, which was visibly filled with red-dyed cancer cells. It could also be observed under fluorescent light, both shown in Figure 3.11.

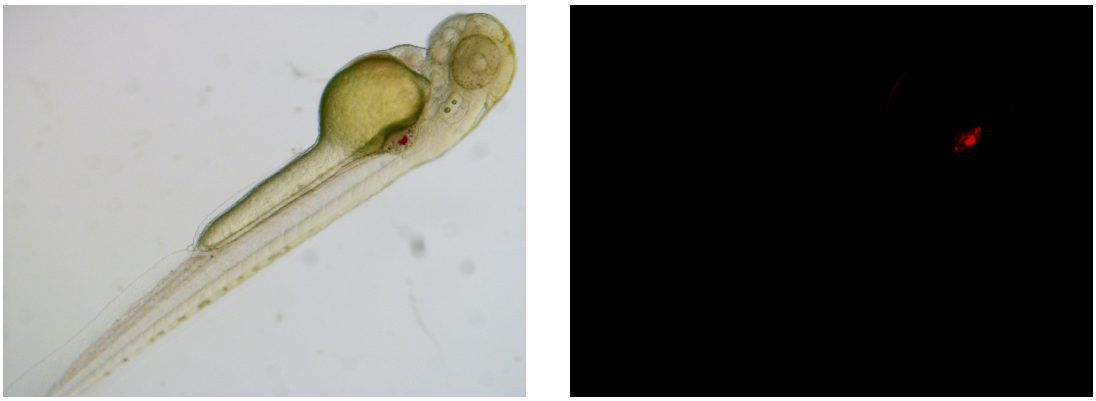

Figure 3.11: Zebrafish larvae after microinjection with dyed melanoma cancer cells, under microscope, under visible light (left), under fluorescent light (right).

Chapter 4

Results and Discussion on Cancer Cell and Zebrafish Larvaes' Experiments

4.1 Zebrafish larvae injected with Melanoma Cancer Cells

Melanoma cancer cells have been cultured at 37°C with 5% CO_2 in a flask. When the flask's confluency reached 70%, the cells were split or stained. When split, they were placed in two brand-new flasks with new medium, so that the cells may continue to proliferate in the incubator. When stained, they were stained with with 40mg/ml DiL red fluorescent dye. Then, the stained melanoma cancer cells were diluted in 30µl of cell culture medium. At this point, they were ready to be injected into the zebrafish larvae.

On the second or third day, post fertilization, zebrafish larvae were decoronated and being gently transferred on a flat agarose gel-coated 1% agarose injecting plate. The embryos were anesthetized by applying on them 2-3 drops of Tricaine solution.

A borosilicate capillary tube secured at both ends is heated in the middle by a needlepulling machine, pulling one end to craft two microneedles with precise, fine tips.

5 µL of suspended stained cancer cells were loaded into the injection microneedle. The needle was inserted and securely mount into the microinjector's siringe pump. The needle tip was broken off with fine tweezers to obtain a tip opening diameter of 5-10 µm and the injection pressure was adjusted as needed.

The needle tip was pointed at the injection site and gently inserted into the zebrafish larvae's perivitelline space, as seen in Figure 4.1. The melanoma cancer cells suspension was microinjected in zebrafish' perivitelline space making sure that the yolk sac was not ruptured and avoid injecting air bubbles or stretching the perivitelline space as either can be lethal to the embryo.

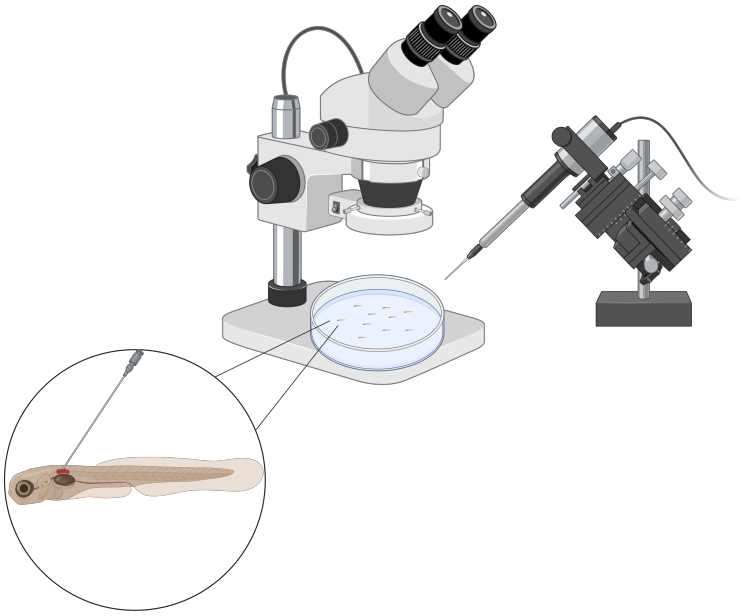

Figure 4.1: Experiments Setup and injection in zebrafish perivitelline space, image made with Biorender.

After the injection, the successful integration of cancer cells was verified through visual confirmation of a slight expansion of the perivitelline area, distinctly populated with red-stained melanoma cancer cells, as seen in Figure 4.2. This observation was also evident under fluorescent light.

Figure 4.2: Successful injections seen through microscope.

Zebrafish that had been successfully injected were placed individually in well plates containing PTU 1X and/or other substances in the swimming medium, depending on the specific experiment requirements.

4.2 Integrating Image Analysis injected Zebrafish Larvae

The zebrafish larvae injection experiments aimed to observe the growth of the primary tumor and metastasis in the tail over a three-day period. Photos were taken

under a microscope on day zero and day three to monitor the development of the primary tumor and detect metastatic cells in the tail, using both standard and fluorescent illumination.

ImageJ software was utilized to analyze these photos, measuring the number of pixels for primary tumors. Metastatic cells were similarly quantified, resulting in average values for each experiment.

The growth percentage for each primary tumor was calculated, and in select experiments, photographs were taken on all three days to ensure the determination of an average growth rate (shown in Table 11.1 and Table 11.2). This additional data collection ensured a more thorough understanding of the dynamic changes in the primary tumor over time, enhancing the precision and reliability of our mathematical model (explained in chapter 8).

The experiment findings showed notable differences in the primary tumor's growth and were contrasted with established data. However, due to its novelty, there is a limited body of academic literature available for comparison.

4.3 Zebrafish Experiments' Results

4.3.1 Melanoma Cancer

The first experiment focused solely on injecting zebrafish with melanoma cancer cells. It was observed that the original tumor injected on day zero showed an average growth of 96.32%. Additionally, an average of 13.3 cancer cells metastasized to the tail by day 3, as shown in the table 4.1.

cancer type	tumor growth	metastasized cancer cells in tail
melanoma	96,32%	13,33

Table 4.1: First experiment of Melanoma Cancer results.

4.3.2 Melanoma Cancer treated with propranolol

The subsequent experiment entailed the utilization of propranolol as a treatment to inhibit the growth of primary tumors and metastasis. Initially, we needed to establish the optimal dosage concentration. Our investigation included concentrations ranging from 1mg/L, 3mg/L, 10mg/L, 30mg/L, to 100mg/L in their swimming solution (PTU 1X). Through this process, we identified two optimal and non-lethal concentrations of which did not have a negative impact on the zebrafish heartbeat were 1mg/L and 3mg/L. These results are consistent with the scholarly publication by Sun et al.[184], suggesting that an ideal concentration of propranolol for zebrafish larvae is around 2.48 mg/L.

Thus, in this experiment, a 1mg/L dosage of propranolol was administered to zebrafish with injected melanoma cancer cells in their swimming fluid. The results showed an average reduction of 13.82% in tumor size and an average metastasis of 20.28 cancer cells in the tail on day 3. With these encouraging findings, we advanced to the next phase of the experiments involving stress factors.

4.3.3 Melanoma Cancer with Stressors

The stressors employed in these studies were epinephrine, dexamethasone and norepinephrine. To conduct the experiments involving these stressors, we conducted additional toxicity tests for each one. Various concentrations of the stressors were introduced into their swimming medium (PTU 1X). The concentration ranges for epinephrine were 10mM, 1mM, 100µM, 10µM, 1µM; for dexamethasone they were 1mM, 250µM, 50µM, 10µM, 2µM; and for norepinephrine they were 1mM, 200µM, 100µM, 50µM.

After evaluation, the optimal concentrations identified that were utilized in the solution zerafish swam in, were: 10µM for epinephrine, 10µM for dexamethasone, and 50µM for norepinephrine.

Epinephrine led to an average tumor growth of 96.36%, with an average of 20.33 cancer cells metastasizing in the tail on day 3. Dexamethasone showed an average tumor enlargement of 71.92%, and there was an average of 31.3 cancer cells that metastasized in the tail on day 3. Norepinephrine resulted in a mean tumor increase of 113.35%, along with an average of 22 cancer cells metastasizing in the tail on day 3.

4.3.4 Melanoma Cancer with Stressors treated with Propranolol

Then, the experiments involving propranolol and stress-inducing factors were carried out. For these experiments, propranolol needed to be added to the melanoma cancer cell medium before the cells were re-suspended in it. To achieve the optimal concentrations of 1mg/L and 3mg/L for propranolol in the cell medium, a concentration at least x100 times greater had to be used due to its injection with the melanoma cancer cells. This adjustment was necessary because only very small quantities of cell liquid are typically injected, usually in the microliter range. As a result, propranolol's ideal concentration in the cell medium was determined to be 100-300µM or equivalent to 1-3 mg/L.

The following experiments were conducted to investigate the potential of propranolol in reducing melanoma cancer in zebrafish larvae, while increasing different stress proteins. When a concentration of 100µM of propranolol was applied in the cell medium, it was observed that epinephrine led to an average increase in tumor size of 73.54%, with an average metastasis of 15.16 cancer cells in the tail on day 3. Exposure to dexamethasone resulted in an average tumor size increase of 50.28%, and an average metastasis of 23.57 cancer cells in the tail on day 3. Finally, when looking at norepinephrine's effects, there was recorded a substantial average increase of 134.98% in tumor size, along with an average metastasis of 14.66 cancer cells in the tail on day 3.

Due to unfortunate outcome of the experiments with 300µM, the observation of the zebrafish was not feasible, resulting in insufficient data for presentation.

4.3.5 Melanoma Cancer with Stressors treated with Propranolol loaded MPEG-*b*-PLLA Diblock copolymers

The last experiment was conducted again, with a modification in which propranolol-MPEG-*b*-PLLA diblock copolymers (nanoparticles or polymeric nanocarriers loaded with the drug) (see Chapter 7.3) were added to the melanoma cancer cell medium instead of propranolol before re-suspending the cells in it. The concentration used matched that of the previously administered propranolol (100µM). Due to the high mortality of zebrafish in the 300µM experiments, we opted not to utilize this concentration for the nanoparticle experiments.

This experiment aimed to explore the potential of propranolol in reducing melanoma cancer in zebrafish larvae while increasing different stress proteins. Propranolol was encapsulated within self-assembling micellar structures formed by MPEG-*b*-PLLA diblock copolymers for delivery. In drug release studies (see Chapter 7.4), it was observed that approximately 82% of the drug diffused passively from the micelles into the aqueous medium within the first 24 hours (see Figure 7.8). Thus, in zebrafish larvae experiments, a faster release of propranolol was anticipated at the first days of incubation, whereas the release rate was constant (a plateau was observed) for the 3rd day of incubation in PTU 1X. This could be beneficial for our study involving zebrafish as the three-day experiment duration aligns with the release rate of propranolol-loaded nanoparticles, facilitating continuous drug exposure during testing.

For epinephrine, there was an average observed increase in tumor size of 122.42%, with an average of 17.5 cancer cells metastasizing to the tail by day 3. In the case of dexamethasone, the tumor showed an average increase of 218.69%, and on average, 14.75 cancer cells were found to have metastasized to the tail by day 3. As for norepinephrine, it led to a mean increase in tumor size of 236.17% and an average of 12.75 cancer cells were observed to have metastasized on day 3 after injection. In comparison, the control group that did not receive stressors but received injections consisting melanoma cancer cells and propranolol nanoparticles had a recorded average tumor growth rate at 201.41% and on average 9.37 cancer cells were found to have metastasized to the tail by day 3.

The results of all experiments are shown in the table 4.2 below.

stressors	concentration	medium	treatment	concentration	medium	tumor growth	metastasized cancer cells in tail
			propranolol	1mg/L	in PTU 1X	-13,82%	20,28
epinephrine	10uM	in PTU 1X				96,36%	20,33
dexamethasone	10uM	in PTU 1X				71,92%	31,3
norepinephrine	50uM	in PTU 1X				113,35%	22
			propranolol	100uM	injection	226,49%	20,28
epinephrine	10uM	in PTU 1X	propranolol	100uM	injection	73,54%	15,16
dexamethasone	10uM	in PTU 1X	propranolol	100uM	injection	50,28%	23,57
norepinephrine	50uM	in PTU 1X	propranolol	100uM	injection	134,98%	14,66
			propranolol nanoparticles	100uM	injection	201,41%	9,37
epinephrine	10uM	in PTU 1X	propranolol nanoparticles	100uM	injection	122,42%	17,5
dexamethasone	10uM	in PTU 1X	propranolol nanoparticles	100uM	injection	218,69%	14,75
norepinephrine	50uM	in PTU 1X	propranolol nanoparticles	100uM	injection	236,17%	12,75

Table 4.2: All experiments results.

4.4 Discussion on in vivo testing on Zebrafish

The extensive series of experiments carried out in this research aimed to clarify the complex dynamics of melanoma cancer advancement in zebrafish larvae. This involved investigating the effects of propranolol, stress-inducing factors, and a novel method involving propranolol-loaded nanoparticles.

The purpose of these experiments was to gather tumor growth data under varying stress conditions for our upcoming mathematical model, explained in the following chapters. Additionally, the experiments aimed to investigate the potential of propranolol in reducing melanoma cancer in zebrafish larvae while increasing expression of different stress proteins. Zebrafish larvae were injected with a 100µM concentration of propranolol using two methods: direct injection of DL-propranolol and encapsulation of DL-propranolol within self-assembling micellar structures formed by mPEG-*b*-PLLA Diblock copolymers. An illustrative representation of our experiments is shown in the Figure 4.3.

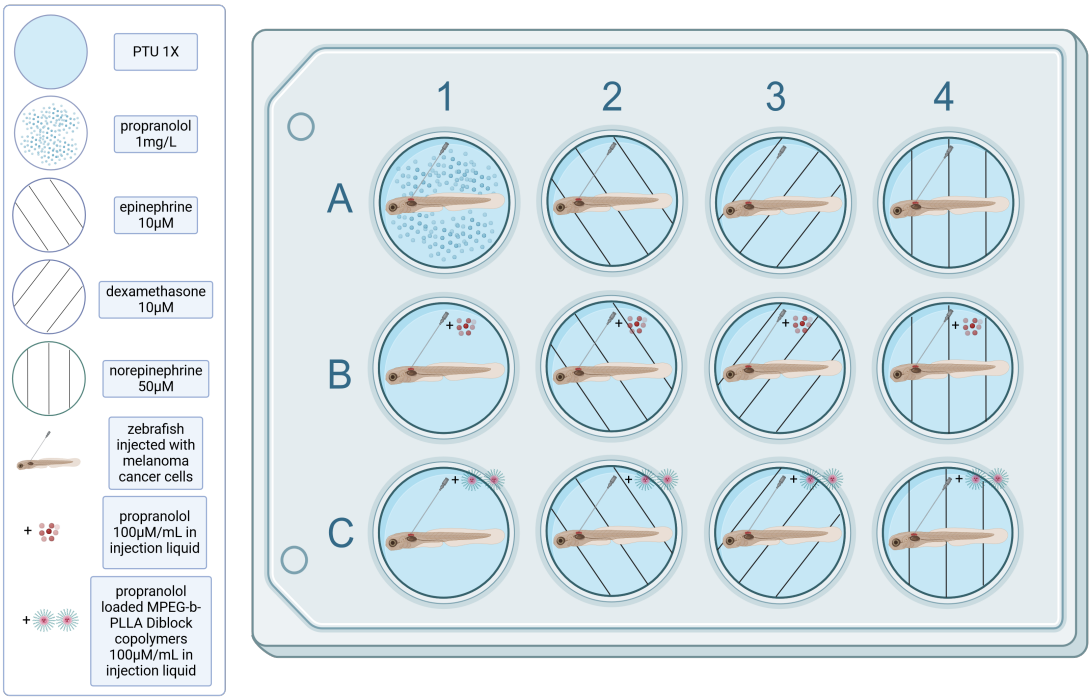

Figure 4.3: Experiments Illustrative Representation, image made with Biorender.

In the first experiment, injecting melanoma cancer cells resulted in an average tumor growth of 96.32% on day three, along with an average metastasis of 13.3 cancer cells to the tail. This served as a baseline for future interventions.

Introducing propranolol at a concentration of 1mg/L in the swimming fluid led to a notable average reduction of 13.82% in tumor size, showing its potential as a therapeutic agent. However, there was an increase in the average metastasis to 20.28 cancer cells in the tail, which requires further consideration.

Introducing stress-inducing substances like epinephrine, norepinephrine, and dexamethasone into the swimming water resulted in different impacts on tumor behavior.

Particularly noteworthy was the substantial average increase in tumor size induced by norepinephrine at 113.35%. Epinephrine and dexamethasone also significantly contributed to tumor growth, with increases of 96.36% and 71.92% respectively, highlighting the potential influence of stress in aggravating cancer development. Dexamethasone, among all stressors, had the highest number of metastasized cells in the fish's tail, averaging 31.3 cells.

The experiments combining propranolol with stress-inducing factors, though limited by the observed high mortality at 300µM concentrations, provided interesting findings. Propranolol exhibited a mitigating effect on tumor growth when coupled with stressors, especially evident in the case of epinephrine and dexamethasone where the average tumor size increase was lower compared to the experiment without propranolol. For epinephrine, the increase reduced from 96.36% to 73.54% (resulting in a reduction of 22.82%), and for dexamethasone, it decreased from 71.92% to 50.28% (resulting in a reduction of 21.64%). This indicates the potential protective role of propranolol in mitigating the adverse effects of stress on cancer progression.

Also, an obvious decrease in metastasized cells in the tail was observed during all instances of stress when propranolol was used in combination with stress-inducing factors, as compared to situations where propranolol was not used. This suggests that there is a potential connection between propranolol and inhibiting the spread of the primary tumor.

The introduction of propranolol-loaded nanoparticles in the last experiment, showcased a novel approach for drug delivery. While presenting challenges, this experiment demonstrated the potential of propranolol within self-assembling micellar structures in reducing tumor growth. Although the groups with stressors and the control group without stressors did not display any notable distinctions from the groups without propranolol nanoparticles, it was clear that metastasized cells were reduced in all cases when propranolol nanoparticles were utilized.

In conclusion, these results highlight the complex relationship between stress responses and cancer progression in zebrafish larvae. Propranolol emerges as a promising candidate in mitigating tumor growth, especially when combined with stress-inducing factors. Furthermore, the nanoparticle approach presents new opportunities for advancing drug delivery techniques. Overall, these findings provide important contributions to the discussion on targeted therapies and stress regulation in cancer research.

Chapter 5

Diblock copolymers for drug delivery

5.1 Polymers and Ring Opening Polymerization

5.1.1 Polymers

According to the International Union of Pure and Applied Chemistry (IUPAC), a polymer is a large molecule composed of repeating structural units, known as monomers [185]. These monomers are covalently bonded together to form a chain-like structure, which can range from a few monomers to millions. Polymers can be natural or synthetic, and they can be found in a wide variety of products, such as plastics, fibers, rubber, and adhesives. Polymers can be synthesized using a variety of methods, such as polymerization, which involves the chemical reaction of monomers to form a polymer chain [186].

5.1.2 Copolymers

A copolymer is a polymer made up of two or more types of monomers. Copolymers can be classified based on the sequence and ratio of the monomers in the polymer chain [187]. There are several types of copolymers, including block copolymers, graft copolymers, and statistical copolymers. Block copolymers have blocks of monomers that are arranged in a specific sequence. The different segments (monomers) of the block copolymer can be arranged in a variety of ways, such as a linear or branched structure, and can self-assemble into specific nanostructures, such as spherical or cylindrical micelles [188], as shown in Figure 5.1.

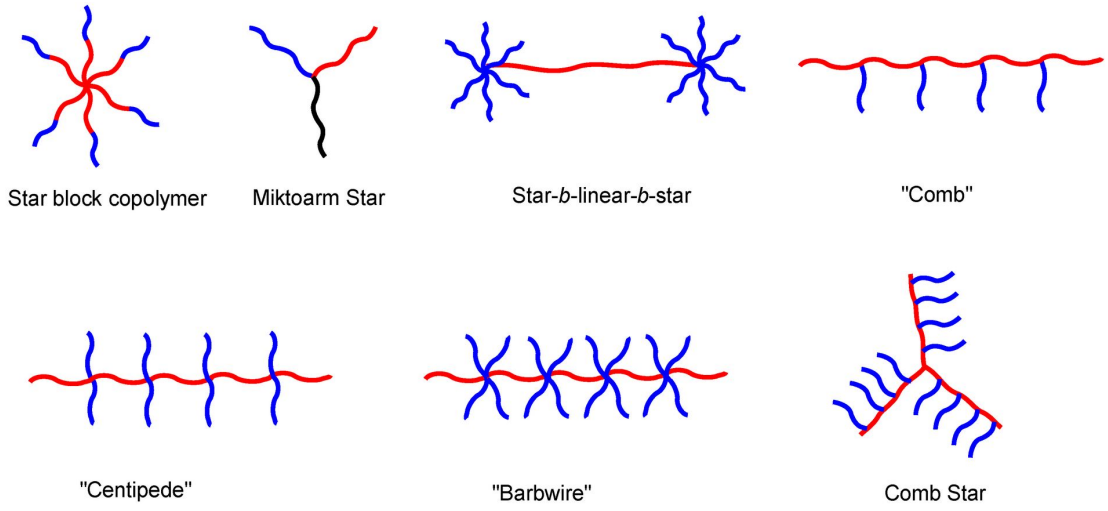

Figure 5.1: Arrangements in block copolymers [189].

Graft copolymers have a main chain of one type of monomer with branches of another type of monomer (Figure 5.2). Statistical copolymers have a random distribution of monomers within the polymer chain [188] [190] [191] [192].

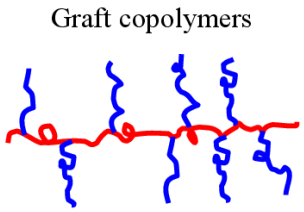

Figure 5.2: Arrangement in graft copolymers [189].

Copolymers can have a wide range of properties, depending on the monomers that make up the polymer and the ratio in which they are combined. They can be synthesized using various polymerization techniques, such as addition polymerization, condensation polymerization, and ring-opening polymerization [187] [193].

5.1.3 Diblock Copolymers

Diblock copolymers are a type of polymer made up of two distinct blocks of repeating chemical units, or monomers, that are chemically bonded together (Figure 5.3). These blocks are referred to as the "A block" and "B block", and they can be made up of different types of monomers. The "A block" and "B block" can have different chemical and physical properties, such as solubility, melting point, and glass transition temperature. This means that the diblock copolymer can exhibit unique properties that depend on the properties of the two blocks and their relative ratio [194].

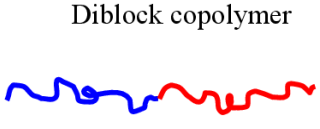

Figure 5.3: Arrangement in diblock copolymers [189].

5.1.4 Ring-opening polymerization

Ring-opening polymerization (ROP) is a type of polymerization process in which a ring-shaped (cyclic) monomer, such as a cyclic ester or amide, is polymerized to form a linear polymer chain, such as acyclic or polymers with fewer cycles [185]. ROP can be carried out using various techniques, including anionic ROP, cationic ROP, and coordinated ROP (Figure 5.4). ROP is often used to synthesize polymers with well-defined structures and molecular weights [195] [196].

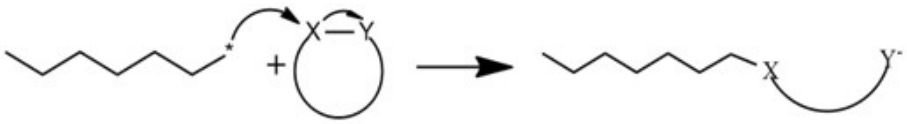

Figure 5.4: General scheme of ROP. The * refers to anionic, cationic or radical chain.

5.2 Drug Delivery

5.2.1 Drug delivery systems

Drug delivery systems (DDS) are methods or devices used to introduce a therapeutic substance into the body and enhance its effectiveness and safety by controlling the timing, rate and location of drug release. [197] These systems can be administered orally, rectally or through the nose, as well as through intravenous or subcutaneous injections. Researchers are constantly seeking new methods of delivery to improve drug efficacy. One aspect of this research is focused on controlling the release rate of drugs to prolong their activity and decrease the frequency of dosing [197]. There has also been a significant amount of research done on targeted drug delivery to specific organs or cells in the body [198] [199]. Nanocarriers such as liposomes, nanoparticles, and micelles have been used to achieve sustained and targeted drug delivery of therapeutic agents [200] [201].

5.2.2 Nanocarriers and their types

Nanocarriers are a type of DDS that are designed to transport drugs or other active agents to specific target sites within the body. These carriers are typically in the nanometer size range, which makes them small enough to be transported through the circulatory system to reach their intended target.

There are several types of nanocarriers (shown in Figure 5.5) that have been developed for drug delivery and other biomedical applications, including [202]:

1. Lipid nanocarriers: Nanoscale drug delivery systems that consist of lipids as the primary component. They are used for encapsulating and transporting therapeutic drugs to target sites within the body.
   (a) Liposomes: Spherical vesicles composed of a phospholipid bilayer that can encapsulate both hydrophilic and hydrophobic compounds [203] [204] [205].

   (b) Solid lipid nanoparticles: Nanoparticles made from solid lipids that can encapsulate hydrophobic drugs and enhance their stability [206] [207] [208].
   (c) Phospholipid micelles: Spherical structures composed of phospholipids, they have a similar structure to cell membranes and are therefore able to mimic the natural environment of cells [209] [210].

2. Polymeric nanocarriers: Particles made from polymers that can encapsulate drugs and target specific cells or tissues [211] [212] [213] [214].
   (a) Polymeric micelles: Nanoscale particles composed of amphiphilic polymers, with a hydrophobic core and a hydrophilic outer shell. They are commonly used as nanocarriers for drug delivery [215] [216] [217].
   (b) Dendrimers: Highly branched, monodisperse nanoparticles with a compact core and numerous peripheral functional groups. They are used in various applications, including drug delivery, imaging, and diagnostics [218] [219] [220].
   (c) Lipid-polymer hybrid nanoparticles: Nanoparticles made by combining lipids and polymers to form a core-shell structure. They can be designed to improve the stability and drug-delivery properties of lipid-based nanoparticles [221] [200] [222].
   (d) Polyelectrolyte complexes: Nanoparticles formed by the self-assembly of oppositely charged polyelectrolytes. They can be used as drug carriers, gene delivery vehicles, and vaccines [223] [224].
   (e) Polymeric vesicles: Spherical, lipid-like structures composed of a bilayer of amphiphilic polymers. They can be used as drug delivery vehicles, as well as in cell membrane mimetic and protein delivery applications [225].

3. Inorganic nanocarriers: Nanocarriers made from inorganic materials, such as metals and metal oxides, that can be used for imaging and therapy [226] [227].
   (a) Gold nanoparticles: Nanoparticles made of gold that have unique physical, chemical, and optical properties, that are used for cancer diagnosis and therapy, as well as for the delivery of drugs, genes, and vaccines. Also, they are used as biosensors, as well as to create new materials with enhanced electrical, optical, and thermal properties [228] [229] [230].
   (b) Magnetic nanoparticles: nanoparticles that exhibit magnetic properties and are typically made of magnetic materials such as iron, cobalt, or nickel. They are used for targeted drug delivery, magnetic resonance imaging (MRI), environmental remediation, energy storage, and catalysis [231] [232] [233].
   (c) Quantum dots: They are tiny semiconductor particles, usually made of materials such as cadmium selenide, that exhibit unique optical and electronic properties. They have unique spectral, optical, and electronic characteristics that are different from those of larger particles and are used in biomedical imaging, displays, solar cells, and lighting [234] [235].

4. Nucleic acid nanoparticles: Nanoparticles made from nucleic acids, such as DNA and RNA, that can be used for gene therapy [236].

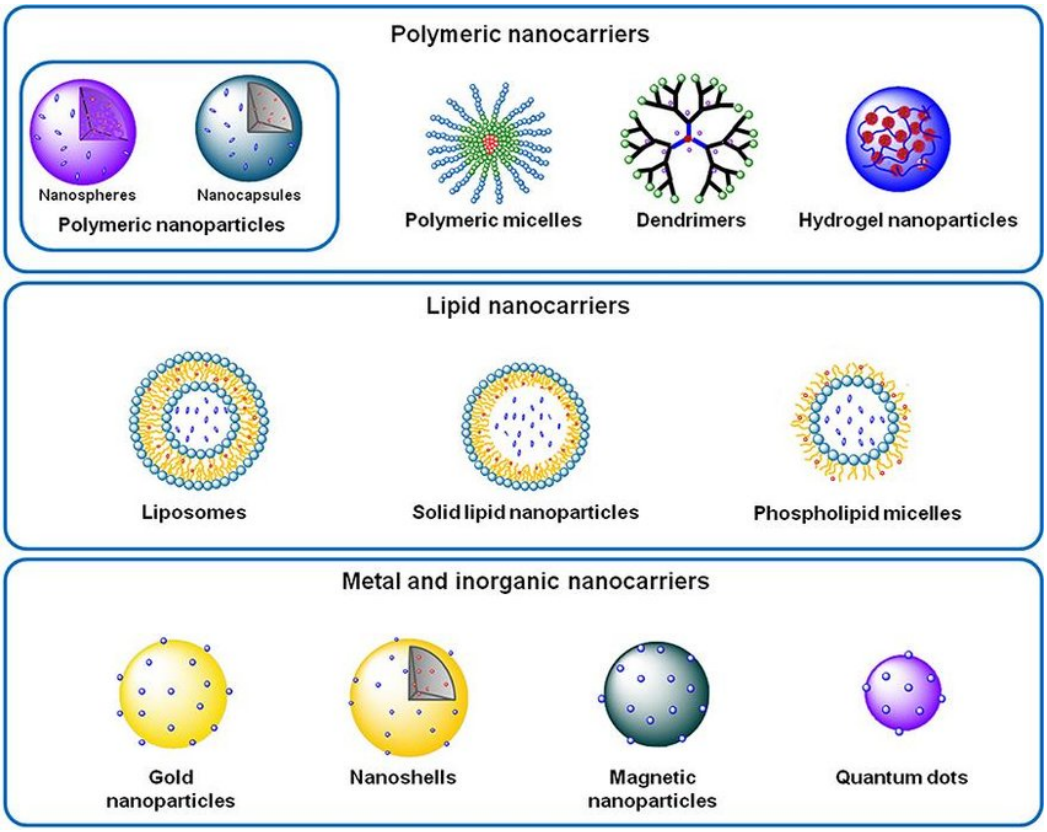

Figure 5.5: Different types of nanocarriers [202].

5.2.3 Polymeric Nanoparticles

Polymeric nanoparticles (PNPs) are a type of nanocarriers. They are spherical particles that are made from polymers and have diameters typically in the range of 20-200 nm. They can be used to encapsulate drugs and other therapeutic agents, and they can be designed to release the drug in a controlled manner [212].

In drug delivery, PNPs are used to deliver drugs to specific cells or tissues in the body [237] [213]. The polymeric matrix of the nanoparticles can be engineered to control the release rate of the drug, allowing for sustained release over an extended period of time. Additionally, PNPs can be functionalized with targeting molecules, such as antibodies or peptides, to selectively deliver drugs to specific cells or tissues [238] [239].

In imaging and diagnostics, PNPs can be used as contrast agents for imaging modalities such as magnetic resonance imaging (MRI), computed tomography (CT), and ultrasound [240] [241] [242]. These nanoparticles can be functionalized with imaging moieties, such as magnetic or fluorescent molecules, to enhance the visibility of diseased cells or tissues [243] [244].

PNPs have several advantages over other drug delivery systems. They protect drugs from degradation, help to target drugs to specific cells or tissues, and can provide sustained release of drugs over an extended period of time. Additionally, PNPs are biocompatible and biodegradable, which reduces the risk of toxicity [245].

They are generally considered to be solid particles and are usually composed of

hydrophobic polymers [246]. These particles can be formed through a variety of methods, including self-assembly, emulsion polymerization, and solvent evaporation.

5.2.4 Polymeric Micelles

Polymeric micelles are spherical structures composed of a hydrophobic core and a hydrophilic shell that are formed by self-assembling amphiphilic polymers in aqueous solutions [215]. They typically range in size from 10 to 200 nanometers (nm). The size of a polymeric micelle can affect its ability to target specific tissues and to evade the body's immune system, among other things. The hydrophobic core of the micelle is formed by the hydrophobic segments of the polymer and serves as a container for hydrophobic drugs, while the hydrophilic shell, composed of hydrophilic segments, surrounds the core and provide stability to the micelle in the aqueous environment (Figure 5.6) [247].

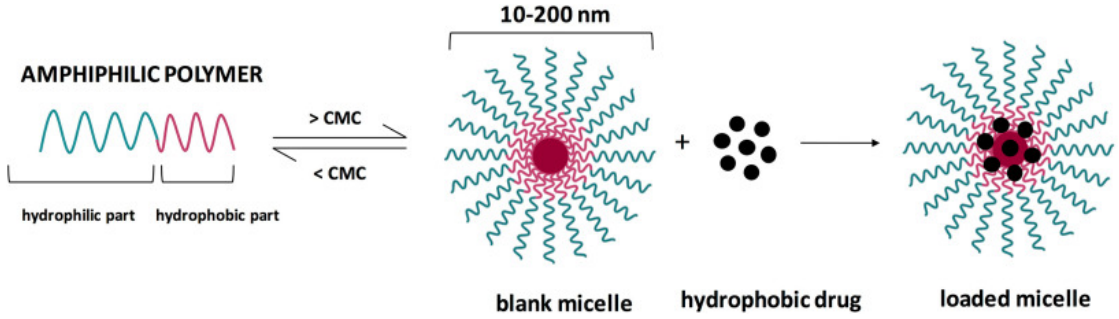

Figure 5.6: Structure of polymeric micelles: The hydrophobic segments of the copolymer tend to aggregate together in the core of the micelle, while the hydrophilic segments form the outer shell. These structures are considered as liquid-like droplets and have a core-shell structure, and have a hydrophobic core and hydrophilic shell [248].

Micelles are formed by the self-assembly of amphiphilic polymers, which are polymers that have both hydrophobic and hydrophilic segments. When these polymers are dissolved in water, the hydrophobic segments tend to aggregate together, forming a core, while the hydrophilic segments extend outwards to interact with water, forming a shell [249].

Polymeric micelles are used in drug delivery as a way to deliver hydrophobic drugs, such as anticancer drugs, to the body [215] [216]. The hydrophobic drug molecules are encapsulated within the hydrophobic core of the micelle, which protects them from degradation and enables their targeted delivery to specific cells or tissues [217]. The hydrophilic shell of the micelle also allows them to circulate in the bloodstream for a longer period of time, which is known as the "stealth effect" [250] and can help the micelle to evade the reticuloendothelial system (RES) and avoid being rapidly cleared from the body [251] [252].

5.2.5 Mechanisms of drug release from Polymeric Micelles

Drug release from a polymeric micelle refers to the process of transporting a drug molecule from the interior of the micelle to the exterior environment [253]. Thus,

polymer degradation, passive diffusion and a combination of the two are the primary mechanisms of drug release from polymeric micelles [196].

More specifically:

1. Polymer degradation: One mechanism of drug release from polymeric micelles is through the degradation of the polymer. The polymer is designed to degrade over time, and as it does so, the encapsulated drug molecules are released. This mechanism is typically used when a slow and sustained release of the drug is desired.
2. Passive diffusion: Another mechanism of drug release is through passive diffusion of the encapsulated drug molecules. The drug molecules are able to diffuse out of the micelle through the polymer membrane due to a concentration gradient. The rate of release is dependent on the solubility of the drug, the size of the micelle, and the thickness of the polymer membrane.
3. Combination of the two: A combination of both polymer degradation and passive diffusion can be used to achieve a controlled release of the drug. The polymer degradation can be used to achieve a sustained release over a longer period of time, while the passive diffusion can be used to achieve a faster initial release.

The drug release process can be divided into two phases: In phase 1, the rapid release of drug molecules into the surrounding environment due to their absorption onto the surface of the nanocarriers. This is referred to as the burst release phase. In phase 2 the rate of release (controlled release phase) is determined by the characteristics of the polymeric system. If the rate of drug diffusion is greater than the rate of polymer degradation, diffusion is the primary process, otherwise, drug release is driven by polymer degradation [254].

5.2.6 Factors affecting Drug Release

There are several factors that can affect the rate and extent of drug release from polymeric micelles [255] [256] [257] [258]. Some of the main factors include:

1. The properties of the polymeric micelle itself, such as the chemical composition, molecular weight, and architecture.
2. The properties of the drug that is being encapsulated, such as its solubility, stability, and pka value.
3. The size and shape of the polymeric micelle, as well as the size and distribution of the drug within the micelle.
4. The pH and temperature of the surrounding environment, as these can affect the stability and solubility of the drug and the polymeric micelle.
5. The presence of other molecules in the surrounding environment, such as enzymes or proteins, which can affect the stability and release of the drug from the micelle.
6. The route of administration and the targeted site of action, as well as the pharmacokinetic and pharmacodynamic profiles of the drug and the polymeric micelle.
7. The surface properties and characteristics of the polymeric micelle, such as the charge, hydrophilicity, and hydrophobicity, which can affect the interactions with the surrounding environment and the release of the drug.

Chapter 6

MPEG-*b*-PLLA Diblock copolymers' Materials and Protocols

6.1 MPEG-*b*-PLLA Diblock copolymers Materials

6.1.1 Poly(ethylene-glycol) methyl ether (mPEG)

Poly(ethylene-glycol) methyl ether also known as Monomethoxy poly(ethylene oxide) or PEG-CH_3 (mPEG), is a type of Polyethylene glycol (PEG) that has a methoxy group at one end of the molecule. PEG is a synthetic, water-soluble polymer, it is a versatile and generally considered safe for human use and widely used substance in the medical, chemical, and biological fields [259]. In the field of chemistry, PEG is used as a polymer solvent, surfactant and also used in the formulation of drug delivery systems, as a coating for nanoparticles to improve their stability and circulation time in the body [196] [260]. PEG conjugates of drugs, proteins, and other therapeutic agents have improved pharmacokinetics and reduced immunogenicity [261]. In medicine, PEG is commonly used as a laxative to treat constipation and as a lubricant for endoscopic procedures [262]. In the pharmaceutical industry, PEG is used as a solubilizer, stabilizer, and enhancer of drug bioavailability [263]. In the life sciences, PEG is used as a protein purification and stabilization agent, as well as a research tool to study protein-protein interactions and protein-nucleic acid interactions [264]. The broad range of applications for PEG, combined with its low toxicity, biocompatibility, and ability to be easily modified, make it an essential tool in many areas of scientific research and clinical practice. Poly(ethylene-glycol) methyl ether (mPEG)'s chemical structure is shown in Figure 6.1.

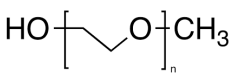

Figure 6.1: Poly(ethylene-glycol) methyl ether (mPEG)'s chemical structure.

mPEG with molecular weight of 5000 gr/mol, used in this project, was purchased from Polysciences Inc.

6.1.2 L-lactide and Poly L-lactide (PLLA)

L-lactide is a lactide stereoisomer, which is a monomer that can be used to synthesize a polymer called Poly(L-lactide). L-lactide is a cyclic ester and is one of the

two stereoisomers of lactide, the other being D-lactide. The two isomers differ in the orientation of their chiral centers. L-lactide, which is derived from lactic acid, a substance found in mammalian metabolism [265]. L-lactide is used as a building block in the synthesis of various biodegradable polymers, particularly in medical applications such as drug delivery and bioresorbable sutures [266] [267]. L-lactide and D-lactide isomers' chemical structure is shown in Figure 6.2.

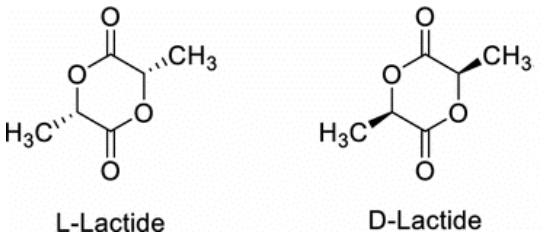

Figure 6.2: Chemical structure of L-lactide and D-lactide isomers [268].

Poly(L-lactide) (PLLA) is a biodegradable and biocompatible polymer that is commonly used in the field of biomedical applications. It is a white, crystalline, and odorless solid. PLLA is soluble in a number of organic solvents, including chloroform, acetone, and methylene chloride [265]. The polymer is thermally stable and decomposes at a relatively high temperature of around 250°C. Its glass transition temperature ranges between 50-70°C, making it a relatively stiff material [269]. PLLA is hydrophobic and has low water solubility, making it suitable for use in hydrophobic environments such as the body [270]. It is also non-toxic and does not induce an immune response, making it suitable for use in medical applications, thus it is used for the manufacture of sutures, implants, and drug delivery systems [271]. In chemical applications, it is used as a component in the production of composites, fibers, and films [272]. In biological applications, PLLA is used as a material for scaffolds in tissue engineering, as well as a material for the encapsulation of cells, enzymes, and drugs [273]. Additionally, it is also used as a substrate for the cultivation of cells and tissues, as well as for the preparation of controlled-release systems for drugs and biologics [274] [275] [267]. Poly(L-lactide) (PLLA)'s chemical structure is shown in Figure 6.3.

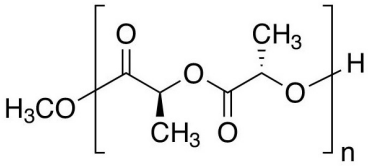

Figure 6.3: Poly(L-lactide) (PLLA)'s chemical structure.

L-lactide used in this project was obtained from Sigma-Aldrich.

6.1.3 4-N,N-Dimethylaminopyridine (DMAP)

4-N,N-Dimethylaminopyridine ($(CH_3)2NC_5H_4N$) (DMAP) is a tertiary amine used as a catalyst in organic chemistry. It is a commonly used catalyst for the condensation of carbonyl compounds with amines to form amides. DMAP also acts as a Lewis

base catalyst in reactions such as Michael additions and alkylations. Additionally, DMAP can be used as a scavenger for acidic impurities in organic synthesis and as a component in the synthesis of other organic compounds [276]. (DMAP)'s chemical structure is shown in Figure 6.4.

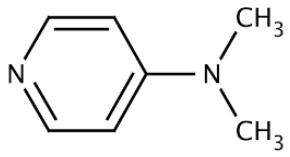

Figure 6.4: 4-N,N-Dimethylaminopyridine (DMAP)'s chemical structure.

DMAP as the catalyst used in this project was obtained from Sigma-Aldrich.

6.1.4 Poly(ethylene-glycol) methyl ether (mPEG)-b-poly(L-lactide) mPEG-*b*-PLLA diblock copolymer

In this project, Poly(ethylene-glycol) methyl ether (mPEG)-*b*-poly(L-lactide) (mPEG-*b*-PLLA) diblock copolymer was used as the polymer to product blank and drug loaded micelles. In the production of micelles, hydrophobic PLLA and hydrophilic mPEG segments are commonly used due to their biodegradable and non-toxic properties. PEG segments also offer the added benefit of preventing non-specific protein binding, known as the "stealth effect". This has led to a significant increase in the study of PLLA/PEG block copolymers as drug delivery systems in recent years [277]. These amphiphilic block copolymers can be synthesized chemically or enzymatically, and the use of PLLA/PEG di- or triblock copolymers to create polymeric micelles with a core-shell structure in aqueous environments was first recognized in the early 1990s [278]. Since then, these types of micelles have been used to deliver a variety of hydrophobic drugs, with the hydrophobic PLLA cores providing high loading efficiency and the brush-like PEG shells allowing for prolonged circulation in the body. The loading efficiency and release rate can be controlled by the ratio of hydrophobic to hydrophilic segments in the micelle [279] [277] [196] [267]. mPEG-*b*-PLLA copolymer's chemical structure is shown in Figure 6.5.

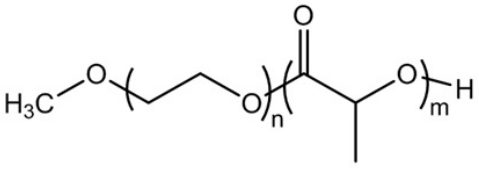

Figure 6.5: mPEG-*b*-PLLA copolymer's chemical structure.

6.1.5 DL-Propranolol and DL-Propranolol Hydrochloride 99%

DL-propranolol is sometimes used to distinguish between the two enantiomers (optical isomers) of propranolol, which are designated as the S- and R-enantiomers. The "D" and "L" prefixes represent the dextrorotatory (right-handed) and levorotatory (left-handed) forms of the compound. DL-propranolol is a racemic mixture of two

enantiomers: S-propranolol and R-propranolol. DL-Propranolol's chemical structure is shown in Figure 6.6.

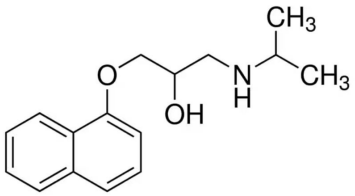

Figure 6.6: DL-Propranolol's chemical structure.

DL-Propranolol Hydrochloride 99% is the hydrochloride salt form of DL-Propranolol, which means that it contains the DL-Propranolol molecule combined with a chloride ion. In comparison, DL-Propranolol refers specifically to the free base form of the drug, without any additional ions or groups attached. The difference between the two forms is primarily in their solubility and stability, with DL-Propranolol Hydrochloride 99% being more soluble in water and having a longer shelf life than the free base form of DL-Propranolol. DL-Propranolol Hydrochloride's 99% chemical structure is shown in Figure 6.7 and ^{1}H NMR spectra in Figure 6.8.

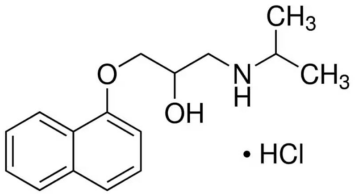

Figure 6.7: DL-Propranolol Hydrochloride's 99% chemical structure.

DL-Propranolol Hydrochloride 99% from Thermo Scientific (CAT: 207320050) was gifted from the Department of Health, Medicine and Caring Sciences (HMV), Linkoping University (LiU), Sweden.

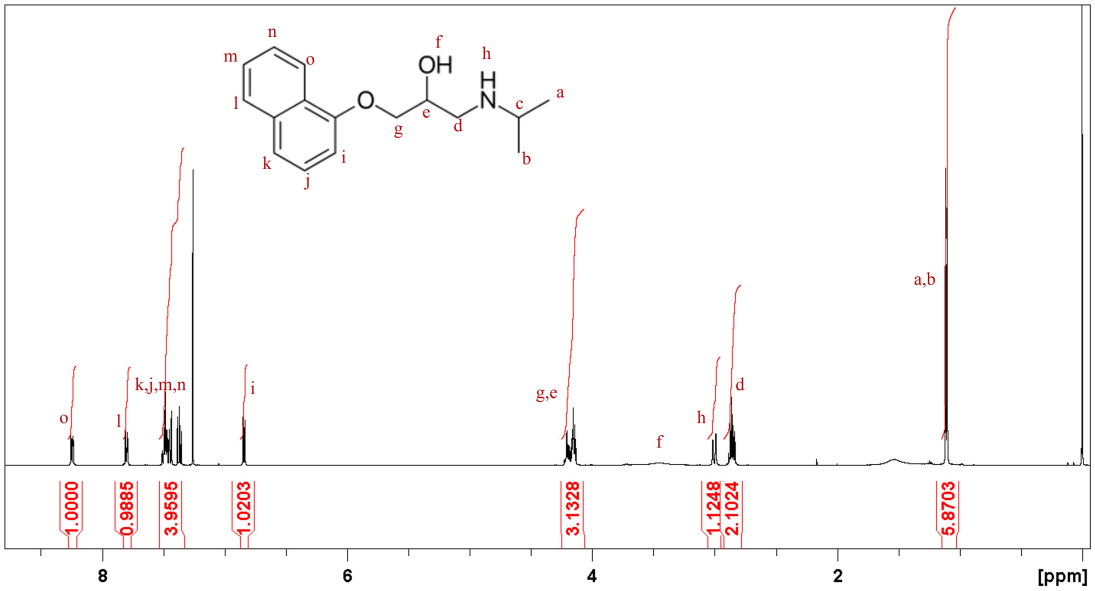

Figure 6.8: ^{1}H NMR spectra of DL-Propranolol.

6.1.6 Other Materials used in this project

Tetrahydrofuran (THF) (HPLC grade ≥ 99.9%) and petroleum ether were purchased from Scharlau S. L. Dichloromethane (≥ 99.9%) was purchased from Sigma-Aldrich. All experiments were conducted using Milli-Q water from a Millipore apparatus with a resistivity of 18.2 MΩ.cm at 298 K.

6.2 MPEG-*b*-PLLA Diblock copolymers' Protocols

6.2.1 Synthesis of poly(ethylene-glycol) methyl ether-b-poly(L-lactide) mPEG-*b*-PLLA diblock copolymers

6.2.1.1 Recrystallization

Recrystallization of lactide is necessary to purify and improve its quality before use. Lactide can contain impurities from the manufacturing process, such as catalysts, byproducts, and oligomers. Recrystallization can remove these impurities and provide a more homogeneous and pure material for use in polymer synthesis. The process typically involves dissolving the lactide in a solvent and slowly cooling the solution to encourage the formation of high-quality crystals, which are then separated and dried. Recrystallization can also improve the solubility, melting point, and thermal stability of the lactide, making it more suitable for use in various applications [280] [281].

In order to recrystallize lactide, dry ethyl acetate was made by placing calcium hydrate and ethyl acetate in a vial for 24 hours under stirring. Afterwards, 10-12gr of dry ethyl acetate was used or every 5g of lactide, and the solid solution was heated at 60°C until the crystals dissolve. Then, the supernatant was disposed and the product was left under vacuum to dry.

6.2.1.2 Synthesis of mPEG-*b*-PLLA copolymer with Ring-opening polymerization

The mPEG-*b*-PLLA copolymer was synthesized by performing a ring-opening polymerization of L-lactide, with mPEG serving as the initiator and DMAP acting as the catalyst. Freeze-dried mPEG (1gr, 0,197 mmol), recrystallized L-lactide (1gr, 13,8 mmol) were degassing in vacuum baseline for 24 hours. Then, the catalyst DMAP (24gr, 1,9828 μmol) was added into the reaction vessel. Right after, the reaction was purched with N_2 for 30 min and then it was placed in an oil bath at 101°C for 24 hours under stirring. Afterwards, the final product of the synthesis was dissolved in dichloromethane and was precipitated in petroleum ether. The supernatant was disposed and the product was left under vacuum to dry.

6.2.1.3 Preparation of the mPEG-*b*-PLLA micelles (blank micelles)

The preparation of the micelles was carried out using the non-selective-selective solvent dissolution method. To begin, 100 mg of the polymer (mPEG-*b*-PLLA diblock copolymer) was dissolved in 10 ml of THF (Tetrahydrofuran). Then, 45 ml of milli-Q water (pH 7.4) was gradually added to the solution using a syringe pump at a

rate of 0.05 ml/min. Afterwards, the organic solvent (THF) was removed under vacuum using a rotary evaporator. Finally, the solution was filtered through a hydrophilic Chromapure PVDF/L filter with a pore size of 0.45 µm and was stored in a refrigerator until it was used. The size of the nanocarriers was analyzed using dynamic light scattering (DLS), and their shape was verified using field emission scanning electron microscopy (FESEM).

6.2.1.4 Preparation of DL-Propranolol Hydrochloride 99% loaded mPEG-*b*-PLLA micelles (drug loaded micelles)

DL-Propranolol Hydrochloride 99% is considered hydrophilic and has been expected to be located outside the micelles [282], thus it was neutralized in order to be encapsulated by mPEG-*b*-PLLA micelles. DL-Propranolol Hydrochloride 99% can be neutralized by adding a base to the solution. A commonly used base for this purpose is sodium hydroxide (NaOH). The base reacts with the hydrochloric acid (HCl) in the drug and forms a salt, sodium chloride (NaCl). The drug becomes insoluble in water and precipitates out, effectively neutralizing it. Therefore, to prepare it for encapsulation, it was dissolved in water and its acid (HCl) was neutralized by adding a base (0.1M NaOH). This reaction formed a salt (NaCl), causing the drug to become insoluble and precipitate out of H_2O solution. Thus, the encapsulation drug was DL-Propranolol.

The encapsulation of DL-Propranolol was performed using the non-selective-selective solvent dissolution method. To begin, 100 mg of the polymer (PEG-*b*-PLLA diblock copolymer) and 10mg of DL-Propranolol was dissolved in 10 ml of THF (Tetrahydrofuran). The rest of the procedure involved following the same steps as previously described for the preparation of polymeric micelles, which included adding milli-Q water (pH 7.4), evaporating the organic solvent under vacuum, filtering the solution through a hydrophilic Chromapure PVDF/L filter, and storing the nanocarriers in the refrigerator. The size and shape of the nanocarriers were analyzed using Dynamic Light Scattering (DLS), and their morphology and size was confirmed using field emission scanning electron microscopy (FESEM) and Dynamic Light Scattering (DLS), respectively.

6.2.1.5 Release studies methodology of DL-Propranolol

To determine the drug release profile of the polymeric micelles, a dialysis experiment was performed. Drug release dialysis is a technique used to study the release of drugs from a drug delivery system. It is based on the principle of dialysis, which is a process that uses a semipermeable membrane to separate molecules based on their size and charge. In drug release dialysis, a sample of the drug delivery system is placed in a dialysis bag, which is made of a semipermeable membrane that allows the drug molecules to diffuse out of the bag while preventing the larger molecules of the drug delivery system from diffusing out. The dialysis bag is then placed in a release medium, such as buffer or serum, and the drug molecules that diffuse out of the bag are collected and analyzed to determine the rate and extent of drug release [283] [284].

To achieve that, 5 ml of the Propranolol loaded mPEG-*b*-PLLA micellar solution

was placed into a dialysis membrane with a molecular weight cut-off of 3,500. This was then put in a vial containing 20 ml of milli-Q water at pH 7.4. The vial was kept at 30°C, which simulated the body temperature of zebrafish. (In future experiments, zebrafish will be injected with a Propranolol Hydrochloride 99% loaded mPEG-*b*-PLLA micellar solution.) At set time intervals, the water in the vial was replaced with fresh water and the samples were collected. These samples were then evaporated under vacuum, dissolved in 3 ml of THF, and analyzed for Propranolol Hydrochloride 99% content using (UV)-visible spectroscopy. The time intervals were of 30 minutes, 1 hour, 2 hours, 3 hours, 4 hours, 24 hours and 48 hours.

6.2.2 Characterization methods

6.2.2.1 Gel Permeation Chromatography (GPC)

Gel permeation chromatography (GPC) is a technique used to separate and analyze polymers and proteins based on their size and molecular weight [285]. It allows determination of molecular characteristics such as average molecular weight and molecular weight distribution. The instrument consists of a pump, one or more separating columns filled with porous beads of varying pore sizes, called a stationary phase, and a detector such as UV or IR. A diluted polymer solution is injected into the flowing solvent and as it passes through the columns, larger polymer particles tend to interact more with the stationary phase, and they therefore spend more time in the column, while smaller molecules pass through the column more quickly. As the polymer solution passes through the column, it is separated into fractions based on the size and molecular weight of the polymer molecules. The fractions are collected as the solution elutes from the column, and they can be analyzed to determine the molecular weight distribution of the polymer. The separation is based on the hydrodynamic volume (Vh) of the molecules in solution, and the separated solution is analyzed with a detector after proper calibration with standards of narrow molar mass distribution [286].

In this project, Gel permeation chromatography (GPC) was employed to determine the molecular weight and PDI (Polydispersity Index) of the polymers. The instrument used was equipped with a Waters-515 isocratic pump, two columns (Mixed-D and Mixed-E from Polymer Labs), a Waters 2745 Dual Absorbance detector, and a Waters 410 refractive index detector. The eluent used was THF (HPLC grade) mixed with 2% TEA and the flow was set at 1 ml/min with the column temperature at 25°C. Typically, 20-30 mg of the polymer was dissolved in 1 ml of THF and filtered through a 0.45 µm pore size PTFE filter before being injected into the system. The molecular weight of the polymer was determined using a calibration curve generated from PMMA standards with molecular weights ranging from 625-138600 g/mol.

6.2.2.2 Proton Nuclear Magnetic Resonance (^{1}H NMR) spectroscopy

NMR spectroscopy is a widely used technique for characterizing molecules. It is particularly useful for studying the chemical structure and dynamics of complex molecules, such as proteins and polymers, and for identifying and quantifying the various chemical groups present in a sample. The most commonly used variants of NMR spectroscopy are ^{1}H NMR and ^{13}C NMR. It involves the use of a magnetic

field and radiofrequency (RF) radiation to manipulate the nuclear spins of atoms in a sample, and the resulting interactions between the spins and the RF radiation are used to obtain information about the molecules in the sample. Therefore, in NMR, the sample is typically placed in a strong, uniform magnetic field, and RF radiation is applied to the sample. The RF radiation causes the nuclear spins in the sample to resonantly absorb the energy and flip their spin states. The resulting absorption of RF energy is detected by an RF detector, and the resulting signal provides details about the environment of the nuclei. The field strength of a nucleus, measured in ppm, that comes into resonance is relative to a reference standard, typically the signal of the deuterated solvent used. Electron clouds shield the nuclei from the external magnetic field, causing them to absorb energy at higher ppm, while functional groups neighboring the nuclei "deshield" the nuclei and cause them to absorb energy at lower ppm. Nuclei that are chemically and magnetically equivalent resonate at the same energy and give a single signal or pattern. Protons on adjacent carbons interact and split each other's resonances into multiple peaks, following the n+1 rule with a coupling constant J. Spin-spin coupling is commonly observed between nuclei that are one, two, or three bonds apart. The area under an NMR peak is proportional to the number of nuclei that give rise to that resonance, and by integrating the peaks, the number of protons can be calculated [287] [288] [289].

The polymers were characterized by ^{1}H NMR spectroscopy on an Avance Bruker 300 MHz spectrometer with tetramethylsilane (TMS) as an internal standard and $CDCl_3$ as the solvent.

6.2.2.3 Scanning electron microscopy (SEM) and Field Emission Scanning Electron Microscopy (FESEM)

Scanning electron microscopy (SEM) is a technique for producing high-resolution images of samples by using a tungsten filament to emit electrons that are focused by an electron optical system. The sample is mounted on a stage that can be moved in three dimensions (x, y, and z), normal to the sample plane [290]. SEM operates in a high vacuum, dry environment to produce the high energy electron beam needed for imaging. The imaging system depends on the sample being electrically conductive so that most incoming electrons go to ground. Images are formed by collecting different signals scattered by the interaction of the high energy electron beam with the sample. The two main signals used to create images are backscattered electrons and secondary electrons that are produced within the primary beam-sample interactive volume. Backscattered electron coefficient increases with increasing atomic number, while the secondary electron coefficient is relatively insensitive to atomic number, affecting how samples need to be prepared. To interpret the information obtained from SEM, it is important to understand how the form and structure of two-dimensional images and chemical data relate to the three-dimensional sample from which they were derived [291]. In some cases, a type of SEM can be used, named Field Emission Scanning Electron Microscopy (FESEM), which utilizes a field emission gun to provide focused, high and low energy electron beams, improving spatial resolution, minimizing damage to sensitive samples and enabling work to be carried out at very low potentials (0.02–5 KV). Thus, the biggest difference between a FESEM and a SEM lies in the electron generation system [292].

In this project, the images of the polymers were acquired using a JEOL JSM-7000F Field Emission Scanning Electron Microscope (FESEM). To prepare the sample for imaging, a drop of the material was placed on a glass panel and allowed to dry at room temperature overnight. Before imaging, the sample was sputter-coated with Au (10mm thick).

6.2.2.4 Dynamic Light Scattering (DLS)

Light scattering is a highly effective method for characterizing the size of polymer nanoparticles in solution. When a monochromatic, coherent laser beam is directed at the particles, it is scattered due to the Brownian motion of the particles in the solution, which changes their distance and causes a time-dependent fluctuation in the scattering intensity [293]. By adjusting the observation angle (ϑ) and thus the scattering vector (q), a measurement of the particle size can be obtained. The interference pattern of scattered light, known as the form factor, is unique to the size and shape of the scatterers. Larger particles have slower Brownian motion. It is critical to maintain the temperature during the measurement with accuracy and stability, as the viscosity of the liquid is temperature dependent. The velocity of the Brownian motion is defined by the translational diffusion coefficient (D) [294]. The Stocks-Einstein equation is used to calculate the particles' size based on the translational diffusion coefficient:

$$R_h = \frac{K_B T}{6\eta\pi D}$$

Where, (R_h) is the hydrodynamic radius, (η) is the viscosity of the solvent, (K_B) is the Boltzmann constant and (T) is the temperature.

In this project, the size of micelles was determined using a Malvern Zetasizer Nano ZS device which had a 4 MW He-Ne laser with a wavelength of λ = 632.8 nm. The measurements were taken at a scattering angle of 90 degrees, with three scans collected for each measurement.

6.2.2.5 (UV)-visible spectroscopy

UV-visible spectroscopy, also known as ultraviolet-visible spectroscopy or simply UV-vis spectroscopy, is a type of spectroscopy that measures the absorbance of ultraviolet and visible light by a sample. The technique is based on the principle that a molecule will absorb light at specific wavelengths that correspond to its electronic transitions. By measuring the absorbance of light in the UV and visible regions, information about the chemical structure and composition of a sample can be obtained [295]. To perform UV-visible spectroscopy, a sample is placed in a cuvette and then exposed to light from a UV or visible light source. The light is passed through the sample and the amount of light absorbed by the sample is then measured. This is typically done by comparing the intensity of the light before it passes through the sample to the intensity of the light after it passes through the sample. The absorption spectrum, which shows the relationship between the wavelength of the light and the amount of light absorbed by the sample, can then be generated. This information can be used to identify specific compounds in the sample and determine the concentration of these compounds [296] [297].

UV-visible spectroscopy can be used to measure drug release by determining the concentration of the drug in the release medium over time. This is done by monitoring the absorbance of the drug in the release medium at a specific wavelength using a UV-visible spectrophotometer. The wavelength selected is typically the maximum absorption wavelength of the drug in the solvent used for the release study. By monitoring the absorbance of the drug over time, it is possible to determine the amount of drug that has been released from the polymeric nanocarrier and calculate its release rate. To ensure accurate results, a calibration curve of the drug in the solvent used for the release study should be prepared and used to quantify the drug concentration in the release medium.

In this project, DL-Propranolol release was determined using a Shimadzu UV-2600i mid-range UV spectrophotometer device whose wavelength range can easily be expanded to the near-infrared region of 1400 nm using the optional integrating sphere.

Chapter 7

Results and Discussion on MPEG-*b*-PLLA Diblock copolymers' Experiments

7.1 Synthesis and characterization of mPEG-*b*-PLLA diblock

The synthesis of mPEG-*b*-PLLA diblock copolymers was achieved through the process of ring-opening polymerization. The figure 7.1 illustrates the synthesis of the mPEG-*b*-PLLA diblock copolymer. PEG served as the starting material, or initiator, in the polymerization of the monomer L-lactide. The polymerization reaction starts at the hydroxyl group of mPEG.

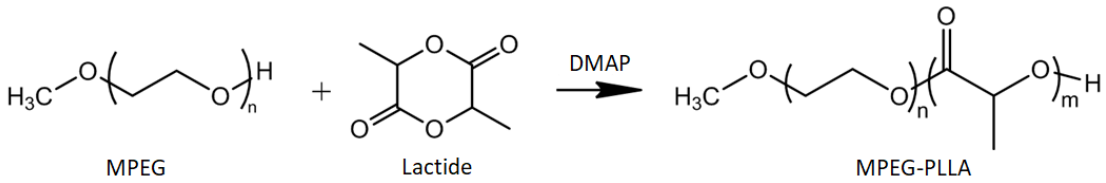

Figure 7.1: Synthesis of mPEG-*b*-PLLA diblock copolymer.

The GPC analysis confirmed the successful synthesis of the mPEG-*b*-PLLA diblock copolymers (Figure 7.2). The molecular weight of the mPEG-*b*-PLLA diblock copolymer was determined to be 26551 g/mol, with a PDI of 1.41. The chromatogram of the diblock copolymer is shown in the Figure 7.2, which shows that the GPC peak of mPEG is appearing at 22.3 min and the copolymer peak is appearing at 21.7 min. The presence of the copolymer peak at lower elution times, implying a higher molecular weight, demonstrates the successful polymerization of L-lactide monomer from the mPEG macroinitiator. The slight overlap between the GPC curves of the block copolymers and the PEG macroinitiators indicates the presence of PLLA homopolymer. As previously mentioned, ring-opening polymerization can be initiated by hydroxyl groups, and the presence of water molecules in the reaction can also initiate the process, leading to the creation of PLLA homopolymers that are challenging to separate from the block copolymer chains.

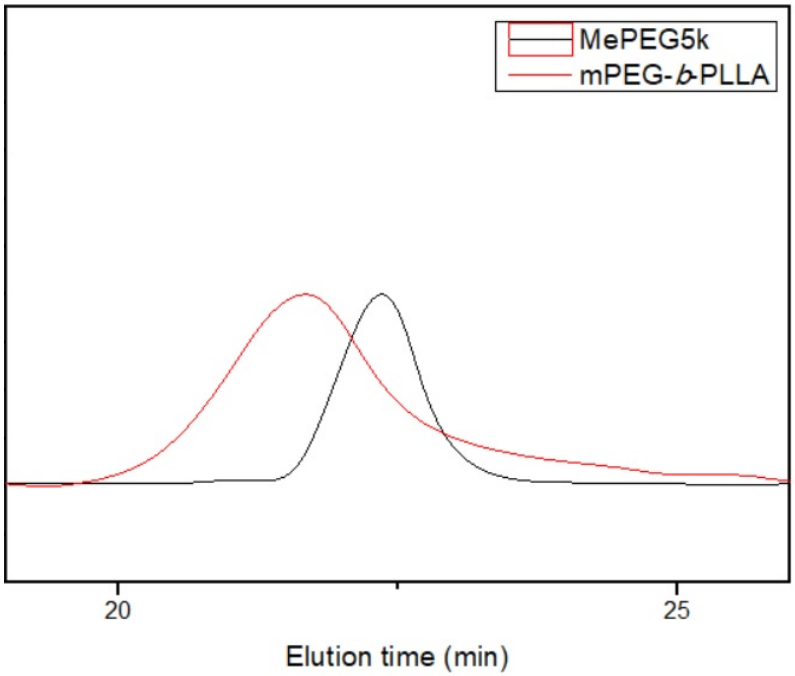

Figure 7.2: GPC of mPEG-*b*-PLLA diblock copolymer.

The composition and chemical structure of the mPEG-*b*-PLLA diblock copolymer were analyzed using ^{1}H NMR spectroscopy. The ^{1}H NMR spectrum of the diblock copolymer is shown in the Figure 7.3. The composition and chemical structure of the diblock copolymer were analyzed using ^{1}H NMR spectroscopy and the ^{1}H NMR spectrum of the diblock is shown in the image below. The peak at 1.6 ppm (a) represents the methyl protons in the repeating unit of the L-lactide monomer, the peak at 5.18 ppm (b) corresponds to the proton in the –CH group of the lactide units, and the peak at 3.66 ppm (c) represents the CH_2 protons of the PEG block. The molecular weight of the diblock copolymer can be calculated by determining the number of hydrogen atoms in the product that are assigned to PLLA. This is done by determining the number of hydrogen atoms in the product assigned to PEG and integrating the corresponding peaks.

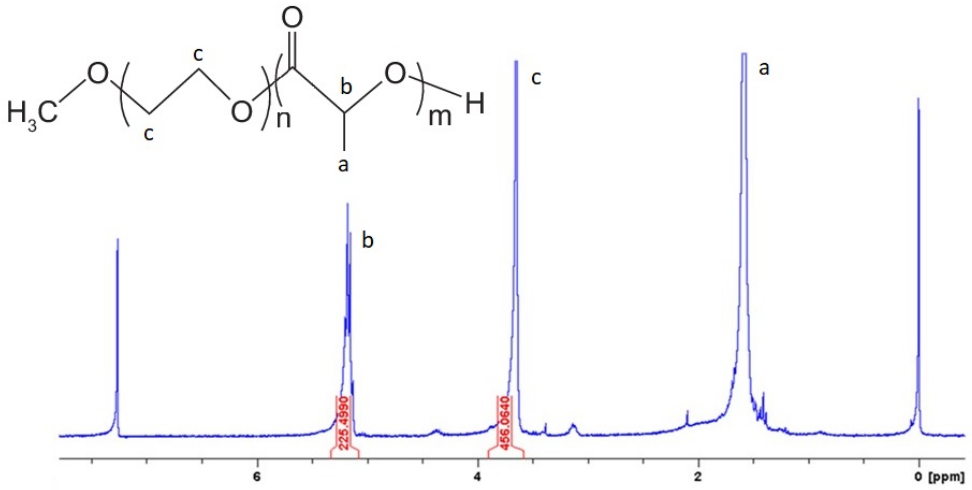

Figure 7.3: ^{1}H NMR spectrum of diblock copolymer.

7.2 Self-assembly of the mPEG-*b*-PLLA diblock copolymer micelles (blank micelles)

The examination of the capability of the amphiphilic copolymers to self-assemble into nanosized structures was conducted. The process involved the use of a non-selective-selective solvent approach to create the nanoparticles. The diblock copolymers were found to have an average micelle size of 13-36 nm, as demonstrated by the DLS measurement with the peak at 18 nm (Figure 7.4). Unfortunately, there were no clear images of mPEG-*b*-PLLA diblock copolymer micelles FESEM to display, but it is a commonly recognized fact that they are in a spherical shape with a micellar structure.

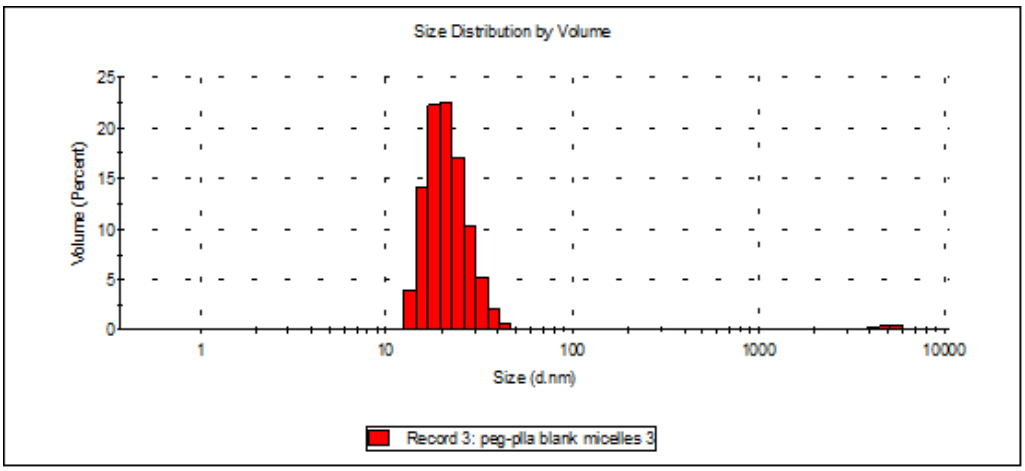

Figure 7.4: DLS measurment of mPEG-*b*-PLLA micelles, peak 18 nm.

7.3 Self-assembly of the DL-Propranolol loaded mPEG-*b*-PLLA micelles (drug loaded micelles)

After propranolol was encapsulated into the nanoparticles and their morphological properties of the nanoparticles were analyzed. As a result of the distribution observed in DLS that fluctuated between 16 nm to 38 nm, with a pick at 22 nm, the drug loaded micelles size were at average 22 nm, as shown in the Figure 7.5.

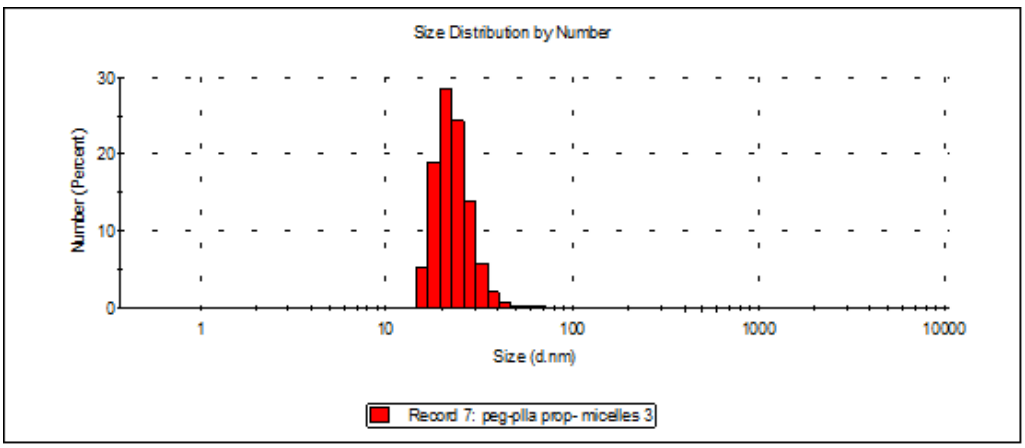

Figure 7.5: DLS measurment of the DL-Propranolol loaded mPEG-*b*-PLLA micelles, peak 22 nm.

The shape and size of the micelles were confirmed through FESEM imaging. The spherical shape of the micelles was evident in the FESEM image (Figure 7.6), and their size was measured to be approximately 92.706 nm. However, it should be noted that the measurement of size obtained through FESEM is smaller than what was observed through DLS due to the dry nature of FESEM and the resultant collapse of the micellar corona.

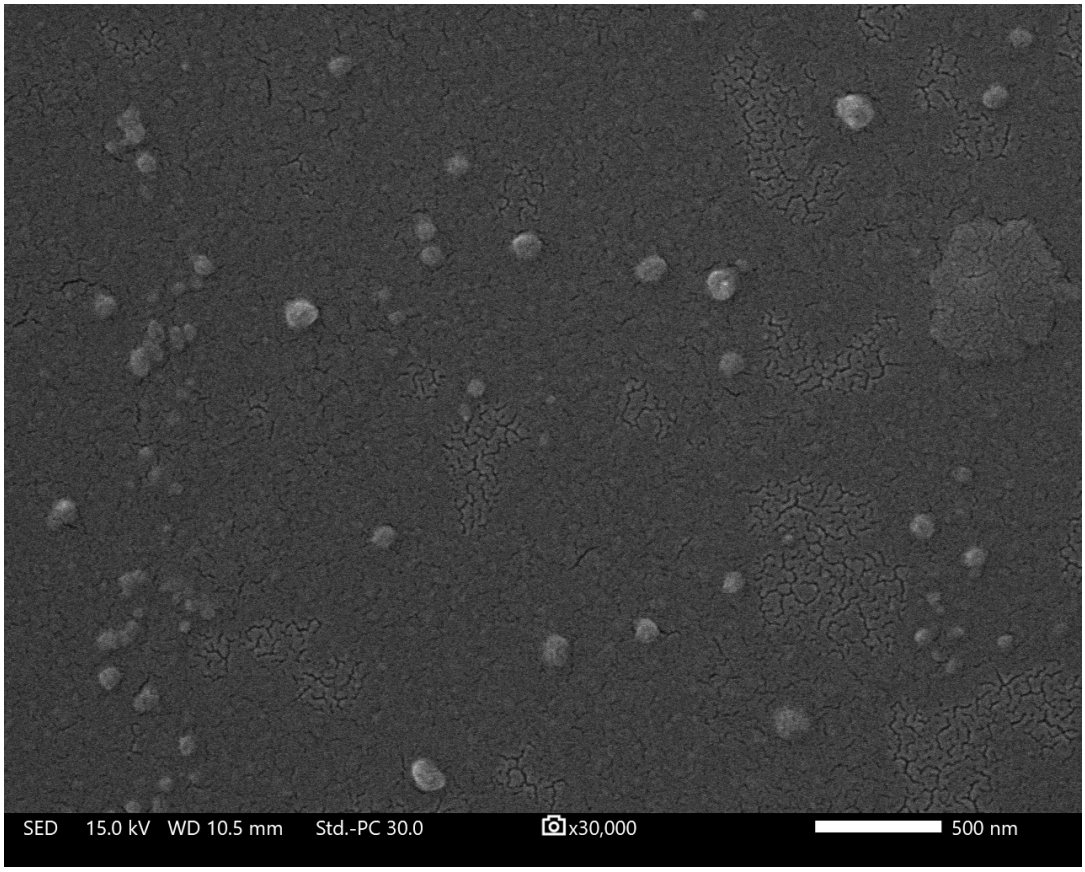

Figure 7.6: FESEM image of the DL-Propranolol loaded mPEG-*b*-PLLA (scale bar, 500nm).

7.4 Release Studies of DL-Propranolol

The previous results demonstrate that the diblock copolymer effectively self-assembled into spherical nanoparticles. Next, the release profile of the drug was examined. In order to do that, calibration (Figure 7.7) was necessary because it allows for accurate and precise measurement of the amount of drug released from the micelles over time. Calibration can be done by using standard reference, ie a known amount of drug and measuring the amount released over time.

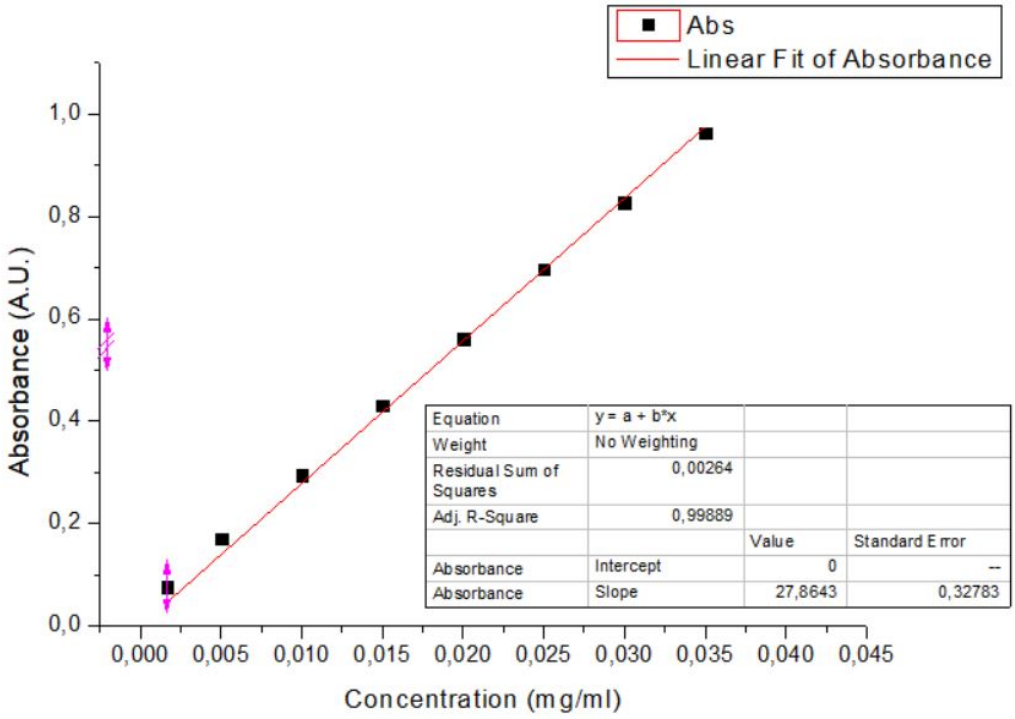

Figure 7.7: DL-Propranolol Callibration.

The release kinetics of DL-Propranolol from the polymeric nanocarriers is presented in the Figure 7.8.

The micelles had a maximum loading of 2.1783 mg. During the first 24 hours, approximately 82% of the drug was released due to passive diffusion of DL-Propranolol from the micelles into the aqueous medium. The system reached a plateau in about 5 days (120 hours).

The objective was to have the drug released from the micelles to the extent of 80% within the first 24 hours, as this will be necessary for our experiments in which the DL-Propranolol loaded mPEG-*b*-PLLA micellar solution will be injected into zebrafish embryos (see Chapter 4.3.5). Zebrafish embryos, after fertilization, typically remain in an embryonic state for about 3-5 days. During this time, they undergo rapid development and morphological changes, including the formation of a head and tail, the development of a neural crest, and the formation of the heart and blood vessels. They can be injected with the drug loaded micellar solution after they have been decoronated. Decoronation of zebrafish embryos typically occurs between 2 and 3 days post fertilization. Thus, there is a time frame of 1 to 3 days to carry out studies about DL-Propranolol loaded mPEG-*b*-PLLA micelles on zebrafish embryos.

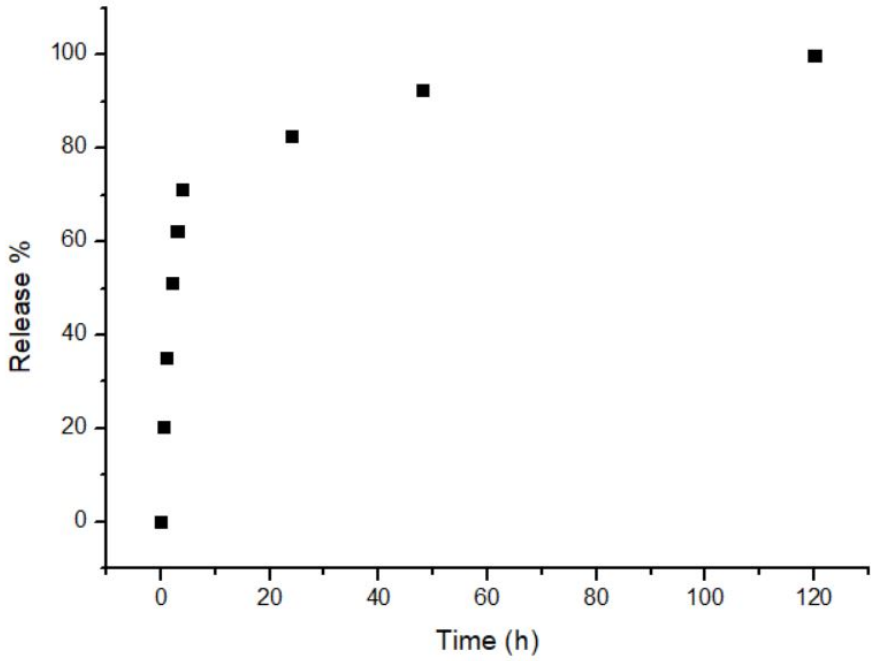

Figure 7.8: DL-Propranolol release from mPEG-*b*-PLLA micelles.

7.5 Discussion on mPEG-*b*-PLLA Diblock copolymers' Experiments

The aim of this part of the thesis, was to create biodegradable diblock copolymers that could self-assemble into micellar structures in order to be used to deliver DL-Propranolol.

mPEG-*b*-PLLA was synthesized and studied using GPC and ^{1}H NMR spectroscopy. The non-selective-selective solvent dissolution method was used to achieve block copolymer self-assembly. DLS was used to determine the size of the nanocarriers, while FESEM determine their morphology. Micelles with a diameter of 18 nm were formed by the diblock copolymer.

The release kinetics of DL-Propranolol from the polymeric nanocarriers was tested by loading the micelles with the drug and placing them in a bath at 30°C, which simulates the body temperature of zebrafish. The results showed that the micelles formed from the diblock copolymer were 22nm and released approximately 2.1783 mg of the drug, reaching a steady state after 48 hours.

See chapter 4.3.5 for the outcomes of zebrafish experiments conducted with stressors using DL-Propranolol loaded mPEG-*b*-PLLA micellar solution.

Chapter 8

Mathematical Modeling

8.1 Biological Phenomena Modelling

The modelling of biological phenomena is a vital aspect of modern scientific research, contributing significantly to our understanding of complex biological systems. This interdisciplinary field harnesses mathematical and computational techniques to simulate, replicate, and analyze biological processes, from the molecular level to entire ecosystems [298]. By creating computational models that mimic biological phenomena, researchers can gain insights into the underlying mechanisms, make predictions [299], and even explore novel avenues for scientific discovery [300] and medical advancements [301], [302].

At its core, biological phenomena modeling involves translating biological observations and principles into mathematical equations and algorithms [298]. For many years, scientists have employed mathematical modeling to get an understanding of the dynamics and mechanisms underlying their experimental observations [303]. In the past few years, the biological community has been exposed to a new word: "systems biology". Even if there is not a precise definition of systems biology, most agree on two aspects of it: the use of mathematical modeling to generate testable predictions and shed light on the behavior of biological systems, and an "-omics" component that involves the thorough gathering of experimental data about a system [304]–[307].

8.2 Modeling Cancer

As recent studies have demonstrated, cancer cells not only take advantage of the microenvironment surrounding them, but they also interact with non-cancerous cells like those on the stroma in order to facilitate tumor spread [308]. Whether conducted in vitro, in vivo, or both, this is a complicated, bidirectional process that is difficult to understand with standard wet-lab studies alone. By providing the ability to track tumor growth, cellular distribution, mobility, and genetic changes that cause aggressive growth and metastasis in real-time, mathematical models and computer simulations can aid in overcoming these restrictions [309], [310].

Although in silico cancer models represent a simplified version of real-word phenomena, we claim that they constitute a sufficient representation of a specific cancer phenomenon that has to be studied. In reality, it is becoming more widely acknowl-

edged that this kind of theoretical approach can be used to: (a) evaluate and improve medical theories; (b) optimize and forecast clinical therapy and outcomes; and (c) simulate experimental processes [311]. It will take time to construct a successful in silico cancer model; the process will be iterative and available experimental data will be utilized for guiding the model's design as well as to confirm and validate the model's output [312].

8.2.1 Continuum Mathematical Models

There exist various approaches to modeling systems, each tailored to capture specific characteristics of the system's behavior. Continuum mathematical models (tumour-scale), often expressed through differential equations, are apt for systems with smoothly changing variables. In the realm of cancer research, a continuum model might describe the intricate interactions between tumors and neurons, capturing the gradual evolution of their dynamics over time disregarding the effects of individual cells in the environment, providing information about the general architecture and distribution of chemicals inside the tumors and neurons. This approach is well-suited to study processes where variables change continuously, mirroring the nuanced nature of biological systems [309], [312]–[316].

8.2.2 Discrete Mathematical Models

On the other hand, discrete mathematical models (cell-scale), commonly represented by a Cellular Automaton (CA), are employed when systems evolve in distinct steps or intervals. CA were first developed by Stanislaw Ulam and John von Neumann in 1946 [317]. A CA consists of cells on a grid. More extensively, a CA defines a spatial matrix where the dynamics are determined by a collection of local interaction rules between adjacent "nodes", which can also determine the communication and transition between grid points. Typically, each grid point is meant to represent a single agent or a group of agents. In cancer research, CA models could simulate the discrete actions of individual cancer cells, providing insights into emergent behaviors and complex interactions. These discrete models employ experimentally derived, computationally coded rules to define the step-wise or discrete interactions between individual cells offering a fine-grained understanding of systems where stepwise changes and individual entities' actions are crucial for comprehensive analysis [309], [312]–[316].

8.2.3 Hybrid Models: Agent-Based Modelling

Hybrid models can combine these approaches, offering a versatile toolkit for tackling diverse aspects of complex systems. As a result, hybrid models, such as ABM, are becoming increasingly popular because they allow for tumor simulations across multiple space-and time-scales. One of the most novel aspects of ABM is its ability to explore "transient, non-equilibrium, non-stationary behavior" of a system and to computationally trace it [318], [319]. ABM are particularly effective in simulating individual entities' behaviors, such as cells', and how they interact within a larger system, offering several benefits over previous approaches of in silico oncology research [309], [312]–[314], [320].

ABM mimic the (inter)actions of autonomous individuals ("agents"), inside complex systems, by representing individual agents and their interactions within a given environment. ABM is the technique of choice to investigate emergent patterns in complex dynamic systems [321]. In complex systems, processes occur simultaneously and the overall behavior of the system is significantly influenced by its individual components [322]. ABM begin with basic principles that lead to the generation of complex patterns: micro behaviors cause macro phenomena. By implementing straightforward rules at the individual level, we observe the emergence of unique characteristics within a particular system. Thus, to enable each agent to independently carry out a set of actions and make decisions, a predetermined set of rules is encoded into it [314].

The ABM outcome is not necessarily related to the initial conditions. The model runs parallel updates of individuals in a discrete manner, and an agent may or may not have memory of their past states [323]. The behaviour of an agent at a given step can also be based on probabilities.

The development of ABM in cancer research has provided a novel way of understanding the complex dynamics and interactions that occur within the tumor microenvironment. Each agent in the model can represent a biological entity, such as a cell, organism, or molecule, and is programmed with specific rules governing its behavior and interactions. These models excel in capturing heterogeneity, stochasticity, and spatial aspects of biological systems, making them ideal for studying phenomena like cell proliferation and death rates, and cell densities [309].

8.3 Agent-Based Modeling Software - Mesa

Mesa is a Python framework created in 2013 and developed by Jackie Kazil and her research team in 2020 [318]. It is designed as an ABM tool for researchers, offering a flexible platform for constructing such models with Python.

Expanding the modeling scope, Mesa Python Framework proves to be a versatile tool for simulating complex interactions in the realm of cancer-stress and cancer-neurogenesis dynamics. In this multifaceted model, Mesa's agent-based approach allows for the representation of not only cancer cells but also stress factors and the process of neurogenesis, i.e. the generation of new neurons (for example in response to stress). Agents can be created to mimic the effects of stress on cancer cells, incorporating rules that simulate how stress affects cell growth, cell death, and metastasis. Additionally, the framework allows for modeling neurogenesis to simulate the neurobiological response to stress. By combining these elements, Mesa enables researchers to study the interconnected dynamics of stress, cancer growth, and neurogenesis as a comprehensive platform for investigating the complex relationship between them.

Chapter 9

Our Models

The design of a mathematical model of a biological system is guided by the necessity to distill the essential behavior of the system and the need to answer specific questions about that system. In our case, our goal was to use the model to design a model describing the interaction between stress and cancer proliferation as well as a model connecting cancer growth with neurogenesis. Thus, this thesis will primarily explore the cancer microenvironment, with a specific focus on two areas:

1. examining how stress impacts cancer growth
2. studying the interaction between neurons and tumors.

There were two separate ABM models developed, each shedding light on different aspects of cancer dynamics.

The first model delves into the relationship between cancer proliferation and stress, drawing insights from experiments conducted on zebrafish. This exploration aims at unravelling the impact of stress on the progression of cancer, utilizing empirical data from zebrafish experiments.

In the second model, the focus shifts to the intricate microenvironment shared by cancer cells and neurons. It explores the chemical interactions within this environment, revealing how cancer proliferation is influenced by neurogenesis.

It is known that cancer is caused by uncontrolled cell division and spread into surrounding tissues. Cells can experience uncontrolled growth if there are mutations to DNA, and therefore, alterations to the genes involved in cell division. A single mutated cell can give rise to a malignant tumor, which consists of cells that divide excessively and invade other tissues. Thus, in both our models, we focus on the mutated malignant cells and begin our simulation from the time when the first malignant cell appears. We are then going to consider two different settings: one within an organism, another in a laboratory setting, where cancer cells have been injected.

9.1 First Model - Cancer Proliferation and Stress

Our first ABM investigates the correlation between stress and cancer proliferation. In this model, we aim to simulate two experiments:

(a) On day zero, zebrafish embryos are injected with melanoma cancer cells and then placed in their regular swimming medium, PTU 1X. The main tumor

growth is measured daily to assess the rate of cancer cell proliferation over a period of three days.

(b) On day zero, zebrafish embryos are injected with melanoma cancer cells and then exposed to swimming medium PTU 1X containing norepinephrine as a stressor. Daily measurements of main tumor growth are taken over a three-day period to evaluate the rate of cancer cell proliferation under these conditions.

Our study focuses on the cancer cells environment and their response to stress. More specifically, from our in vivo experiments on zebrafish larvae, we examined the data obtained from zebrafish that were only injected with melanoma cancer cells and compared it to the data from zebrafish that were injected with melanoma cells and also exposed to molecular stressors, such as epinephrine, norepinephrine and dexamethasone, in their swimming medium. The findings revealed that stress leads to an increase in the size of the primary tumor proliferation. As norepinephrine is identified as the main sympathetic (SyNS) neurotransmitter linked to tumors, we specifically selected experiments involving norepinephrine as the stress inducer.

A typical assumption for simplifying the development of an ABM, is that cellular proliferation requires enough room to grow or divide into, and sufficient nutrients available to maintain cell viability. In this model, each cancer cell is represented as an agent and it is placed on a grid that simulates the microenvironment. As previously mentioned, in ABM, agents follow specific rules throughout the simulation.

The rules in our model include:

1. An agent may be placed on the grid at any time step
2. An agent may undergo proliferation based on surrounding environmental stress conditions
3. An agent may experience programmed cell death (apoptosis)

For the first experiment we simulate, at step zero, a single cancer cell is positioned randomly in a pixel of a 30x30 grid (see Appendix). Subsequently, 200 - 215 new agents are placed randomly around its perimeter within a radius of 7 pixels width and 7 pixels height, simulating the quantity of cancer cells injected into the zebrafish in experiments. Analysis of zebrafish tumor images revealed that each tumor contained approximately 200 - 215 pixels worth of cancer cells (see Appendix). This explains why the radius is set at 7 pixels as it allows for around 224 potential locations for each new agent surrounding the first cancer cell. Respectively, for the experiment we simulate, at step zero, we start by placing a single cancer cell randomly in a pixel of a 60x60 grid (see Appendix). Then, we position 750 - 830 new agents around its perimeter within a radius of 14 pixels width and height to imitate the quantity of cancer cells injected into zebrafish during experiments. Analysis of images from zebrafish tumors indicated that each tumor contained approximately 750 - 830 pixels worth of cancer cells (see Appendix). This choice for the radius enables around 841 potential locations for each new agent surrounding the initial cancer cell. At the end of step zero, these agents represent the initially injected tumor in zebrafish experiments.

The cancer cells/agents from the injected tumor, in our model follow specific growth patterns. In every step, every agent has the opportunity to proliferate. We have identified a proliferation rate of 0.3 (see Appendix) based on our experiments in

zebrafish as the normal rate at which these cells multiply. Each cancer cell/agent generates a random number between 0 and 1, and if this number is less than the determined proliferation rate, a new cell is created in its vicinity within the grid by selecting an empty position nearby. The stress effect in our model is measured with a different proliferation rate number (0.4) (see Appendix), also identified from our experiments.

9.2 Second Model - Cancer Proliferation and Neurogenesis

Our second ABM explores the correlation between cancer growth and neurogenesis, which refers to the emergence of new neurons, in the tumor microenvironment.

In this model, we aim to simulate the following experiment:

> On day zero, in a laboratory setting, cancer cells are placed in a controlled environment in a petri dish. Neurons were previously added to the same dish on the day -1. Their interactions are observed over a span of 3 days in this laboratory setup.

Our study focuses on the microenvironment of a tumor and the existing or newly appearing neurons in its vicinity and we examine the the interactions between them. More specifically, it has been discovered that tumor cells release NGF, which stimulates the growth and enhances the survival of neurons, and therefore neurogenesis [26], [27]. Neurons secrete NTR (such as epinephrine, norepinephrine and acetylcholine) which enhance tumor cell survival, growth and trigger migration and metastasis [1], [38]. A visual representation of the model can be found in the images 9.1 9.2 below.

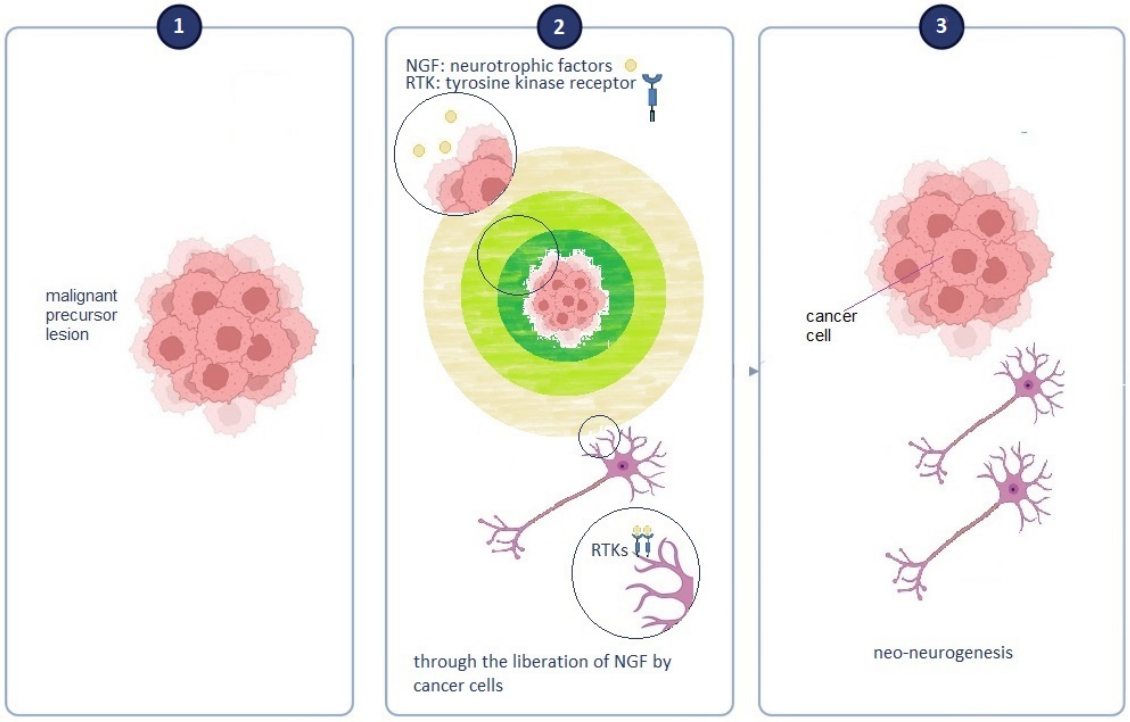

Figure 9.1: NGF secreted by tumor cells promotes neurogenesis, image made with Biorender.

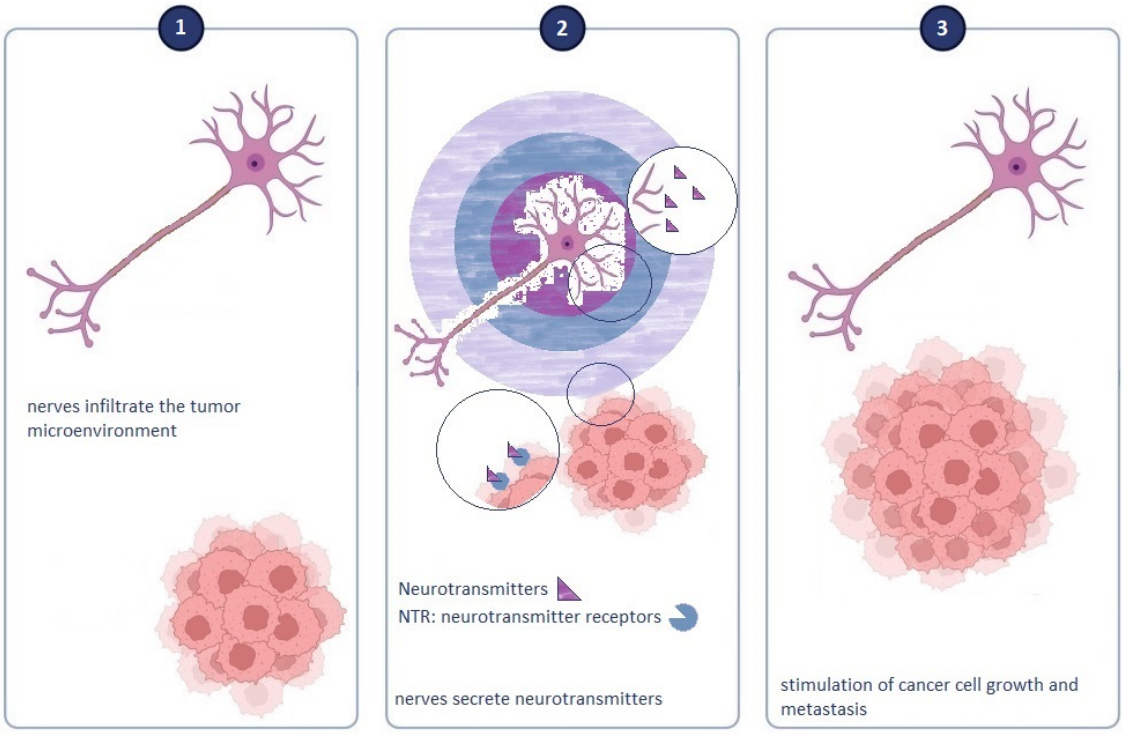

Figure 9.2: Neurons secrete NTR which enhance tumor cell growth and their dissemination, image made with Biorender.

It is known that not all cells in the primary tumor are actively proliferating [324]. Therefore, the model incorporates this by estimating the rate of cell proliferation (see Appendix) based on data obtained from experiments involving zebrafish with a certain degree of likelihood or probability. We introduce a parameter that serves as a key determinant, representing the likelihood of a cancer cell undergoing proliferation. We employ the random.random() function and we introduce a stochastic element to our model, allowing for variability in cell behavior. Then with a condition, we capture a probabilistic framework where a new cell is created in a neighboring location if the randomly generated number falls below the specified proliferation rate. This approach reflects the heterogeneity observed in real-world tumors, where not all cells actively proliferate.

Moreover, the same probability principle applies to neurogenesis. Utilizing the random.random() function results in the creation of a new neuron in a neighboring location if a randomly generated number is less than the designated neurogenesis rate.

As agents, we define cancer cell agents and neuron agents. Agents exist and proliferate on a grid; chemical concetrations of NGF and NTR, instead, are represented as values in two background matrices. The grid details the positions of each agent, while the other two are background matrices each one containing values that correspond to the chemical concentration of NGF and NTR, secreted by cancer cells and neurons respectively. Our approach involved overlapping these matrices onto the grid, which, as far as we are aware, has not been previously utilized.

At step zero, one cancer cell is positioned randomly in a pixel of a 30x30 grid. At the same step, new agents are being placed randomly along its perimeter within a

specified width and height determined by values for x and y. These dimensions allow us to represent the initial malignant tumor at our desired size. Also, at step zero, a neuron is positioned randomly within the grid.

It is assumed that in a tumor-free experiment neurons do not undergo neurogenesis. However, the presence of cancer cells and their secretion of NGF, result in the probability of emergence of new neurons and the enhancement of nerve growth. On the other hand, in an experiment involving exclusively cancer cells, it is assumed that the cancer cells are proliferating at a normal rate. However, when neurons and their release of NTR are introduced, there is an increase in the proliferation rate of the cancer cells. Thus, if the randomly generated number for a potential cancer agent's proliferation falls below the specified proliferation rate, there is an increasing likelihood of a new cell being formed in the neighboring location.

NGF secreted by cancer cells and NTR secreted by neurons are represented as chemicals. A Gaussian diffusion kernel defines how the NGF and NTR concentration spreads spatially, and a diffusion coefficient parameter, different for NGF and NTR respectively, scales the strength of this diffusion (see Appendix). To elaborate further, we use the Gaussian Kernel Function to generate a two-dimensional Gaussian distribution, which is then used as a convolution kernel. The convolution operation applies the diffusion kernel to the input matrix, resulting in a diffused matrix that represents the spatial distribution of NGF and NTR concentrations after the diffusion process. The resulting Gaussian kernel is normalized by dividing it by the sum of all its values and then multiplied by the diffusion coefficient.

The 2D Gaussian function is given by:

$$G(x, y) = \frac{1}{2\pi\sigma^2} e^{-\frac{x^2+y^2}{2\sigma^2}}$$

where:

- (x, y) are the coordinates in the kernel,
- σ (sigma) represents the standard deviation of the Gaussian distribution,
- π is the mathematical constant pi (approximately 3.14)
- e is the mathematical constant Euler's number (approximately 2.71)

In particular, a larger σ value results in a wider and smoother Gaussian curve, while a smaller sigma value leads to a narrower and more peaked curve.

A depiction of simulating the diffusion of NGF from a cancer cell using the Gaussian kernel is presented in the figure 9.3, illustrating progression at 1, 10, 50, and 100 intervals. This visual demonstrates how a single cancer cell diffuses NGF within the matrix.

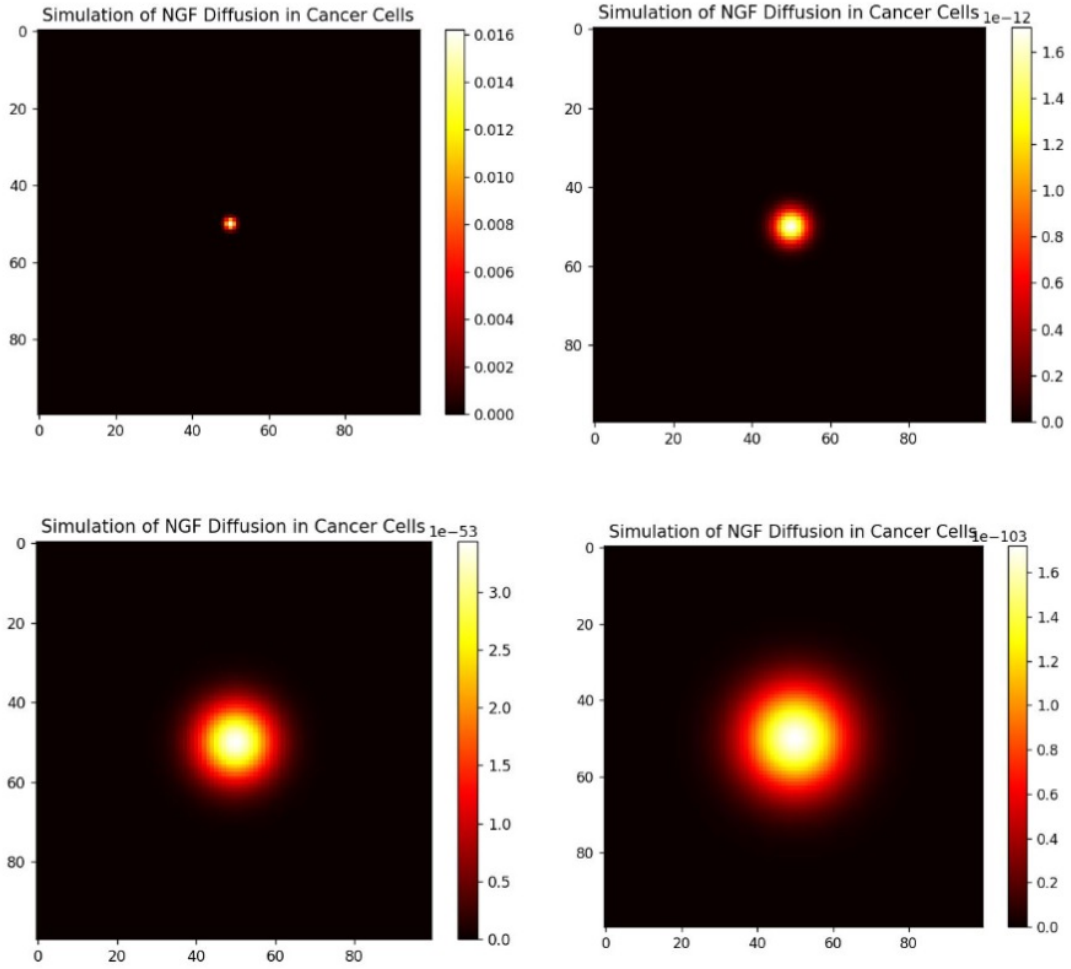

Figure 9.3: Simulation of NGF Diffusion of a Cancer Cell with Gaussian kernel, in 1, 10, 50 and 100 steps.

For the simplification of our ABM, we make the assumption that cellular growth and division have adequate space and a sufficient supply of nutrients to sustain cell viability. In this model, each cancer cell is represented as an agent and occupies one pixel on the grid. Neurons are represented solely by the NTR they diffuse via their axons, which feature branch-like extensions. The length of each neuron is comparable to 20 pixels on the grid, serving as an analogy when compared to a single cancer cell's extent. The grid represents the tumor-neuron microenvironment.

9.2.1 Modeling Neurons

Modeling a neuron agent in a 2D space while representing one cancer cell agent in each grid pixel proved to be challenging. To address this complexity, we decided to display only the neuron's emitted chemical (NTR) on the grid, prioritizing the modeling of the cell body and axon shape.

The structural depiction of a neuron (see Figure 9.4), as opposed to the model formulation, includes the following:

- Cell Body (Soma): The model typically depicts the central cell body, which contains the nucleus and other cellular organelles.
- Dendrites: Branching structures extending from the cell body, representing the neuron's capacity to receive signals from other neurons.
- Axon: A long projection conveying signals away from the cell body, often ending in axon terminals.
- Axon Terminals: The endpoints of the axon, where communication with other neurons or target cells occurs.

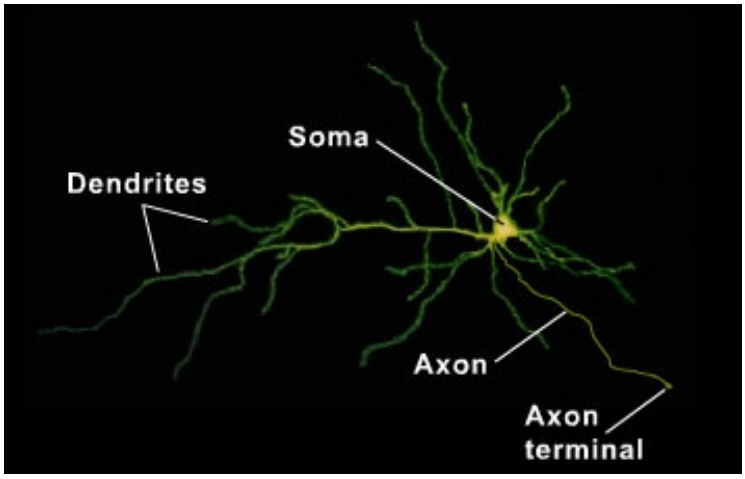

Figure 9.4: Representation of a neuron, image adapted from the American Society for Neuroscience [325].

The shape of each neuron is calculated with a method (called body) based on a list of angles. The method iterates through the list of angles, determining the coordinates of points along the axons using trigonometric functions. The calculated points are stored in the body list. The method accounts for different cases based on the range of angles, adjusting the calculation of coordinates accordingly. Then, in the resulting body coordinates, 20 pixels are being painted grey (as seen in Figure 9.5), to represent a neuron's NTR release in an analogy of one pixel representing one cancer cell.

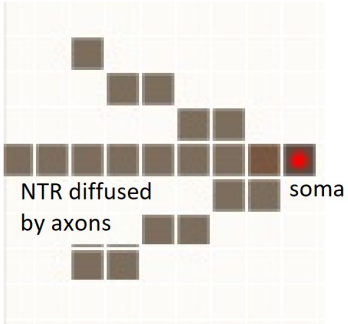

Figure 9.5: 2-Dimentional Representation of a neuron with the red dot representing the neuron's soma and the grey pixels representating the NTR released by axons.

In the following, we refer to the initial placing of chemicals produced by agents as "drop size". This indicates that within the background matrix of cancer cells, each cell agent will emit a maximum amount of NGF. Similarly, for neurons in

the neuron's background matrix, the maximum NTR amount they release is this quantity. For neurons, the highest quantity they release will be divided by 20, representing the number of pixels occupied by a neuron in the grid. Calculations for the initial drop size (or the maximum amount of chemicals NGF and NTR) are located in the Appendix.

The rate at which new neurons appear (neurogenesis rate) increases as NGF concertation increases. But the impact of NGF on growth is not linear, it saturates as NGF concentration increases. In the model, the factor $\frac{G}{\sigma_1+\sigma_2 \cdot G}$ is added to model extra-growth based on the concentration G, of NGF, in each position (x,y) of the background matrix. A graph of the function $\frac{G}{\sigma_1+\sigma_2 \cdot G}$ is plotted in Figure 9.6.

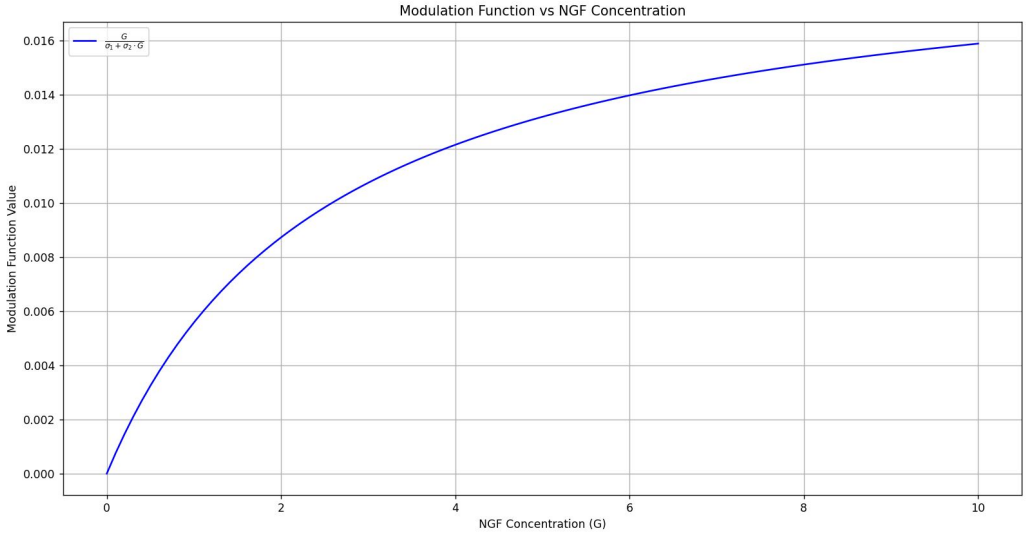

Figure 9.6: Function $\frac{G}{\sigma_1+\sigma_2 \cdot G}$ over the NGF concentration.

σ_1 and σ_2 are parameters that influence the behavior of the function determining the sensitivity of the growth response to the concentration of NGF. More specifically, σ_1 represents a basal sensitivity or a constant factor, while σ_2 introduces a linear dependency on the concentration of NGF, detected by neurons. In this function, as G increases, the denominator also increases, resulting in a smaller fraction and thus a diminishing effect on the growth rate. This introduces a level of diminishing returns or saturation, where very high concentrations of NGF have a reduced impact on growth, shown in Figure 9.7. To find the value of σ_1 and σ_2, refer to the Appendix.

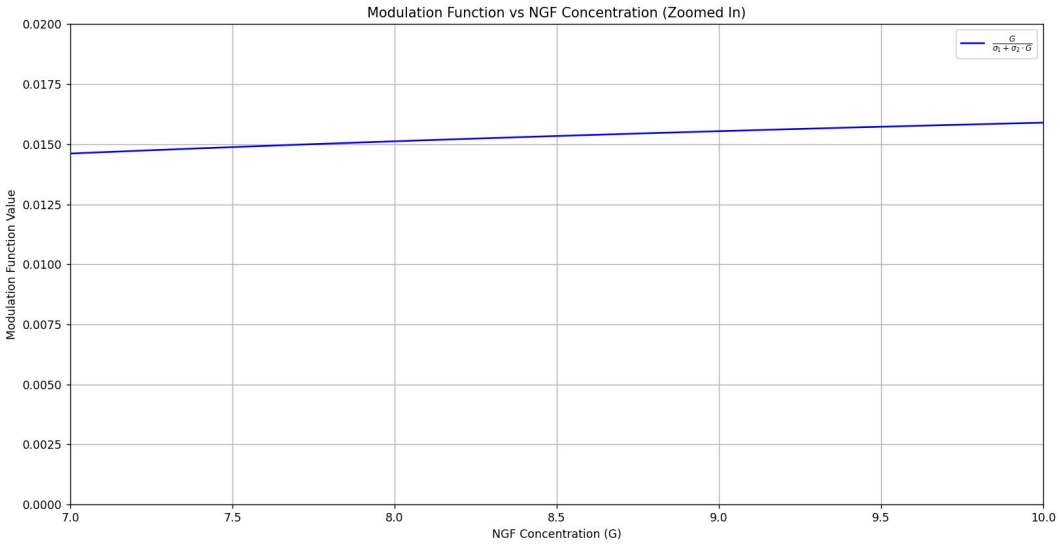

Figure 9.7: Function $\frac{G}{\sigma_1+\sigma_2 \cdot G}$ over the NGF concentration, where very high concentrations of NGF have a reduced impact on growth.

We also model the occurrence of apoptosis in the simulation, ensuring that cells and nerves are appropriately removed from the system at the designated time points. At each iteration of our simulations, a check is implemented to determine if the age of an agent surpasses the estimated life-span, if so, agents undergo apoptosis (programmed cell death). After completing the iteration, the simulation proceeds to remove the identified agents from both the schedule and the grid.

9.2.2 Initial conditions

In every step the simulation represents a day of the experiment. All the values are considered to be at their non-tumor level (normal level) at the beginning of the model simulation.

We also assume the following initial conditions for NGF and NTR production rate, meaning that the initial drop size or the maximum amount of these chemicals for every agent is set to be the values of:

- 2.22 picograms released from every cancer cell: initial drop size of NGF
- 10^{-6} picograms at each of the 20 pixels of every neuron: initial NTR drop size

the moment we start the simulation.

The initial tumor proliferation rate assumed, corresponding our zebrafish data, is 0.3. The value of tumor proliferation rate after the effect of NGF produced by neurons was calculated to be 0.4. More for their calculation on Appendix.

The cancer cell death rate is $1.27 \cdot 10^{-2} \frac{1}{day}$. We have not introduced neuronal cell death in our model.

Chapter 10

Models' Results

10.1 Results of: First Model - Cancer Proliferation and Stress

10.1.1 Cancer Cell Proliferation

The initial condition of our simulation is shown in the Figure 10.1. 200 - 215 new cancer cell agents are placed on the grid.

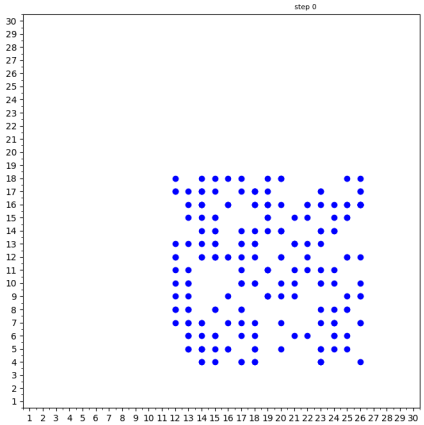

Figure 10.1: Simulation screenshot at step 0.

In the simulation Figure 10.2, we observe blue dots that symbolize agents of cancer cells. The simulation operates for a period of three steps, representing three days. At each iteration, there is visible proliferation of cancer cells. In figure 10.3 shows the evolution of cancer cell growth over time, it is a good approximation of cancer cell population growth taken in zebrafish experiments.

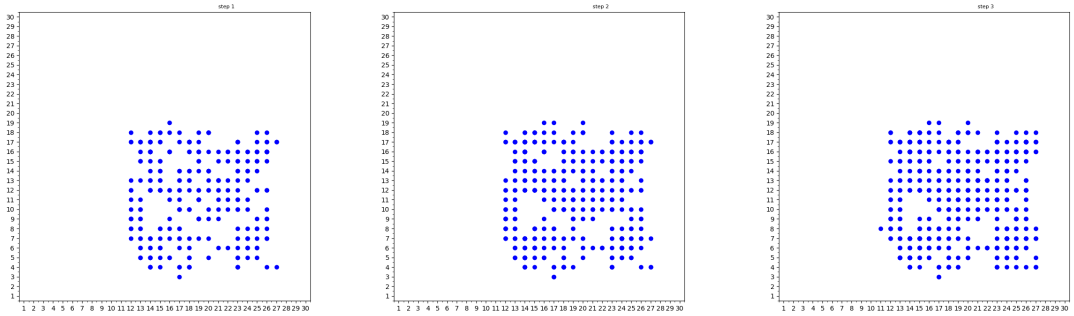

Figure 10.2: Simulation screenshot of Cancer Cell Proliferation at step 1, 2 and 3 (indicating 3 days).

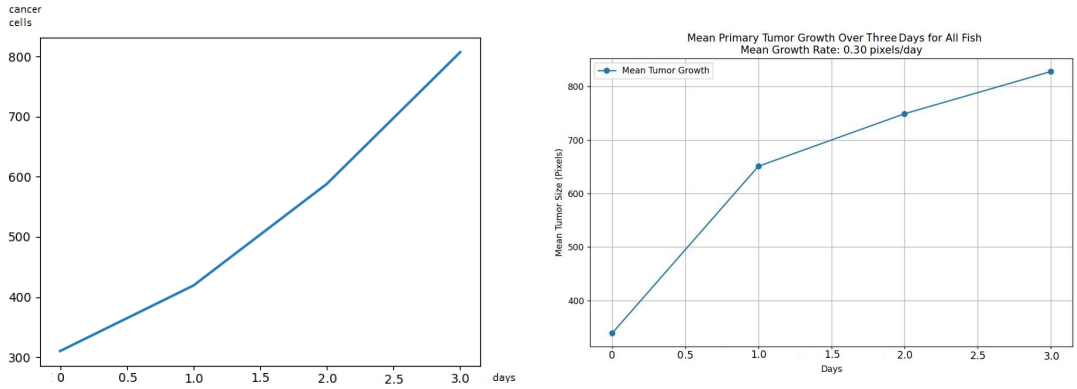

Figure 10.3: Graph for Cancer Proliferation simulation (left) and Graph for Cancer Proliferation Mean Rate from zebrafish experiments (right).

10.1.2 Cancer Cell Proliferation with Stress

The following Figures are from the simulation of cancer cell proliferation with incorporating the stress factor. The initial step of our simulation is shown in the Figure 10.4, where 750 - 830 new agents are being placed on the grid.

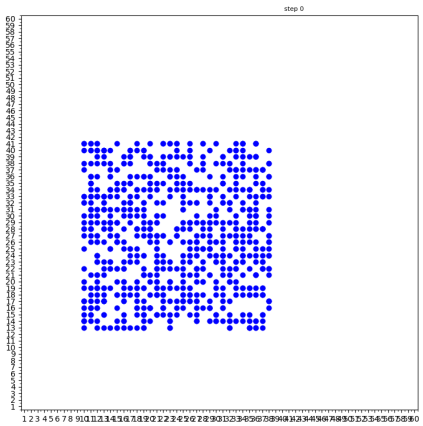

Figure 10.4: Simulation screenshot in step 0.

Figure 10.5 shows the simulation of cancer cell growth in the span of 3 days, taking into account the influence of stress. In the simulation Figure 10.5, we observe blue dots that symbolize agents of cancer cells. At each iteration, there is visible proliferation of cancer cells. The findings clearly indicate that cell proliferation occurs at a faster rate under the influence of stress compared to when stress effect is absent. The graph 10.6 showing their population, is consistent with our findings from zebrafish experiments.

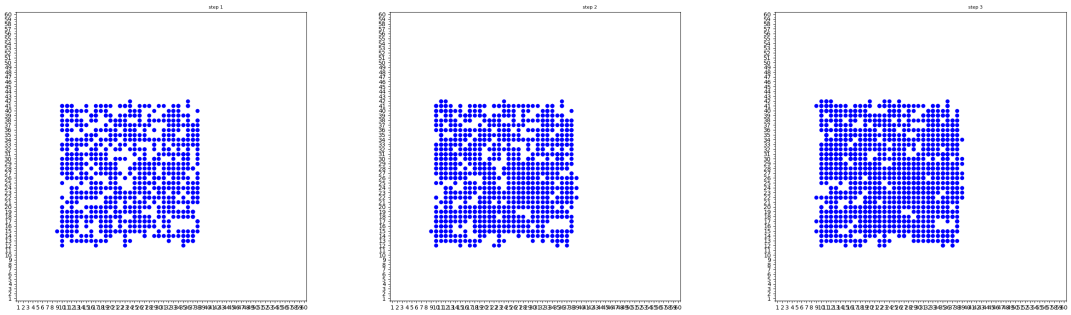

Figure 10.5: Simulation screenshot of Cancer Cell Proliferation with the Stress effect in step 1, 2 and 3 (indicating 3 days).

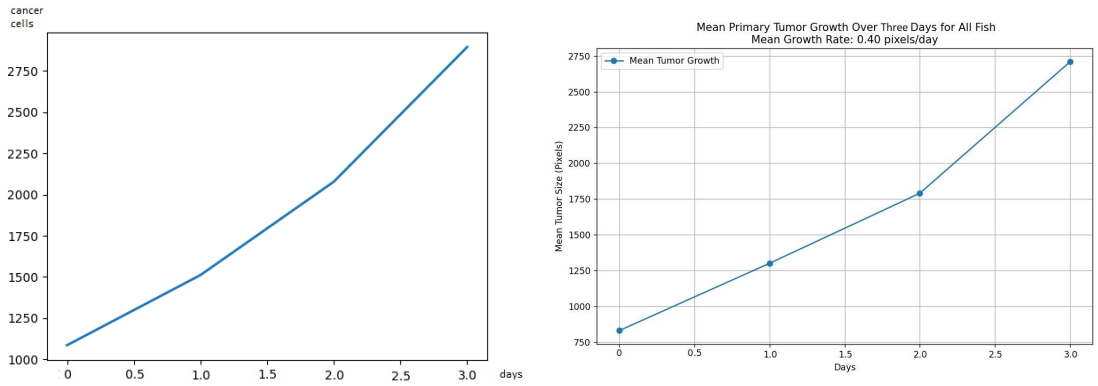

Figure 10.6: Graph for Cancer Proliferation simulation with the Stress effect (left) and Graph for Cancer Proliferation Mean Rate from zebrafish experiments with the Stress effect from norepinephrine (right).

10.2 Results of: Second Model - Cancer Proliferation and Neurogenesis

The Figure 10.7 shows a simulation where green dots represent cancer cell agents (tumor) that grow in response to neurons in their environment. Neuron agents are depicted by the previously described shape with their soma represented as a red dot.

In the beginning of the simulation, the tumor grows at the typical rate of cancer proliferation, indicating that each cancer cell has the potential to divide and generate a new cell within its environment.

Cancer cells release NGF into the surrounding environment, while neurons emit NTR. With green color we simulate the NGF release from cancer cells. With orange color we simulate the NTR release from neuron's soma and axons. When the level of detected NGF exceeds a certain threshold, the neuron's soma turns blue (a blue dot appears in soma's position) and has the potential to undergo neurogenesis. If a cancer cell surpasses the specified threshold of NTR released from the neuron, it changes to yellow and proliferates at a faster rate, indicating an increased likelihood of spreading.

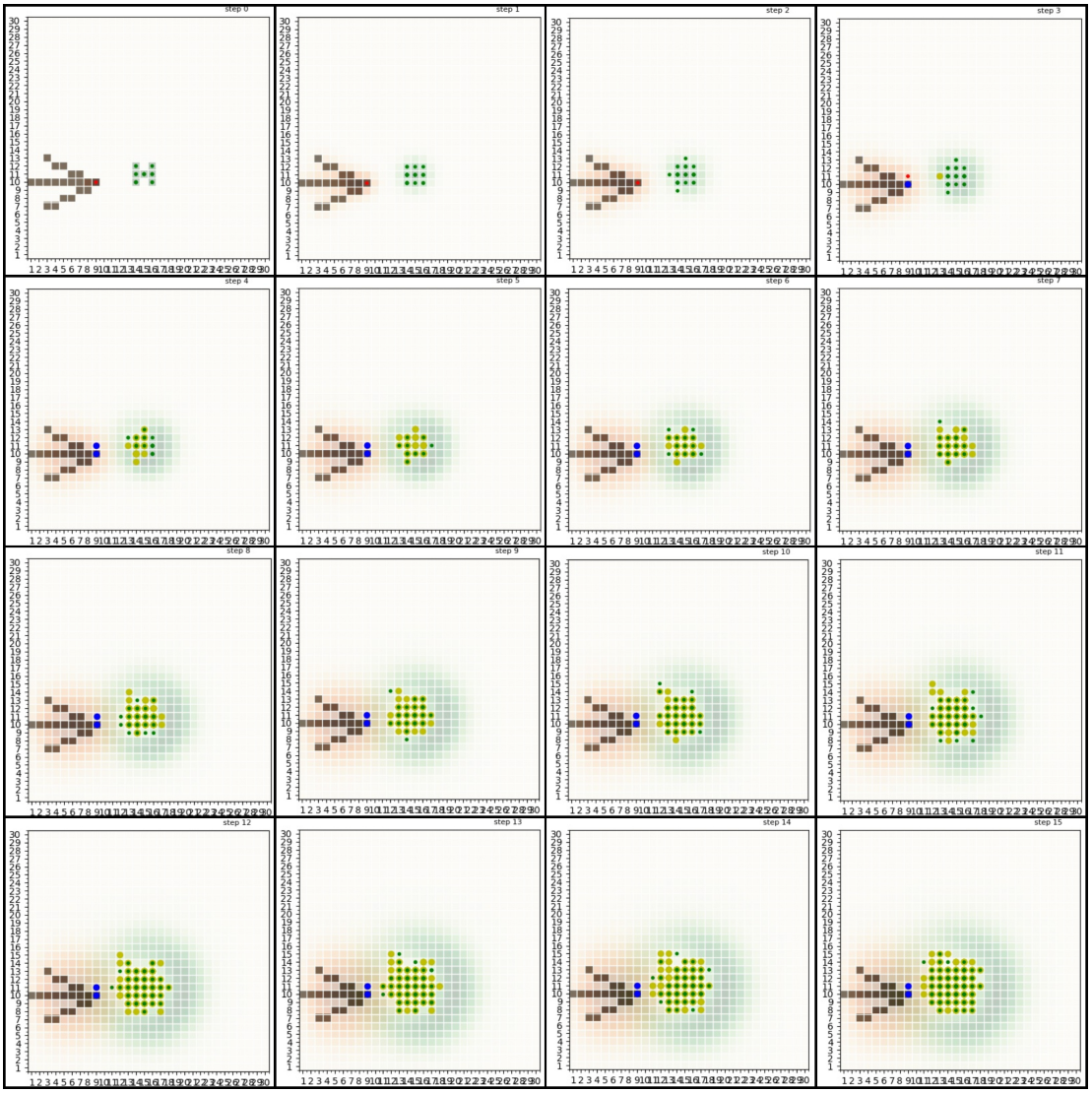

Figure 10.7: Simulation of Cancer Proliferation and Neurogenesis, in 16 steps, indicating 16 days. Green dots represent cancer cell agents and blue dots represent the neuron's soma. With green color we simulate the NGF release from cancer cells. With orange color we simulate the NTR release from neuron's soma and axons. When a yellow dot appears, the proliferation rate of this cancer cell increases. When a red dot appears, the neuron has the potential to undergo neurogenesis. "Secondary" neurons are only represented as single dots/agents for clarity.

Chapter 11

Conclusions and Future Work

In this thesis, we attempted to elucidate the interactions between tumors and neurons and the indication of stress. To achieve this objective, two distinct models were developed and experimental procedures were employed to refine these models. Additionally, an investigation was conducted to assess the efficacy of propranolol-loaded nanoparticles in treating cancer as a potential targeted therapy option.

In our results we see basic representations of cancer cells interactions with neurons and with stress. Our zebrafish experiments showed that propranolol reduces cancer cell proliferation of the primary melanoma tumor 13.82%. Furthermore, propralonol loaded nanoparticles showed reduced the metastatic propensity of primary tumor cells. It is evident that more experiments need to be conducted to fully justify our results.

In summary, to our knowledge our in silico approach is a first attempt of modelling cancer-neuron interactions and the effect of stress using ABM, calibrated by experimental evidence. In our ABM we were able to capture the tumor (growth) dynamics in analogy to the zebrafish experiments. Additionally, our ABM highlighted the stress effect on tumor growth. In the future we would like to add several more variables in our model, such as components of the extracellular matrix (fibroblasts, macrophages) as well as lymphatic and blood vessels.

Appendix

Grids (for the First and Second Model)

In histopathological examinations, the size of melanoma cells typically falls within the range of 10 to 25 micrometers in diameter. As a standard practice, we have designated the width and height of a pixel to be approximately 25μM, for both the first and the second model. Each cancer cell is denoted by a blue circular marker on the grid, for the first model and by a green circular marker, for the second model. We chose a 30x30 grid to represent the tumor microenvironment, in the first model without the stress effect and the second model. For the first model with the stress effect we selected a 60x60 pixel grid.

Grid capacity (for the First Model)

For the simulation without the stress effect, we anticipate introducing 200-215 new cancer cells into the grid, in analogy to zebrafish experiments, on day zero as an initial condition, and conducting a simulation for a duration of three days, reflecting our experimental timeline with zebrafish studies. In order to accommodate optimal proliferation of cancer cells, we have determined that an ideal grid capacity would be 30 by 30 pixels.

In the simulation involving the stress effect, we introduce 750 - 830 new cancer cell agents into the grid, on day zero, following the zebrafish experiments. The duration of the experiment remains 3 days, which aligns with our zebrafish study's timeline. To facilitate efficient growth of cancer cells, we have identified that an optimal grid size would be 60 by 60 pixels.

Grid capacity (for the Second Model)

As mentioned previously, melanoma cells generally have diameters ranging from 10 to 25 micrometers, while neuron cell bodies (somas) typically range in diameter from about 5 to 100 micrometers. However, the majority of somas fall within the range of 10 to 30 micrometers. In this model, one pixel (25x25μM) is used as the standard for representing a neuron's soma, while NTR release from axons is represented by 19 pixels. Axons are not included in the model's simulation due to their thin and long nature; therefore, each neuron is represented by using 20 pixels on the grid. To support the maximum growth of cancer cells and provide sufficient space for neurons, it has been established that an optimal grid size would be 30 pixels by 30 pixels.

Initial tumor proliferation rate (for the First and Second Model)

For the initial tumor proliferation rate we assume, corresponding our zebrafish data, the following:

We calculate the mean growth rate of a tumor over a four-day period based on the given tumor sizes and corresponding time points. It utilizes the logarithmic growth model, where the growth rate r between consecutive days is computed using the formula:

$$r = \frac{\log(N_{i+1}) - \log(N_i)}{t_{i+1} - t_i}$$

where N_i and t_i represent the tumor size and time point on the i-th day, respectively [326]. The growth rates for each pair of consecutive days are stored in a list named growth rates. The mean growth rate is then calculated by taking the sum of the growth rates and dividing it by the number of intervals. The result providing the average growth rate of the tumor over the specified time period for one zebrafish. Finally, by calculating the mean growth rate of each zebrafish and dividing it by the total number of fish in our experiment, we determine the average (melanoma) cancer growth rate.

The calculation of tumor proliferation rate from zebrafish experiments is shown in the table 11.1 below.

	melanoma cancer cells proliferation				**mean growth rate**
	in pixels				
	day 0	day 1	day 2	day 3	
fish 1	425	974	973	684	0.1586
fish 2	184	662	758	1100	0.5960
fish 3	385	506	790	891	0.2797
fish 4	495	933	973	1062	0.2545
fish 5	186	306	423	480	0.3160
fish 6	359	524	577	750	0.2456
average growth rate					0.3084

Table 11.1: Tumor proliferation rate quantification from zebrafish experiments

Thus, the initial tumor proliferation rate for both the First and Second Model is defined as 0.3.

Stress induced tumor proliferation rate (for the First Model) and tumor proliferation rate after the effect of NTR produced by Neurons (for the Second Model)

From our zebrafish experiments using norepinephrine as the stressor, we calculated for the first model the impact of norepinephrine on tumor proliferation rate. Also, as stated previously, in the second model, as a simplification for NTR production by neurons, the rate is determined with the rate of norepinephrine production.

Therefore, in order to measure the effect of norepinephrine in tumor growth for both the first and the second model, we used the results from the aforementioned zebrafish experiments with norepinephrine and the same formula $r = \frac{\log(N_{i+1})-\log(N_i)}{t_{i+1}-t_i}$, where N_i and t_i represent the tumor size and time point on the i-th day used for the initial tumor proliferation rate.

The calculation of tumor proliferation rate determined with the effect of norepinephrine from zebrafish experiments is shown in the table 11.2 below.

	cancer cells proliferation with norepinephrine's effect				**mean growth rate**
	in pixels				
	day 0	day 1	day 2	day 3	
fish 1	622	527	964	1670	0.3292
fish 2	545	1596	2084	4674	0.7163
fish 3	1585	1644	1254	1777	0.0381
fish 4	865	1118	1958	2129	0.3002
fish 5	539	1620	2692	3292	0.6032
average growth rate					0.3974

Table 11.2: Tumor proliferation rate quantification from zebrafish experiments

Thus, stress induced tumor proliferation rate is defined (for the First Model) and tumor proliferation rate after the effect of NTR produced by Neurons (for the Second Model) is defined as 0.4 (≃0.3974).

Nerve extra growth up regulated by NGF from Tumors (for the Second Model)

σ_1 is defined as $1.29{\cdot}10^2$ $\frac{pg{\cdot}day}{mm^3}$ [17] and σ_2 is defined as 50 in day units [17].

Diffusion coefficients (for the Second Model)

First of all, we calculate the value of 1 second corresponding to 1 day. One minute has 60 seconds, one hour has 60 minutes, one day has 24 hours

1 sec = $\frac{1}{60}{\cdot}\frac{1}{60}{\cdot}\frac{1}{24}$ day = $\frac{1}{86400}$ day

We know that 1 pixel = $(25\mu m)^2$.

So, we calculate the value of 1 cm corresponding to 25µm (pixel's width).

$1cm = 10^4\mu m = 10^4{\cdot}\frac{25}{25}\mu m = \frac{1}{25}{\cdot}10^4{\cdot}(25\mu m)$

Then, we calculate the value of 1 cm corresponding to $(25\mu m)^2$ (pixel's dimentions).

$1cm = [\frac{1}{25}{\cdot}10^4{\cdot}(25\mu m)]^2 = \frac{10^8}{25^2}{\cdot}(25\mu m)^2$

Finally, we calculate how many $\frac{cm^2}{s}$ correspond to $\frac{pixel}{day}$.

$1\frac{cm^2}{s} = \frac{10^8}{25^2}{\cdot}(25\mu m)^2 \;/\; \frac{1}{86400}day = \frac{10^8}{625}{\cdot}86400{\cdot}\frac{(25\mu m)^2}{86400} = \frac{10^8}{625}{\cdot}86400\frac{pixel}{day} = 138.24{\cdot}10^8\frac{pixel}{day}$

NTR diffusion coefficient (for the Second Model)

NTR diffusion coefficient is simplified by calculating the diffusion coefficient for norepinephrine and then applying it to every pixel per day. Norepinephrine's diffusion coefficient was found in M. Rice's original academic article [327].

$D = 0.69 \cdot 10^{-5}$ cm^2/sec

$D = 0.69 \cdot 10^{-5}$ cm^2/sec =

$0.69 \cdot 10^{-5} \frac{cm^2}{s} \cdot 138.24 \cdot 10^8 \frac{pixel}{day}$ =

$95.3856 \cdot 10^{-5} \cdot 10^8$ pixel =

$95.3856 \cdot 10^3$ pixel

Thus, we use the value $95.3856 \cdot 10^3$ pixel for NTR diffusion coefficient.

NGF diffusion coefficient (for the Second Model)

NGF diffusion coefficient has been calculated from the initial amount $D=2.75 \cdot 10^{-7}$ cm^2/sec that has been stated in [328]. We, then, appied this coefficient to pixel per day.

$D=2.75 \cdot 10^{-7}$ cm^2/sec =

$2.75 \cdot 10^{-7} \frac{cm^2}{s} \cdot 138.24 \cdot 10^8 \frac{pixel}{day}$ =

$380.16 \cdot 10$ pixel =

$3.8016 \cdot 10^3$ pixel

Thus, the value $3.8016 \cdot 10^3$ was used as NGF diffusion coefficient.

NGF production rate by cancer cells (or NGF initial drop size) (for the Second Model)

The initial drop size of NGF released from cancer cells is 2.22 picograms per day, as reported as the production rate of NGF by tumor cells in [17] and [26].

NTR production rate by neurons (or NTR initial drop size) (for the Second Model)

NTR production rate by neurons is simplified by determining the rate at which norepinephrine is produced, since norepinephrine is recognized as the primary sympathetic (SyNS) neurotransmitter associated with tumors and there is limited documentation on the impact of epinephrine on tumor cell proliferation [17], [38]. Norepinephrine production rate by neurons results as the initial drop size of NTR is 1.6 picograms per day as stated in the academic articles [17] and [329].

We assume that the neuron was placed in the petri dish 1 minute prior to the addition of cancer cells and the beginning of the simulation. The production of

norepinephrine by 1 neuron is 1.6 $\frac{pg}{cell} \cdot \frac{1}{day}$, and 1 neuron occupies roughly 20 pixels within the grid.

Each pixel contains $\frac{1.6}{20}$pg = 0.08pg of norepinephrine after 1 day. After 1 minute, we calculate:

$\frac{0.08}{86400} \simeq 9.259 \cdot 10^{-7}\text{pg} \simeq 10 \cdot 10^{-7} \simeq 10^{-6}\text{pg}$

Thus, each neuron's NTR release is represented with an initial NTR drop size of 10^{-6} picograms at each of the 20 pixels within the neurons.

Cancer Cell Death Rate (for the First and Second Model)

It is known that the tumor cell death rate is $1.27 \cdot 10^{-2} \frac{1}{day}$ [17], [330]. To calculate how many cancer cells die per day based on the tumor cell death rate, we use the formula: Cell Death Rate = Tumor Cell Death Rate·Number of Cancer Cells

If the tumor cell death rate is given as $1.27 \cdot 10^{-2} \frac{1}{day}$ and the initial number of cancer cells is N_0, the calculation would be:

Number of Cancer Cells Died Per Day = $1.27 \cdot 10^{-2} \cdot N_0$

Acronyms

^{1}H NMR Proton Nuclear Magnetic Resonance

ABM Agent-Based Modelling

ANS Autonomic Nervous System

BDNF Brain-Derived Neurotrophic Factor

CA Cellular Automaton

CNS Central Nervous System

DCX+ Doublecortin

DDS Drug delivery systems

DiL 1,1'-Dioctadecyl-3,3,3',3'-tetramethylindocarbocyanine perchlorate

DLS Dynamic Light Scattering

DMAP 4-N,N-Dimethylaminopyridine ($(CH_3)2NC_5H_4N$)

FESEM Field Emission Scanning Electron Microscopy

FGF-2 Fibroblast Growth Factor 2

GPCRs G protein-coupled receptors

HPA Hypothalamic-Pituitary-Adrenal

IGF Insulin-Like Growth Factor

IUPAC International Union of Pure and Applied Chemistry

mPEG Poly(ethylene-glycol) methyl ether also known as Monomethoxy poly(ethylene oxide) or PEG-CH_3

mPEG-*b*-PLLA Poly(ethylene-glycol) methyl ether (mPEG)-*b*-poly(L-lactide)

NGF Nerve Growth Factor

NGFR Nerve Growth Factor receptor

NTR Neurotransmitters

NTR receptors Neurotransmitters receptors

PaNS Parasympathetic Nervous System

PBS Phosphate-buffered saline

PDX Patient-derived xenografts

PEG Polyethylene glycol

PLLA Poly(L-lactide)

PNI Perineural invasion

PNS Peripheral Nervous System

PTU 1-phenyl-2-thiourea

RF radiofrequency

ROP Ring-opening polymerization

S4F Semaphorin 4F

SEM Scanning electron microscopy

SoNS Somatic Nervous System

SyNS Sympathetic Nervous System

TMS tetramethylsilane

Tricaine ethyl 3-aminobenzoate methane-sulfonate

Trks Tyrosine-receptor kinases

UV Ultraviolet

VEGF Vascular Endothelial Growth Factor

Bibliography

[1] C. Magnon, S. J. Hall, J. Lin, *et al.*, "Autonomic nerve development contributes to prostate cancer progression", *Science*, vol. 341, no. 6142, p. 1236361, 2013.

[2] G. M. Cooper, *The cancer book: A guide to understanding the causes, prevention, and treatment of cancer*. Jones & Bartlett Learning, 1993.

[3] R. A. Weinberg, "How cancer arises", *Scientific American*, vol. 275, no. 3, pp. 62–70, 1996.

[4] V. A. Bohr, C. A. Smith, D. S. Okumoto, and P. C. Hanawalt, "Dna repair in an active gene: Removal of pyrimidine dimers from the dhfr gene of cho cells is much more efficient than in the genome overall", *Cell*, vol. 40, no. 2, pp. 359–369, 1985.

[5] I. Mellon, V. A. Bohr, C. A. Smith, and P. C. Hanawalt, "Preferential dna repair of an active gene in human cells.", *Proceedings of the National Academy of Sciences*, vol. 83, no. 23, pp. 8878–8882, 1986.

[6] B. Bridges, "An approach to the assessment of the risk to man from dna damaging agents.", *Archives of toxicology. Supplement. Archiv fur Toxikologie. Supplement*, vol. 3, pp. 271–281, 1980.

[7] A. Berlin, A. H. Wolff, Y. Hasegawa, W. H. Organization, *et al.*, "The use of biological specimens for the assessment of human exposure to environmental pollutants: Proceedings of the international workshop at luxembourg, 18-22 april 1977", *(No Title)*, 1979.

[8] A. Dayan, "Monitoring human exposure to carcinogenic and mutagenic agents", *Journal of Clinical Pathology*, vol. 39, no. 3, p. 347, 1986.

[9] D. Schadendorf, A. C. van Akkooi, C. Berking, *et al.*, "Melanoma", *The Lancet*, vol. 392, no. 10151, pp. 971–984, 2018.

[10] D. Schadendorf and A. Hauschild, "Melanoma—the run of success continues", *Nature reviews Clinical oncology*, vol. 11, no. 2, pp. 75–76, 2014.

[11] D. G. Coit, R. Andtbacka, C. K. Bichakjian, *et al.*, "Melanoma", *Journal of the National Comprehensive Cancer Network*, vol. 7, no. 3, pp. 250–275, 2009.

[12] M. S. Lawrence, P. Stojanov, P. Polak, *et al.*, "Mutational heterogeneity in cancer and the search for new cancer-associated genes", *Nature*, vol. 499, no. 7457, pp. 214–218, 2013.

[13] J. K. Mai and G. Paxinos, *The human nervous system*. Academic press, 2011.

[14] C. R. Noback, D. A. Ruggiero, N. L. Strominger, and R. J. Demarest, *The human nervous system: structure and function*. Springer Science & Business Media, 2005.

[15] R. Nieuwenhuys, J. Voogd, and C. Van Huijzen, *The human central nervous system: a synopsis and atlas*. Springer Science & Business Media, 2007.

[16] A. T. Michael-Titus and P. Shortland, *The Nervous System, E-Book: Systems of the Body Series*. Elsevier Health Sciences, 2022.

[17] G. Lolas, A. Bianchi, and K. N. Syrigos, "Tumour-induced neoneurogenesis and perineural tumour growth: A mathematical approach", *Scientific reports*, vol. 6, no. 1, pp. 1–10, 2016.

[18] S. E. Hyman, "Neurotransmitters", *Current biology*, vol. 15, no. 5, R154–R158, 2005.

[19] E. S. Valenstein, *The war of the soups and the sparks: The discovery of neurotransmitters and the dispute over how nerves communicate*. Columbia University Press, 2005.

[20] D. Purves, G. Augustine, D. Fitzpatrick, *et al.*, "Peptide neurotransmitters. neuroscience", *Sinauer Associates*, 2001.

[21] V. Ralevic, "Purines as neurotransmitters and neuromodulators in blood vessels", *Current vascular pharmacology*, vol. 7, no. 1, pp. 3–14, 2009.

[22] F. E. Bloom, "Neurotransmitter diversity and its functional significance", *Journal of the Royal Society of Medicine*, vol. 78, no. 3, pp. 189–192, 1985.

[23] R. Sapolsky and T. Company, *Biology and Human Behavior: The Neurological Origins of Individuality* (Great Courses τ. 3). Teaching Company, LLC, 2005, ISBN: 9781598030815. [Online]. Available: `https://books.google.gr/books?id=5YBwPAAACAAJ`.

[24] S.-H. Jiang, L.-P. Hu, X. Wang, J. Li, and Z.-G. Zhang, "Neurotransmitters: Emerging targets in cancer", *Oncogene*, vol. 39, no. 3, pp. 503–515, 2020.

[25] D. Chakroborty, U. R. Chowdhury, C. Sarkar, R. Baral, P. S. Dasgupta, S. Basu, *et al.*, "Dopamine regulates endothelial progenitor cell mobilization from mouse bone marrow in tumor vascularization", *The Journal of clinical investigation*, vol. 118, no. 4, pp. 1380–1389, 2008.

[26] L. Dolle, E. Yazidi-Belkoura, E. Adriaenssens, V. Nurcombe, H. Hondermarck, *et al.*, "Nerve growth factor overexpression and autocrine loop in breast cancer cells", *Oncogene*, vol. 22, no. 36, pp. 5592–5601, 2003.

[27] D. Palm and F. Entschladen, "Neoneurogenesis and the neuro-neoplastic synapse", *Neuronal Activity in Tumor Tissue*, vol. 39, pp. 91–98, 2007.

[28] R. Levi-Montalcini and P. U. Angeletti, "Nerve growth factor.", *Physiological Reviews*, vol. 48, no. 3, pp. 534–569, 1968.

[29] N. Ferrara, "Vascular endothelial growth factor", *European Journal of Cancer*, vol. 32, no. 14, pp. 2413–2422, 1996.

[30] D. K. Binder and H. E. Scharfman, "Brain-derived neurotrophic factor", *Growth factors (Chur, Switzerland)*, vol. 22, no. 3, p. 123, 2004.

[31] D. Le Roith, "Insulin-like growth factors", *New England Journal of Medicine*, vol. 336, no. 9, pp. 633–640, 1997.

[32] M. A. Nugent and R. V. Iozzo, "Fibroblast growth factor-2", *The international journal of biochemistry & cell biology*, vol. 32, no. 2, pp. 115–120, 2000.

[33] M. Amit, S. Na'Ara, and Z. Gil, "Mechanisms of cancer dissemination along nerves", *Nature reviews Cancer*, vol. 16, no. 6, pp. 399–408, 2016.

[34] J. Kim, R. Villadsen, T. Sørlie, *et al.*, "Tumor initiating but differentiated luminal-like breast cancer cells are highly invasive in the absence of basal-like activity", *Proceedings of the National Academy of Sciences*, vol. 109, no. 16, pp. 6124–6129, 2012.

[35] D. A. Silverman, V. K. Martinez, P. M. Dougherty, J. N. Myers, G. A. Calin, and M. Amit, "Cancer-associated neurogenesis and nerve-cancer cross-talk", *Cancer research*, vol. 81, no. 6, pp. 1431–1440, 2021.

[36] W. Wang, L. Li, N. Chen, *et al.*, "Nerves in the tumor microenvironment: Origin and effects", *Frontiers in Cell and Developmental Biology*, vol. 8, p. 601738, 2020.

[37] C. Liebig, G. Ayala, J. A. Wilks, D. H. Berger, and D. Albo, "Perineural invasion in cancer: A review of the literature", *Cancer: Interdisciplinary International Journal of the American Cancer Society*, vol. 115, no. 15, pp. 3379–3391, 2009.

[38] K. Lang and P. Bastian, "Neurotransmitter effects on tumor cells and leukocytes", *Neuronal Activity in Tumor Tissue*, vol. 39, pp. 99–121, 2007.

[39] A. H. Zahalka and P. S. Frenette, "Nerves in cancer", *Nature Reviews Cancer*, vol. 20, no. 3, pp. 143–157, 2020.

[40] G. E. Ayala, H. Dai, M. Powell, *et al.*, "Cancer-related axonogenesis and neurogenesis in prostate cancer", *Clinical Cancer Research*, vol. 14, no. 23, pp. 7593–7603, 2008.

[41] A. Krüttgen, I. Schneider, and J. Weis, "The dark side of the ngf family: Neurotrophins in neoplasias", *Brain pathology*, vol. 16, no. 4, pp. 304–310, 2006.

[42] P. Mauffrey, N. Tchitchek, V. Barroca, *et al.*, "Progenitors from the central nervous system drive neurogenesis in cancer", *Nature*, vol. 569, no. 7758, pp. 672–678, 2019.

[43] M. Dunn, M. B. Morgan, and T. W. Beer, "Perineural invasion: Identification, significance, and a standardized definition", *Dermatologic surgery*, vol. 35, no. 2, pp. 214–221, 2009.

[44] I. Hirai, W. Kimura, K. Ozawa, *et al.*, "Perineural invasion in pancreatic cancer", *Pancreas*, vol. 24, no. 1, pp. 15–25, 2002.

[45] A. A. Bapat, G. Hostetter, D. D. Von Hoff, and H. Han, "Perineural invasion and associated pain in pancreatic cancer", *Nature Reviews Cancer*, vol. 11, no. 10, pp. 695–707, 2011.

[46] P. Jobling, J. Pundavela, S. M. Oliveira, S. Roselli, M. M. Walker, and H. Hondermarck, "Nerve–cancer cell cross-talk: A novel promoter of tumor progression", *Cancer research*, vol. 75, no. 9, pp. 1777–1781, 2015.

[47] J. L. Saloman, K. M. Albers, D. Li, *et al.*, "Ablation of sensory neurons in a genetic model of pancreatic ductal adenocarcinoma slows initiation and progression of cancer", *Proceedings of the National Academy of Sciences*, vol. 113, no. 11, pp. 3078–3083, 2016.

[48] R. E. Stopczynski, D. P. Normolle, D. J. Hartman, *et al.*, "Neuroplastic changes occur early in the development of pancreatic ductal adenocarcinoma", *Cancer research*, vol. 74, no. 6, pp. 1718–1727, 2014.

[49] B. March, S. Faulkner, P. Jobling, *et al.*, "Tumour innervation and neurosignalling in prostate cancer", *Nature Reviews Urology*, vol. 17, no. 2, pp. 119–130, 2020.

[50] N. Voronina, J. K. Wong, D. Hübschmann, *et al.*, "The landscape of chromothripsis across adult cancer types", *Nature communications*, vol. 11, no. 1, p. 2320, 2020.

[51] A. H. Zahalka, A. Arnal-Estapé, M. Maryanovich, *et al.*, "Adrenergic nerves activate an angio-metabolic switch in prostate cancer", *Science*, vol. 358, no. 6361, pp. 321–326, 2017.

[52] C.-M. Zhao, Y. Hayakawa, Y. Kodama, *et al.*, "Denervation suppresses gastric tumorigenesis", *Science translational medicine*, vol. 6, no. 250, 250ra115–250ra115, 2014.

[53] B. W. Renz, R. Takahashi, T. Tanaka, *et al.*, "β2 adrenergic-neurotrophin feedforward loop promotes pancreatic cancer", *Cancer cell*, vol. 33, no. 1, pp. 75–90, 2018.

[54] D. Hanahan and R. A. Weinberg, "Hallmarks of cancer: The next generation", *cell*, vol. 144, no. 5, pp. 646–674, 2011.

[55] A. Rutledge, P. Jobling, M. M. Walker, J. W. Denham, and H. Hondermarck, "Spinal cord injuries and nerve dependence in prostate cancer", *Trends in cancer*, vol. 3, no. 12, pp. 812–815, 2017.

[56] W. Wang, H. Zhao, S. Zhang, *et al.*, "Patterns of expression and function of the p75ngfr protein in pancreatic cancer cells and tumours", *European Journal of Surgical Oncology (EJSO)*, vol. 35, no. 8, pp. 826–832, 2009.

[57] S. D. Deshmukh, J. K. Willmann, and R. B. Jeffrey, "Pathways of extrapancreatic perineural invasion by pancreatic adenocarcinoma: Evaluation with 3d volume-rendered mdct imaging", *American journal of roentgenology*, vol. 194, no. 3, pp. 668–674, 2010.

[58] I. E. Demir, H. Friess, and G. O. Ceyhan, "Nerve-cancer interactions in the stromal biology of pancreatic cancer", *Frontiers in physiology*, vol. 3, p. 97, 2012.

[59] Y. Lei, L. Tang, Y. Xie, *et al.*, "Gold nanoclusters-assisted delivery of ngf sirna for effective treatment of pancreatic cancer", *Nature communications*, vol. 8, no. 1, pp. 1–15, 2017.

[60] A. España-Ferrufino, L. S. Lino-Silva, and R. A. Salcedo-Hernández, "Extramural perineural invasion in pt3 and pt4 gastric carcinomas", *Journal of pathology and translational medicine*, vol. 52, no. 2, pp. 79–84, 2018.

[61] J. Deng, Q. You, Y. Gao, *et al.*, "Prognostic value of perineural invasion in gastric cancer: A systematic review and meta-analysis", *PloS one*, vol. 9, no. 2, e88907, 2014.

[62] B. B. Oven Ustaalioglu, A. Bilici, M. Seker, *et al.*, "Prognostic factors for operated gallbladder cancer", *Journal of Gastrointestinal Cancer*, vol. 50, pp. 451–457, 2019.

[63] L. Schmitd, C. Scanlon, and N. D'silva, "Perineural invasion in head and neck cancer", *Journal of dental research*, vol. 97, no. 7, pp. 742–750, 2018.

[64] P. Huyett, U. Duvvuri, R. L. Ferris, J. T. Johnson, B. M. Schaitkin, and S. Kim, "Perineural invasion in parotid gland malignancies", *Otolaryngology–Head and Neck Surgery*, vol. 158, no. 6, pp. 1035–1041, 2018.

[65] J. R. Cracchiolo, B. Xu, J. C. Migliacci, *et al.*, "Patterns of recurrence in oral tongue cancer with perineural invasion", *Head & neck*, vol. 40, no. 6, pp. 1287–1295, 2018.

[66] Y. Zhu, G. Zhang, Y. Yang, *et al.*, "Perineural invasion in early-stage cervical cancer and its relevance following surgery", *Oncology Letters*, vol. 15, no. 5, pp. 6555–6561, 2018.

[67] L. Cui, Y. Shi, and G. N. Zhang, "Perineural invasion as a prognostic factor for cervical cancer: A systematic review and meta-analysis", *Archives of Gynecology and Obstetrics*, vol. 292, pp. 13–19, 2015.

[68] H. Ozaki, T. Hiraoka, R. Mizumoto, *et al.*, "The prognostic significance of lymph node metastasis and intrapancreatic perineural invasion in pancreatic cancer after curative resection", *Surgery today*, vol. 29, pp. 16–22, 1999.

[69] C. Beard, M. Chen, K. Cote, *et al.*, "Perineural invasion is associated with increased relapse after external beam radiotherapy for men with low-risk prostate cancer and may be a marker for occult, high-grade cancer", *International Journal of Radiation Oncology* Biology* Physics*, vol. 58, no. 1, pp. 19–24, 2004.

[70] N. Duraker, S. Şişman, and G. Can, "The significance of perineural invasion as a prognostic factor in patients with gastric carcinoma", *Surgery today*, vol. 33, pp. 95–100, 2003.

[71] M. Zare-Bandamiri, M. Fararouei, S. Zohourinia, N. Daneshi, and M. Dianatinasab, "Risk factors predicting colorectal cancer recurrence following initial treatment: A 5-year cohort study", *Asian Pacific journal of cancer prevention: APJCP*, vol. 18, no. 9, p. 2465, 2017.

[72] Y. Huang, L. He, D. Dong, *et al.*, "Individualized prediction of perineural invasion in colorectal cancer: Development and validation of a radiomics prediction model", *Chinese Journal of Cancer Research*, vol. 30, no. 1, p. 40, 2018.

[73] T. Kinugasa, T. Mizobe, S. Shiraiwa, Y. Akagi, and K. Shirouzu, "Perineural invasion is a prognostic factor and treatment indicator in patients with rectal cancer undergoing curative surgery: 2000-2011 data from a single-center study", *Anticancer Research*, vol. 37, no. 7, pp. 3961–3968, 2017.

[74] H. Chen, D. Liu, L. Guo, X. Cheng, N. Guo, and M. Shi, "Chronic psychological stress promotes lung metastatic colonization of circulating breast cancer cells by decorating a pre-metastatic niche through activating β-adrenergic signaling", *The Journal of pathology*, vol. 244, no. 1, pp. 49–60, 2018.

[75] G. O. Ceyhan, F. Bergmann, M. Kadihasanoglu, *et al.*, "The neurotrophic factor artemin influences the extent of neural damage and growth in chronic pancreatitis", *Gut*, vol. 56, no. 4, pp. 534–544, 2007.

[76] S. Dai, Y. Mo, Y. Wang, *et al.*, "Chronic stress promotes cancer development", *Frontiers in oncology*, vol. 10, p. 1492, 2020.

[77] L. S. Sklar and H. Anisman, "Stress and cancer.", *Psychological bulletin*, vol. 89, no. 3, p. 369, 1981.

[78] C. Sandi and J. Haller, "Stress and the social brain: Behavioural effects and neurobiological mechanisms", *Nature Reviews Neuroscience*, vol. 16, no. 5, pp. 290–304, 2015.

[79] C. Alonso, M. Guilarte, M. Vicario, *et al.*, "Maladaptive intestinal epithelial responses to life stress may predispose healthy women to gut mucosal inflammation", *Gastroenterology*, vol. 135, no. 1, pp. 163–172, 2008.

[80] J. Santos and M. Perdue, "Stress and neuroimmune regulation of gut mucosal function", *Gut*, vol. 47, no. suppl 4, pp. iv49–iv51, 2000.

[81] P. R. Braadland, H. Ramberg, H. H. Grytli, and K. A. Taskén, "β-adrenergic receptor signaling in prostate cancer", *Frontiers in oncology*, vol. 4, p. 375, 2015.

[82] B. Cui, Y. Luo, P. Tian, *et al.*, "Stress-induced epinephrine enhances lactate dehydrogenase a and promotes breast cancer stem-like cells", *The Journal of clinical investigation*, vol. 129, no. 3, pp. 1030–1046, 2019.

[83] A. Chang, C. P. Le, A. K. Walker, *et al.*, "β2-adrenoceptors on tumor cells play a critical role in stress-enhanced metastasis in a mouse model of breast cancer", *Brain, behavior, and immunity*, vol. 57, pp. 106–115, 2016.

[84] A. Androulidaki, E. Dermitzaki, M. Venihaki, *et al.*, "Corticotropin releasing factor promotes breast cancer cell motility and invasiveness", *Molecular Cancer*, vol. 8, pp. 1–12, 2009.

[85] V. Riley, "Mouse mammary tumors: Alteration of incidence as apparent function of stress", *Science*, vol. 189, no. 4201, pp. 465–467, 1975.

[86] C. McNeil, *Stress reduction: Three trials test its impact on breast cancer progression*, 1998.

[87] X. Zhi, B. Li, Z. Li, *et al.*, "Adrenergic modulation of ampk-dependent autophagy by chronic stress enhances cell proliferation and survival in gastric cancer", *International journal of oncology*, vol. 54, no. 5, pp. 1625–1638, 2019.

[88] X. Zhang, Y. Zhang, Z. He, *et al.*, "Chronic stress promotes gastric cancer progression and metastasis: An essential role for adrb2", *Cell Death & Disease*, vol. 10, no. 11, p. 788, 2019.

[89] H.-J. Jang, H.-J. Boo, H. J. Lee, H.-Y. Min, and H.-Y. Lee, "Chronic stress facilitates lung tumorigenesis by promoting exocytosis of igf2 in lung epithelial cells", *Cancer Research*, vol. 76, no. 22, pp. 6607–6619, 2016.

[90] A. N. Saul, T. M. Oberyszyn, C. Daugherty, *et al.*, "Chronic stress and susceptibility to skin cancer", *Journal of the National Cancer Institute*, vol. 97, no. 23, pp. 1760–1767, 2005.

[91] J. Parker, S. L. Klein, M. K. McClintock, *et al.*, "Chronic stress accelerates ultraviolet-induced cutaneous carcinogenesis", *Journal of the American Academy of Dermatology*, vol. 51, no. 6, pp. 919–922, 2004.

[92] R. E. Engeszer, L. B. Patterson, A. A. Rao, and D. M. Parichy, "Zebrafish in the wild: A review of natural history and new notes from the field", *Zebrafish*, vol. 4, no. 1, pp. 21–40, 2007.

[93] G. Streisinger, C. Walker, N. Dower, D. Knauber, and F. Singer, "Production of clones of homozygous diploid zebra fish (brachydanio rerio)", *Nature*, vol. 291, no. 5813, pp. 293–296, 1981.

[94] J. S. Eisen, "History of zebrafish research", in *The zebrafish in biomedical research*, Elsevier, 2020, pp. 3–14.

[95] S. Zhao, J. Huang, and J. Ye, "A fresh look at zebrafish from the perspective of cancer research", *Journal of Experimental & Clinical Cancer Research*, vol. 34, pp. 1–9, 2015.

[96] A. J. Hill, H. Teraoka, W. Heideman, and R. E. Peterson, "Zebrafish as a model vertebrate for investigating chemical toxicity", *Toxicological sciences*, vol. 86, no. 1, pp. 6–19, 2005.

[97] R. J. Major and K. D. Poss, "Zebrafish heart regeneration as a model for cardiac tissue repair", *Drug Discovery Today: Disease Models*, vol. 4, no. 4, pp. 219–225, 2007.

[98] E. Plantié, M. Migocka-Patrzałek, M. Daczewska, and K. Jagla, "Model organisms in the fight against muscular dystrophy: Lessons from drosophila and zebrafish", *Molecules*, vol. 20, no. 4, pp. 6237–6253, 2015.

[99] C. A. MacRae and R. T. Peterson, "Zebrafish as tools for drug discovery", *Nature reviews Drug discovery*, vol. 14, no. 10, pp. 721–731, 2015.

[100] D. M. Parichy, "Evolution of danio pigment pattern development", *Heredity*, vol. 97, no. 3, pp. 200–210, 2006.

[101] F. R. Khan and S. S. Alhewairini, "Zebrafish (danio rerio) as a model organism", *Current trends in cancer management*, vol. 27, pp. 3–18, 2018.

[102] A. V. Gore, K. Monzo, Y. R. Cha, W. Pan, and B. M. Weinstein, "Vascular development in the zebrafish", *Cold Spring Harbor perspectives in medicine*, vol. 2, no. 5, a006684, 2012.

[103] J. Kanungo, E. Cuevas, S. F Ali, and M. G. Paule, "Zebrafish model in drug safety assessment", *Current Pharmaceutical Design*, vol. 20, no. 34, pp. 5416–5429, 2014.

[104] A. V. Kalueff, A. M. Stewart, and R. Gerlai, "Zebrafish as an emerging model for studying complex brain disorders", *Trends in pharmacological sciences*, vol. 35, no. 2, pp. 63–75, 2014.

[105] J. R. Guyon, L. S. Steffen, M. H. Howell, T. J. Pusack, C. Lawrence, and L. M. Kunkel, "Modeling human muscle disease in zebrafish", *Biochimica et Biophysica Acta (BBA)-Molecular Basis of Disease*, vol. 1772, no. 2, pp. 205–215, 2007.

[106] B. M. Weinstein, "Vascular cell biology in vivo: A new piscine paradigm?", *Trends in cell biology*, vol. 12, no. 9, pp. 439–445, 2002.

[107] G. J. Lieschke, A. C. Oates, M. O. Crowhurst, A. C. Ward, and J. E. Layton, "Morphologic and functional characterization of granulocytes and macrophages in embryonic and adult zebrafish", *Blood, The Journal of the American Society of Hematology*, vol. 98, no. 10, pp. 3087–3096, 2001.

[108] C. Santoriello, L. I. Zon, *et al.*, "Hooked! modeling human disease in zebrafish", *The Journal of clinical investigation*, vol. 122, no. 7, pp. 2337–2343, 2012.

[109] J. Jung, "Human tumor xenograft models for preclinical assessment of anticancer drug development", *Toxicological research*, vol. 30, pp. 1–5, 2014.

[110] J. Yin, G. Zhao, H. Kalirai, *et al.*, "Zebrafish patient-derived xenograft model as a preclinical platform for uveal melanoma drug discovery", *Pharmaceuticals*, vol. 16, no. 4, p. 598, 2023.

[111] H. Gao, J. M. Korn, S. Ferretti, *et al.*, "High-throughput screening using patient-derived tumor xenografts to predict clinical trial drug response", *Nature medicine*, vol. 21, no. 11, pp. 1318–1325, 2015.

[112] K. R. Astell and D. Sieger, "Zebrafish in vivo models of cancer and metastasis", *Cold Spring Harbor perspectives in medicine*, vol. 10, no. 8, 2020.

[113] L. Mercatali, F. La Manna, A. Groenewoud, *et al.*, "Development of a patient-derived xenograft (pdx) of breast cancer bone metastasis in a zebrafish model", *International journal of molecular sciences*, vol. 17, no. 8, p. 1375, 2016.

[114] S. Okada, K. Vaeteewoottacharn, and R. Kariya, "Establishment of a patient-derived tumor xenograft model and application for precision cancer medicine", *Chemical and Pharmaceutical Bulletin*, vol. 66, no. 3, pp. 225–230, 2018.

[115] J. Jung, H. S. Seol, and S. Chang, "The generation and application of patient-derived xenograft model for cancer research", *Cancer research and treatment: official journal of Korean Cancer Association*, vol. 50, no. 1, pp. 1–10, 2018.

[116] A. T. Byrne, D. G. Alférez, F. Amant, *et al.*, "Interrogating open issues in cancer precision medicine with patient-derived xenografts", *Nature Reviews Cancer*, vol. 17, no. 4, pp. 254–268, 2017.

[117] N. Amirouchene-Angelozzi, F. Nemati, D. Gentien, *et al.*, "Establishment of novel cell lines recapitulating the genetic landscape of uveal melanoma and preclinical validation of mtor as a therapeutic target", *Molecular Oncology*, vol. 8, no. 8, pp. 1508–1520, 2014.

[118] X. Li and M. Li, "The application of zebrafish patient-derived xenograft tumor models in the development of antitumor agents", *Medicinal Research Reviews*, vol. 43, no. 1, pp. 212–236, 2023.

[119] H. Amawi, A. A. Aljabali, S. H. Boddu, *et al.*, "The use of zebrafish model in prostate cancer therapeutic development and discovery", *Cancer Chemotherapy and Pharmacology*, vol. 87, pp. 311–325, 2021.

[120] J. W. Astin and P. S. Crosier, "Lymphatics, cancer and zebrafish", *Cancer and Zebrafish: Mechanisms, Techniques, and Models*, pp. 199–218, 2016.

[121] C. Tulotta, S. He, W. Van Der Ent, *et al.*, "Imaging cancer angiogenesis and metastasis in a zebrafish embryo model", *Cancer and Zebrafish: Mechanisms, Techniques, and Models*, pp. 239–263, 2016.

[122] A. V. Gore, L. M. Pillay, M. Venero Galanternik, and B. M. Weinstein, "The zebrafish: A fintastic model for hematopoietic development and disease", *Wiley Interdisciplinary Reviews: Developmental Biology*, vol. 7, no. 3, e312, 2018.

[123] N. Osmani and J. G. Goetz, "Multiscale imaging of metastasis in zebrafish", *Trends in cancer*, vol. 5, no. 12, pp. 766–778, 2019.

[124] J. F. Amatruda, J. L. Shepard, H. M. Stern, and L. I. Zon, "Zebrafish as a cancer model system", *Cancer cell*, vol. 1, no. 3, pp. 229–231, 2002.

[125] D. A. Morilak, G. Barrera, D. J. Echevarria, *et al.*, "Role of brain norepinephrine in the behavioral response to stress", *Progress in Neuro- Psychopharmacology and Biological Psychiatry*, vol. 29, no. 8, pp. 1214–1224, 2005.

[126] J. P. Herman and W. E. Cullinan, "Neurocircuitry of stress: Central control of the hypothalamo–pituitary–adrenocortical axis", *Trends in neurosciences*, vol. 20, no. 2, pp. 78–84, 1997.

[127] P. Sawchenko, H.-Y. Li, and A. Ericsson, "Circuits and mechanisms governing hypothalamic responses to stress: A tale of two paradigms", *Progress in brain research*, vol. 122, pp. 61–78, 2000.

[128] T. A. Day, "Defining stress as a prelude to mapping its neurocircuitry: No help from allostasis", *Progress in Neuro-Psychopharmacology and Biological Psychiatry*, vol. 29, no. 8, pp. 1195–1200, 2005.

[129] J. Axelrod and T. D. Reisine, "Stress hormones: Their interaction and regulation", *Science*, vol. 224, no. 4648, pp. 452–459, 1984.

[130] I. J. Kopin, "Definitions of stress and sympathetic neuronal responses.", *Annals of the New York Academy of Sciences*, vol. 771, pp. 19–30, 1995.

[131] T. O'connor, D. O'halloran, and F. Shanahan, "The stress response and the hypothalamic-pituitary-adrenal axis: From molecule to melancholia", *Qjm*, vol. 93, no. 6, pp. 323–333, 2000.

[132] P. J. Steenbergen, M. K. Richardson, and D. L. Champagne, "The use of the zebrafish model in stress research", *Progress in Neuro-Psychopharmacology and Biological Psychiatry*, vol. 35, no. 6, pp. 1432–1451, 2011.

[133] A. B. Silverberg, S. D. Shah, M. W. Haymond, and P. E. Cryer, "Norepinephrine: Hormone and neurotransmitter in man.", *American Journal of Physiology-Endocrinology and Metabolism*, vol. 234, no. 3, E252, 1978.

[134] J. A. Herd, "Cardiovascular response to stress", *Physiological reviews*, vol. 71, no. 1, pp. 305–330, 1991.

[135] R. M. Weinshilboum, N. B. Thoa, D. G. Johnson, I. J. Kopin, and J. Axelrod, "Proportional release of norepinephrine and dopamine-β-hydroxylase from sympathetic nerves", *Science*, vol. 174, no. 4016, pp. 1349–1351, 1971.

[136] G. F. WOOTEN, N. B. THOA, I. J. KOPIN, and J. AXELROD, "Enhanced release of dopamine β-hydroxylase and norepinephrine from sympathetic nerves by dibutyryl cyclic adenosine 3', 5'-monophosphate and theophylline", *Molecular Pharmacology*, vol. 9, no. 2, pp. 178–183, 1973.

[137] G. J. Palmer, M. G. Ziegler, and C. R. Lake, "Response of norepinephrine and blood pressure to stress increases with age", *Journal of Gerontology*, vol. 33, no. 4, pp. 482–487, 1978.

[138] P. E. Cryer, "Isotope derivative measurements of plasma norepinephrine and epinephrine in man", *Diabetes*, vol. 25, no. 11, pp. 1071–1082, 1976.

[139] J. Wortsman, "Role of epinephrine in acute stress", *Endocrinology and Metabolism Clinics*, vol. 31, no. 1, pp. 79–106, 2002.

[140] S. L. Lightman, M. T. Birnie, and B. L. Conway-Campbell, "Dynamics of acth and cortisol secretion and implications for disease", *Endocrine reviews*, vol. 41, no. 3, bnaa002, 2020.

[141] E. R. De Kloet, M. S. Oitzl, and M. Joëls, "Stress and cognition: Are corticosteroids good or bad guys?", *Trends in neurosciences*, vol. 22, no. 10, pp. 422–426, 1999.

[142] B. A. Barton and G. K. Iwama, "Physiological changes in fish from stress in aquaculture with emphasis on the response and effects of corticosteroids", *Annual Review of fish diseases*, vol. 1, pp. 3–26, 1991.

[143] F. Sharif, P. J. Steenbergen, J. R. Metz, and D. L. Champagne, "Long-lasting effects of dexamethasone on immune cells and wound healing in the zebrafish", *Wound Repair and Regeneration*, vol. 23, no. 6, pp. 855–865, 2015.

[144] C. Kiank, B. Holtfreter, A. Starke, A. Mundt, C. Wilke, and C. Schutt, "Stress susceptibility predicts the severity of immune depression and the failure to combat bacterial infections in chronically stressed mice", *Brain, behavior, and immunity*, vol. 20, no. 4, pp. 359–368, 2006.

[145] L. I. Partecke, S. Speerforck, A. Kading, *et al.*, "Chronic stress increases experimental pancreatic cancer growth, reduces survival and can be antagonised by beta-adrenergic receptor blockade", *Pancreatology*, vol. 16, no. 3, pp. 423–433, 2016.

[146] S. W. Cole and A. K. Sood, "Molecular pathways: Beta-adrenergic signaling in cancer", *Clinical cancer research*, vol. 18, no. 5, pp. 1201–1206, 2012.

[147] P. H. Thaker, L. Y. Han, A. A. Kamat, *et al.*, "Chronic stress promotes tumor growth and angiogenesis in a mouse model of ovarian carcinoma", *Nature medicine*, vol. 12, no. 8, pp. 939–944, 2006.

[148] D. G. Bernabé, A. C. Tamae, É. R. Biasoli, and S. H. Oliveira, "Stress hormones increase cell proliferation and regulates interleukin-6 secretion in human oral squamous cell carcinoma cells", *Brain, behavior, and immunity*, vol. 25, no. 3, pp. 574–583, 2011.

[149] J. W.-L. Eng, K. M. Kokolus, C. B. Reed, B. L. Hylander, W. W. Ma, and E. A. Repasky, "A nervous tumor microenvironment: The impact of adrenergic stress on cancer cells, immunosuppression, and immunotherapeutic response", *Cancer Immunology, Immunotherapy*, vol. 63, pp. 1115–1128, 2014.

[150] K. v. quc Lu'o'ng and L. T. H. Nguyn, "The roles of beta-adrenergic receptors in tumorigenesis and the possible use of beta-adrenergic blockers for cancer treatment: Possible genetic and cell-signaling mechanisms", *Cancer management and research*, pp. 431–445, 2012.

[151] G. L. Stiles, M. G. Caron, and R. J. Lefkowitz, "Beta-adrenergic receptors: Biochemical mechanisms of physiological regulation", *Physiological reviews*, vol. 64, no. 2, pp. 661–743, 1984.

[152] R. Mehvar and D. R. Brocks, "Stereospecific pharmacokinetics and pharmacodynamics of beta-adrenergic blockers in humans", 2001.

[153] R. Rabkin, D. P. Stables, N. W. Levin, and M. M. Suzman, "The prophylactic value of propranolol in angina pectoris", *The American journal of cardiology*, vol. 18, no. 3, pp. 370–380, 1966.

[154] J. W. Black, "Ahlquist and the development of beta-adrenoceptor antagonists.", *Postgraduate Medical Journal*, vol. 52, pp. 11–13, 1976.

[155] M. P. Stapleton, "Sir james black and propranolol. the role of the basic sciences in the history of cardiovascular pharmacology.", *Texas Heart Institute Journal*, vol. 24, no. 4, p. 336, 1997.

[156] E. Besterman and D. Friedlander, "Clinical experiences with propranolol.", *Postgraduate Medical Journal*, vol. 41, no. 479, p. 526, 1965.

[157] B. Prichard and P. Gillam, "Treatment of hypertension with propranolol", *Br Med J*, vol. 1, no. 5635, pp. 7–16, 1969.

[158] S. Goldstein, "Propranolol therapy in patients with acute myocardial infarction: The beta-blocker heart attack trial.", *Circulation*, vol. 67, no. 6 Pt 2, pp. I53–7, 1983.

[159] M. Ogrodowczyk, K. Dettlaff, and A. Jelinska, "Beta-blockers: Current state of knowledge and perspectives", *Mini reviews in medicinal chemistry*, vol. 16, no. 1, pp. 40–54, 2016.

[160] P. Turner, K. Granville-Grossman, and J. Smart, "Effect of adrenergic receptor blockade on the tachycardia of thyrotoxicosis and anxiety state", *The Lancet*, vol. 286, no. 7426, pp. 1316–1318, 1965.

[161] A. V. Srinivasan, "Propranolol: A 50-year historical perspective", *Annals of Indian academy of neurology*, vol. 22, no. 1, p. 21, 2019.

[162] R. Dulbecco and M. Vogt, "Plaque formation and isolation of pure lines with poliomyelitis viruses", *The Journal of experimental medicine*, vol. 99, no. 2, pp. 167–182, 1954.

[163] T. Mezhebovsky, E. Routhier, P. Sass, and Z. Shahrokh, "Enabling freeze-thaw stability of pbs-based formulations of a monoclonal antibody", *BioPharm Int*, vol. 29, pp. 33–39, 2016.

[164] A. A. Thorat and R. Suryanarayanan, "Characterization of phosphate buffered saline (pbs) in frozen state and after freeze-drying", *Pharmaceutical research*, vol. 36, pp. 1–11, 2019.

[165] T. A. McCoy, M. Maxwell, and P. F. Kruse Jr, "Amino acid requirements of the novikoff hepatoma in vitro.", *Proceedings of the Society for Experimental biology and Medicine*, vol. 100, no. 1, pp. 115–118, 1959.

[166] G. Moore, E. Ito, K. Ulrich, and A. Sandberg, "Culture of human leukemia cells", *Cancer*, vol. 19, no. 5, pp. 713–723, 1966.

[167] G. Moore, D. Mount, G. Tara, and N. Schwartz, "Growth of human tumor cells in suspension cultures", *Cancer Research*, vol. 23, no. 11, pp. 1735–1741, 1963.

[168] H.-K. S. Leiros, B. O. Brandsdal, O. A. Andersen, *et al.*, "Trypsin specificity as elucidated by lie calculations, x-ray structures, and association constant measurements", *Protein science*, vol. 13, no. 4, pp. 1056–1070, 2004.

[169] I. Johnson, *Molecular Probes Handbook: A Guide to Fluorescent Probes and Labeling Technologies*. Life Technologies Corporation, 2010, ISBN: 9780982927915. [Online]. Available: `https://books.google.gr/books?id=djuacQAACAAJ`.

[170] R. Haugland, "Molecular probes. handbook of molecular probes and research chemicals. molecular probes", *Inc., Eugene, Oregon*, 1989.

[171] G. Y. Wiederschain, "The molecular probes handbook. a guide to fluorescent probes and labeling technologies", *Biochemistry (Moscow)*, vol. 76, no. 11, pp. 1276–1277, 2011.

[172] F. Ledley, H. Soriano, B. O'Malley Jr, D. Lewis, G. Darlington, and M. Finegold, "Dii as a marker for cellular transplantation into solid organs.", *Biotechniques*, vol. 13, no. 4, pp. 580–582, 1992.

[173] M. G. Honig and R. I. Hume, "Dil and dio: Versatile fluorescent dyes for neuronal labelling and pathway tracing", *Trends in neurosciences*, vol. 12, no. 9, pp. 333–341, 1989.

[174] T. A. McCoy and R. E. Neuman, "The cultivation of walker carcinosarcoma 256 in vitro from cell suspensions", *Journal of the National Cancer Institute*, vol. 16, no. 5, pp. 1221–1229, 1956.

[175] M. Westerfield, "The zebrafish book; a guide for the laboratory use of zebrafish (danio rerio)", *(No Title)*, 2007.

[176] C. Nusslein-Volhard and R. Dahm, *Zebrafish*. Oxford University Press, 2002.

[177] M. A. Ansari, Z. Fatima, and S. Hameed, "Antifungal action of methylene blue involves mitochondrial dysfunction and disruption of redox and membrane homeostasis in c. albicans", *The open microbiology journal*, vol. 10, p. 12, 2016.

[178] J. Karlsson, J. Von Hofsten, and P.-E. Olsson, "Generating transparent zebrafish: A refined method to improve detection of gene expression during embryonic development", *Marine biotechnology*, vol. 3, pp. 522–527, 2001.

[179] J. R. Meyers, "Zebrafish: Development of a vertebrate model organism", *Current Protocols Essential Laboratory Techniques*, vol. 16, no. 1, e19, 2018.

[180] C. Leyden, T. Brueggemann, F. Debinski, C. A. Simacek, F. A. Dehmelt, and A. B. Arrenberg, "Efficacy of tricaine (ms-222) and hypothermia as anesthetic agents for blocking sensorimotor responses in larval zebrafish", *Frontiers in Veterinary Science*, vol. 9, p. 864 573, 2022.

[181] K. Lidster, G. D. Readman, M. J. Prescott, and S. F. Owen, "International survey on the use and welfare of zebrafish danio rerio in research", *Journal of fish biology*, vol. 90, no. 5, pp. 1891–1905, 2017.

[182] W.-C. Huang, Y.-S. Hsieh, I.-H. Chen, *et al.*, "Combined use of ms-222 (tricaine) and isoflurane extends anesthesia time and minimizes cardiac rhythm side effects in adult zebrafish", *Zebrafish*, vol. 7, no. 3, pp. 297–304, 2010.

[183] P. A. Erickson, N. A. Ellis, and C. T. Miller, "Microinjection for transgenesis and genome editing in threespine sticklebacks", *JoVE (Journal of Visualized Experiments)*, no. 111, e54055, 2016.

[184] L. Sun, L. Xin, Z. Peng, *et al.*, "Toxicity and enantiospecific differences of two β-blockers, propranolol and metoprolol, in the embryos and larvae of zebrafish (danio rerio)", *Environmental toxicology*, vol. 29, no. 12, pp. 1367–1378, 2014.

[185] A. Jenkins, P. Kratochvil, R. Stepto, and U. Suter, "Glossary of basic terms in polymer science (iupac recommendations 1996)", *Pure and applied chemistry*, vol. 68, no. 12, pp. 2287–2311, 1996.

[186] W. H. Carothers, "Polymers and polyfunctionality", *Transactions of the Faraday Society*, vol. 32, pp. 39–49, 1936.

[187] K. Ito and Y. Yamashita, "Copolymer composition and microstructure", *Journal of Polymer Science Part A: General Papers*, vol. 3, no. 6, pp. 2165–2187, 1965.

[188] I. W. Hamley, "Block copolymers", *Encyclopedia of Polymer Science and Technology*, vol. 1, 2002.

[189] H. Feng, X. Lu, W. Wang, N.-G. Kang, and J. W. Mays, "Block copolymers: Synthesis, self-assembly, and applications", *Polymers*, vol. 9, no. 10, p. 494, 2017.

[190] H. Mark, "The synthesis and applicability of block and graft copolymers", *Textile Research Journal*, vol. 23, no. 5, pp. 294–298, 1953.

[191] W. Ring, I. Mita, A. Jenkins, and N. Bikales, "Source-based nomenclature for copolymers (recommendations 1985)", *Pure and applied chemistry*, vol. 57, no. 10, pp. 1427–1440, 1985.

[192] J. Kinsinger, J. Bartlett, and W. Rauscher, "On the colligative nature of the specific refractive increment for statistical copolymers", *Journal of Applied Polymer Science*, vol. 6, no. 23, pp. 529–532, 1962.

[193] Y. Hu, W. A. Daoud, K. K. L. Cheuk, and C. S. K. Lin, "Newly developed techniques on polycondensation, ring-opening polymerization and polymer modification: Focus on poly (lactic acid)", *Materials*, vol. 9, no. 3, p. 133, 2016.

[194] G. S. Kwon, "Diblock copolymer nanoparticles for drug delivery", *Critical Reviews™ in Therapeutic Drug Carrier Systems*, vol. 15, no. 5, 1998.

[195] P. Dubois, O. Coulembier, and J.-M. Raquez, *Handbook of ring-opening polymerization*. John Wiley & Sons, 2009.

[196] R. Z. Xiao, Z. W. Zeng, G. L. Zhou, J. J. Wang, F. Z. Li, and A. M. Wang, "Recent advances in peg–pla block copolymer nanoparticles", *International journal of nanomedicine*, vol. 5, p. 1057, 2010.

[197] K. K. Jain, "Drug delivery systems-an overview", *Drug delivery systems*, pp. 1–50, 2008.

[198] S. S. Venkatraman, P. Jie, F. Min, B. Y. C. Freddy, and G. Leong-Huat, "Micelle-like nanoparticles of pla–peg–pla triblock copolymer as chemotherapeutic carrier", *International journal of pharmaceutics*, vol. 298, no. 1, pp. 219–232, 2005.

[199] C.-H. Tsai, P.-Y. Wang, I.-C. Lin, H. Huang, G.-S. Liu, and C.-L. Tseng, "Ocular drug delivery: Role of degradable polymeric nanocarriers for ophthalmic application", *International journal of molecular sciences*, vol. 19, no. 9, p. 2830, 2018.

[200] L. Zhang, J. M. Chan, F. X. Gu, *et al.*, "Self-assembled lipid- polymer hybrid nanoparticles: A robust drug delivery platform", *ACS nano*, vol. 2, no. 8, pp. 1696–1702, 2008.

[201] W. Gao, J. M. Chan, and O. C. Farokhzad, "Ph-responsive nanoparticles for drug delivery", *Molecular pharmaceutics*, vol. 7, no. 6, pp. 1913–1920, 2010.

[202] R. D. Dhande, A. A. Patel, and H. P. Thakkar, "Nanopharmaceuticals: A boon or bane",

[203] R. Davidson, A. Scott, M. Maini, A. Bryceson, and S. Croft, "Liposomal amphotericin b in drug-resistant visceral leishmaniasis", *The Lancet*, vol. 337, no. 8749, pp. 1061–1062, 1991.

[204] P. Guaglianone, K. Chan, E. DelaFlor-Weiss, *et al.*, "Phase i and pharmacologie study of liposomal daunorubicin (daunoxome)", *Investigational new drugs*, vol. 12, pp. 103–110, 1994.

[205] A. Gabizon, T. Peretz, A. Sulkes, *et al.*, "Systemic administration of doxorubicin -containing liposomes in cancer patients: A phase i study", *European Journal of Cancer and Clinical Oncology*, vol. 25, no. 12, pp. 1795–1803, 1989.

[206] V. J. Lingayat, N. S. Zarekar, and R. S. Shendge, "Solid lipid nanoparticles: A review", *Nanoscience and Nanotechnology Research*, vol. 4, no. 2, pp. 67–72, 2017.

[207] W. Mehnert and K. Mader, "Solid lipid nanoparticles: Production, characterization and applications", *Advanced drug delivery reviews*, vol. 64, pp. 83–101, 2012.

[208] G. P. Zara, R. Cavalli, A. Bargoni, A. Fundarò, D. Vighetto, and M. R. Gasco, "Intravenous administration to rabbits of non-stealth and stealth doxorubicin-loaded solid lipid nanoparticles at increasing concentrations of stealth agent: Pharmacokinetics and distribution of doxorubicin in brain and other tissues", *Journal of drug targeting*, vol. 10, no. 4, pp. 327–335, 2002.

[209] A. Banerjee and H. Onyuksel, "Peptide delivery using phospholipid micelles", *Wiley Interdisciplinary Reviews: Nanomedicine and Nanobiotechnology*, vol. 4, no. 5, pp. 562–574, 2012.

[210] C. R. Sanders II, B. J. Hare, K. P. Howard, and J. H. Prestegard, "Magnetically-oriented phospholipid micelles as a tool for the study of membrane-associated molecules", *Progress in Nuclear Magnetic Resonance Spectroscopy*, vol. 26, pp. 421–444, 1994.

[211] A. Krishnadas, I. Rubinstein, and H. Onyuksel, "Sterically stabilized phospholipid mixed micelles: In vitro evaluation as a novel carrier for water-insoluble drugs", *Pharmaceutical research*, vol. 20, pp. 297–302, 2003.

[212] G. Cavallaro, L. Maniscalco, M. Licciardi, and G. Giammona, "Tamoxifen-loaded polymeric micelles: Preparation, physico-chemical characterization and in vitro evaluation studies", *Macromolecular Bioscience*, vol. 4, no. 11, pp. 1028–1038, 2004.

[213] D. Le Garrec, S. Gori, L. Luo, *et al.*, "Poly (n-vinylpyrrolidone)-block-poly (d, l-lactide) as a new polymeric solubilizer for hydrophobic anticancer drugs: In vitro and in vivo evaluation", *Journal of controlled release*, vol. 99, no. 1, pp. 83–101, 2004.

[214] S. C. Yang, L. F. Lu, Y. Cai, J. B. Zhu, B. W. Liang, and C. Z. Yang, "Body distribution in mice of intravenously injected camptothecin solid lipid nanoparticles and targeting effect on brain", *Journal of controlled release*, vol. 59, no. 3, pp. 299–307, 1999.

[215] G. S. Kwon and T. Okano, "Polymeric micelles as new drug carriers", *Advanced drug delivery reviews*, vol. 21, no. 2, pp. 107–116, 1996.

[216] H. M. Aliabadi and A. Lavasanifar, "Polymeric micelles for drug delivery", *Expert opinion on drug delivery*, vol. 3, no. 1, pp. 139–162, 2006.

[217] S. Croy and G. Kwon, "Polymeric micelles for drug delivery", *Current pharmaceutical design*, vol. 12, no. 36, pp. 4669–4684, 2006.

[218] A. S. Chauhan, N. K. Jain, P. V. Diwan, and A. J. Khopade, "Solubility enhancement of indomethacin with poly (amidoamine) dendrimers and targeting to inflammatory regions of arthritic rats", *Journal of drug targeting*, vol. 12, no. 9-10, pp. 575–583, 2004.

[219] P. Tripathi, A. Khopade, S. Nagaich, S. Shrivastava, S. Jain, and N. Jain, "Dendrimer grafts for delivery of 5-fluorouracil.", *Die Pharmazie*, vol. 57, no. 4, pp. 261–264, 2002.

[220] M. Hussain, M. Shchepinov, M. Sohail, *et al.*, "A novel anionic dendrimer for improved cellular delivery of antisense oligonucleotides", *Journal of Controlled Release*, vol. 99, no. 1, pp. 139–155, 2004.

[221] K. Hadinoto, A. Sundaresan, and W. S. Cheow, "Lipid–polymer hybrid nanoparticles as a new generation therapeutic delivery platform: A review", *European journal of pharmaceutics and biopharmaceutics*, vol. 85, no. 3, pp. 427–443, 2013.

[222] B. Mandal, H. Bhattacharjee, N. Mittal, *et al.*, "Core–shell-type lipid–polymer hybrid nanoparticles as a drug delivery platform", *Nanomedicine: Nanotechnology, Biology and Medicine*, vol. 9, no. 4, pp. 474–491, 2013.

[223] A. F. Thunemann, M. Muller, H. Dautzenberg, J.-F. Joanny, and H. Lowen, "Polyelectrolyte complexes", *Polyelectrolytes with defined molecular architecture II*, pp. 113–171, 2004.

[224] M. Muller, "Sizing, shaping and pharmaceutical applications of polyelectrolyte complex nanoparticles", *Polyelectrolyte Complexes in the Dispersed and Solid State II: Application Aspects*, pp. 197–260, 2014.

[225] L. Jia, R. Wang, and Y. Fan, "Encapsulation and release of drug nanoparticles in functional polymeric vesicles", *Soft Matter*, vol. 16, no. 12, pp. 3088–3095, 2020.

[226] C. Altavilla and E. Ciliberto, "Inorganic nanoparticles: Synthesis, applications and perspectives—an overview", *Inorganic Nanoparticles: Synthesis, Applications, and Perspectives. ed by Altavilla C and Ciliberto E, CRC Press, New York*, pp. 1–17, 2011.

[227] Z. P. Xu, Q. H. Zeng, G. Q. Lu, and A. B. Yu, "Inorganic nanoparticles as carriers for efficient cellular delivery", *Chemical Engineering Science*, vol. 61, no. 3, pp. 1027–1040, 2006.

[228] D. A. Giljohann, D. S. Seferos, W. L. Daniel, M. D. Massich, P. C. Patel, and C. A. Mirkin, "Gold nanoparticles for biology and medicine", *Spherical Nucleic Acids*, pp. 55–90, 2020.

[229] R. Sardar, A. M. Funston, P. Mulvaney, and R. W. Murray, "Gold nanoparticles: Past, present, and future", *Langmuir*, vol. 25, no. 24, pp. 13 840–13 851, 2009.

[230] A. Kumar, H. Ma, X. Zhang, *et al.*, "Gold nanoparticles functionalized with therapeutic and targeted peptides for cancer treatment", *Biomaterials*, vol. 33, no. 4, pp. 1180–1189, 2012.

[231] R. Kodama, "Magnetic nanoparticles", *Journal of magnetism and magnetic materials*, vol. 200, no. 1-3, pp. 359–372, 1999.

[232] T. Indira and P. Lakshmi, "Magnetic nanoparticles–a review", *International Journal of Pharmaceutical Sciences and Nanotechnology (IJPSN)*, vol. 3, no. 3, pp. 1035–1042, 2010.

[233] A. Avasthi, C. Caro, E. Pozo-Torres, M. P. Leal, and M. L. Garcia-Martin, "Magnetic nanoparticles as mri contrast agents", *Surface-modified Nanobiomaterials for Electrochemical and Biomedicine Applications*, pp. 49–91, 2020.

[234] M. M. Rahman, M. R. Karim, H. F. Alharbi, B. Aldokhayel, T. Uzzaman, and H. Zahir, "Cadmium selenide quantum dots for solar cell applications: A review", *Chemistry–An Asian Journal*, vol. 16, no. 8, pp. 902–921, 2021.

[235] M. A. Reed, "Quantum dots", *Scientific American*, vol. 268, no. 1, pp. 118–123, 1993.

[236] M. A. Dobrovolskaia, "Nucleic acid nanoparticles at a crossroads of vaccines and immunotherapies", *Molecules*, vol. 24, no. 24, p. 4620, 2019.

[237] S. Raj, S. Khurana, R. Choudhari, *et al.*, "Specific targeting cancer cells with nanoparticles and drug delivery in cancer therapy", in *Seminars in cancer biology*, Elsevier, vol. 69, 2021, pp. 166–177.

[238] Y. Hoshino, T. Kodama, Y. Okahata, and K. J. Shea, "Peptide imprinted polymer nanoparticles: A plastic antibody", *Journal of the American Chemical Society*, vol. 130, no. 46, pp. 15 242–15 243, 2008.

[239] Y. Zhong, F. Meng, C. Deng, and Z. Zhong, "Ligand-directed active tumor - targeting polymeric nanoparticles for cancer chemotherapy", *Biomacromolecules*, vol. 15, no. 6, pp. 1955–1969, 2014.

[240] Y. Liu, Z. Chen, C. Liu, D. Yu, Z. Lu, and N. Zhang, "Gadolinium-loaded polymeric nanoparticles modified with anti-vegf as multifunctional mri contrast agents for the diagnosis of liver cancer", *Biomaterials*, vol. 32, no. 22, pp. 5167–5176, 2011.

[241] J. Balegamire, M. Vandamme, E. Chereul, *et al.*, "Iodinated polymer nanoparticles as contrast agent for spectral photon counting computed tomography", *Biomaterials Science*, vol. 8, no. 20, pp. 5715–5728, 2020.

[242] E. Kang, H. S. Min, J. Lee, *et al.*, "Nanobubbles from gas-generating polymeric nanoparticles: Ultrasound imaging of living subjects", *Angewandte Chemie*, vol. 122, no. 3, pp. 534–538, 2010.

[243] P. Howes, M. Green, A. Bowers, *et al.*, "Magnetic conjugated polymer nanoparticles as bimodal imaging agents", *Journal of the American Chemical Society*, vol. 132, no. 28, pp. 9833–9842, 2010.

[244] A. Reisch and A. S. Klymchenko, "Fluorescent polymer nanoparticles based on dyes: Seeking brighter tools for bioimaging", *Small*, vol. 12, no. 15, pp. 1968–1992, 2016.

[245] M. Zohri, T. Gazori, S. Mirdamadi, A. Asadi, and I. Haririan, "Polymeric nanoparticles: Production, applications and advantage", *Internet J Nanotechnol*, vol. 3, no. 1, 2009.

[246] T. Akagi, M. Baba, and M. Akashi, "Preparation of nanoparticles by the self-organization of polymers consisting of hydrophobic and hydrophilic segments: Potential applications", *Polymer*, vol. 48, no. 23, pp. 6729–6747, 2007.

[247] M.-C. Jones and J.-C. Leroux, "Polymeric micelles–a new generation of colloidal drug carriers", *European journal of pharmaceutics and biopharmaceutics*, vol. 48, no. 2, pp. 101–111, 1999.

[248] M. Ghezzi, S. Pescina, C. Padula, *et al.*, "Polymeric micelles in drug delivery: An insight of the techniques for their characterization and assessment in biorelevant conditions", *Journal of Controlled Release*, vol. 332, pp. 312–336, 2021.

[249] D. Dendukuri, T. A. Hatton, and P. S. Doyle, "Synthesis and self-assembly of amphiphilic polymeric microparticles", *Langmuir*, vol. 23, no. 8, pp. 4669–4674, 2007.

[250] Y. Sanada, I. Akiba, K. Sakurai, *et al.*, "Hydrophobic molecules infiltrating into the poly (ethylene glycol) domain of the core/shell interface of a polymeric micelle: Evidence obtained with anomalous small-angle x-ray scattering", *Journal of the American Chemical Society*, vol. 135, no. 7, pp. 2574–2582, 2013.

[251] J. Akimoto, M. Nakayama, and T. Okano, "Temperature-responsive polymeric micelles for optimizing drug targeting to solid tumors", *Journal of controlled release*, vol. 193, pp. 2–8, 2014.

[252] U. Gaur, S. K. Sahoo, K. De Tapas, P. C. Ghosh, A. Maitra, and P. Ghosh, "Biodistribution of fluoresceinated dextran using novel nanoparticles evading reticuloendothelial system", *International journal of pharmaceutics*, vol. 202, no. 1-2, pp. 1–10, 2000.

[253] K. E. Uhrich, S. M. Cannizzaro, R. S. Langer, and K. M. Shakesheff, "Polymeric systems for controlled drug release", *Chemical reviews*, vol. 99, no. 11, pp. 3181–3198, 1999.

[254] T. Niwa, H. Takeuchi, T. Hino, N. Kunou, and Y. Kawashima, "Preparations of biodegradable nanospheres of water-soluble and insoluble drugs with d, l-lactide/glycolide copolymer by a novel spontaneous emulsification solvent diffusion method, and the drug release behavior", *Journal of controlled release*, vol. 25, no. 1-2, pp. 89–98, 1993.

[255] W. Zhou, C. Li, Z. Wang, W. Zhang, and J. Liu, "Factors affecting the stability of drug-loaded polymeric micelles and strategies for improvement", *Journal of Nanoparticle Research*, vol. 18, pp. 1–18, 2016.

[256] Y. Wang, P. Li, T. Truong-Dinh Tran, J. Zhang, and L. Kong, "Manufacturing techniques and surface engineering of polymer based nanoparticles for targeted drug delivery to cancer", *Nanomaterials*, vol. 6, no. 2, p. 26, 2016.

[257] Z. L. Yang, X. R. Li, K. W. Yang, and Y. Liu, "Amphotericin b-loaded poly (ethylene glycol)–poly (lactide) micelles: Preparation, freeze-drying, and in vitro release", *Journal of Biomedical Materials Research Part A: An Official Journal of The Society for Biomaterials, The Japanese Society for Biomaterials, and The Australian Society for Biomaterials and the Korean Society for Biomaterials*, vol. 85, no. 2, pp. 539–546, 2008.

[258] Y. Luo, X. Yao, J. Yuan, T. Ding, and Q. Gao, "Preparation and drug controlled-release of polyion complex micelles as drug delivery systems", *Colloids and Surfaces B: Biointerfaces*, vol. 68, no. 2, pp. 218–224, 2009.

[259] R. Greenwald, "Peg drugs: An overview", *Journal of Controlled Release*, vol. 74, no. 1-3, pp. 159–171, 2001.

[260] T. Riley, C. Heald, S. Stolnik, *et al.*, "Core- shell structure of pla- peg nanoparticles used for drug delivery", *Langmuir*, vol. 19, no. 20, pp. 8428–8435, 2003.

[261] T. T. Hoang Thi, E. H. Pilkington, D. H. Nguyen, J. S. Lee, K. D. Park, and N. P. Truong, "The importance of poly (ethylene glycol) alternatives for overcoming peg immunogenicity in drug delivery and bioconjugation", *Polymers*, vol. 12, no. 2, p. 298, 2020.

[262] I. J. Koppen, I. J. Broekaert, M. Wilschanski, *et al.*, "Role of polyethylene glycol in the treatment of functional constipation in children", *Journal of pediatric gastroenterology and nutrition*, vol. 65, no. 4, pp. 361–363, 2017.

[263] M. A. Quadir, S. W. Morton, Z. J. Deng, *et al.*, "Peg–polypeptide block copolymers as ph-responsive endosome-solubilizing drug nanocarriers", *Molecular Pharmaceutics*, vol. 11, no. 7, pp. 2420–2430, 2014.

[264] Y.-C. Lin, H.-H. Tseng, and D. K. Wang, "Uncovering the effects of peg porogen molecular weight and concentration on ultrafiltration membrane properties and protein purification performance", *Journal of Membrane Science*, vol. 618, p. 118 729, 2021.

[265] F. Ebrahimi and H. Ramezani Dana, "Poly lactic acid (pla) polymers: From properties to biomedical applications", *International Journal of Polymeric Materials and Polymeric Biomaterials*, vol. 71, no. 15, pp. 1117–1130, 2022.

[266] D. W. Grijpma and A. J. Pennings, "(co) polymers of l-lactide, 2. mechanical properties", *Macromolecular Chemistry and Physics*, vol. 195, no. 5, pp. 1649–1663, 1994.

[267] K. Stefaniak and A. Masek, "Green copolymers based on poly (lactic acid) — short review", *Materials*, vol. 14, no. 18, p. 5254, 2021.

[268] N. Sharmin and C. D. Rudd, "Structure, thermal properties, dissolution behaviour and biomedical applications of phosphate glasses and fibres: A review", *Journal of Materials Science*, vol. 52, no. 15, pp. 8733–8760, 2017.

[269] S. Saeidlou, M. A. Huneault, H. Li, and C. B. Park, "Poly (lactic acid) crystallization", *Progress in Polymer Science*, vol. 37, no. 12, pp. 1657–1677, 2012.

[270] H. Tsuji and Y. Ikada, "Properties and morphologies of poly (l-lactide): 1. annealing condition effects on properties and morphologies of poly (l-lactide)", *Polymer*, vol. 36, no. 14, pp. 2709–2716, 1995.

[271] W. H. De Jong, J. E. Bergsma, J. E. Robinson, and R. R. Bos, "Tissue response to partially in vitro predegraded poly-l-lactide implants", *Biomaterials*, vol. 26, no. 14, pp. 1781–1791, 2005.

[272] W. Hoogsteen, A. Postema, A. Pennings, G. Ten Brinke, and P. Zugenmaier, "Crystal structure, conformation and morphology of solution-spun poly (l-lactide) fibers", *Macromolecules*, vol. 23, no. 2, pp. 634–642, 1990.

[273] T. C. Gamboa-Martinez, J. L. Gomez Ribelles, and G. Gallego Ferrer, "Fibrin coating on poly (l-lactide) scaffolds for tissue engineering", *Journal of Bioactive and Compatible Polymers*, vol. 26, no. 5, pp. 464–477, 2011.

[274] R. Falk, T. W. Randolph, J. D. Meyer, R. M. Kelly, and M. C. Manning, "Controlled release of ionic compounds from poly (l-lactide) microspheres produced by precipitation with a compressed antisolvent", *Journal of controlled release*, vol. 44, no. 1, pp. 77–85, 1997.

[275] C. Lee and S. Hong, "An overview of the synthesis and synthetic mechanism of poly (lactic acid)", *Mod. Chem. Appl*, vol. 2, no. 4, pp. 1–5, 2014.

[276] B. Neises and W. Steglich, "Esterification of carboxylic acids with dicyclohexylcarbodiimide /4-dimethylaminopyridine: Tert-butyl ethyl fumarate: (e)-2-butenedioic acid, ethyl 1, 1-dimethylethyl ester", *Organic Syntheses*, vol. 63, pp. 183–183, 2003.

[277] J. Li, S. Guo, M. Wang, L. Ye, and F. Yao, "Poly (lactic acid)/poly (ethylene glycol) block copolymer based shell or core cross-linked micelles for controlled release of hydrophobic drug", *RSC Advances*, vol. 5, no. 25, pp. 19 484–19 492, 2015.

[278] A. Lucke, J. Teßmar, E. Schnell, G. Schmeer, and A. Gφpferich, "Biodegradable poly (d, l-lactic acid)-poly (ethylene glycol)-monomethyl ether diblock copolymers: Structures and surface properties relevant to their use as biomaterials", *Biomaterials*, vol. 21, no. 23, pp. 2361–2370, 2000.

[279] T. H. Nguyen, A. Petchsuk, P. Tangboriboonrat, M. Opaprakasit, A. Sharp, and P. Opaprakasit, "Synthesis and characterizations of plla/peg block copolymers", in *Advanced Materials Research*, Trans Tech Publ, vol. 93, 2010, pp. 198–201.

[280] X. Zhang, U. P. Wyss, D. Pichora, and M. F. Goosen, "An investigation of the synthesis and thermal stability of poly (dl-lactide)", *Polymer Bulletin*, vol. 27, pp. 623–629, 1992.

[281] K. Soppimath and T. Aminabhavi, "Ethyl acetate as a dispersing solvent in the production of poly (dl-lactide-co-glycolide) microspheres: Effect of process parameters and polymer type", *Journal of microencapsulation*, vol. 19, no. 3, pp. 281–292, 2002.

[282] N. K. Pandit and D. Wang, "Salt effects on the diffusion and release rate of propranolol from poloxamer 407 gels", *International journal of pharmaceutics*, vol. 167, no. 1-2, pp. 183–189, 1998.

[283] M. Yu, W. Yuan, D. Li, A. Schwendeman, and S. P. Schwendeman, "Predicting drug release kinetics from nanocarriers inside dialysis bags", *Journal of Controlled Release*, vol. 315, pp. 23–30, 2019.

[284] G. Moreno-Bautista and K. C. Tam, "Evaluation of dialysis membrane process for quantifying the in vitro drug-release from colloidal drug carriers", *Colloids and Surfaces A: Physicochemical and Engineering Aspects*, vol. 389, no. 1-3, pp. 299–303, 2011.

[285] J. C. Moore, "Gel permeation chromatography. i. a new method for molecular weight distribution of high polymers", *Journal of Polymer Science Part A: General Papers*, vol. 2, no. 2, pp. 835–843, 1964.

[286] S. Balke, A. Hamielec, B. LeClair, and S. Pearce, "Gel permeation chromatography", *Industrial & Engineering Chemistry Product Research and Development*, vol. 8, no. 1, pp. 54–57, 1969.

[287] J. Urenjak, S. R. Williams, D. G. Gadian, and M. Noble, "Proton nuclear magnetic resonance spectroscopy unambiguously identifies different neural cell types", *Journal of Neuroscience*, vol. 13, no. 3, pp. 981–989, 1993.

[288] H. Booth, *Rm silverstein, gc bassler and tc morrill. spectrometric identification of organic compounds. wiley, chichester, 1991, pp. x+ 419,£ 50.25 (cloth), isbn 0 471 63404 2*, 1992.

[289] M. Balci, *Basic 1H-and 13C-NMR spectroscopy*. Elsevier, 2005.

[290] D. C. Joy and C. S. Joy, "Low voltage scanning electron microscopy", *Micron*, vol. 27, no. 3-4, pp. 247–263, 1996.

[291] K. D. Vernon-Parry, "Scanning electron microscopy: An introduction", *III-Vs Review*, vol. 13, no. 4, pp. 40–44, 2000.

[292] J. Pawley, "The development of field-emission scanning electron microscopy for imaging biological surfaces", *SCANNING-NEW YORK AND BADEN BADEN THEN MAHWAH-*, vol. 19, pp. 324–336, 1997.

[293] J. Stetefeld, S. A. McKenna, and T. R. Patel, "Dynamic light scattering: A practical guide and applications in biomedical sciences", *Biophysical reviews*, vol. 8, pp. 409–427, 2016.

[294] F. Babick, "Dynamic light scattering (dls)", in *Characterization of Nanoparticles*, Elsevier, 2020, pp. 137–172.

[295] M. Picollo, M. Aceto, and T. Vitorino, "Uv-vis spectroscopy", *Physical sciences reviews*, vol. 4, no. 4, 2019.

[296] H.-H. Perkampus, *UV-VIS Spectroscopy and its Applications*. Springer Science & Business Media, 2013.

[297] F. S. Rocha, A. J. Gomes, C. N. Lunardi, S. Kaliaguine, and G. S. Patience, "Experimental methods in chemical engineering: Ultraviolet visible spectroscopy—uv-vis", *The Canadian Journal of Chemical Engineering*, vol. 96, no. 12, pp. 2512–2517, 2018.

[298] A. Kriete and R. Eils, "Introducing computational systems biology", in *Computational Systems Biology*, Elsevier, 2006, pp. 1–14.

[299] E. C. Butcher, E. L. Berg, and E. J. Kunkel, "Systems biology in drug discovery", *Nature biotechnology*, vol. 22, no. 10, pp. 1253–1259, 2004.

[300] S. Merler, M. Ajelli, L. Fumanelli, *et al.*, "Spatiotemporal spread of the 2014 outbreak of ebola virus disease in liberia and the effectiveness of non-pharmaceutical interventions: A computational modelling analysis", *The Lancet Infectious Diseases*, vol. 15, no. 2, pp. 204–211, 2015.

[301] S. Y. Jessica and N. Bagheri, "Multi-class and multi-scale models of complex biological phenomena", *Current opinion in biotechnology*, vol. 39, pp. 167–173, 2016.

[302] W. L. Jorgensen, "The many roles of computation in drug discovery", *Science*, vol. 303, no. 5665, pp. 1813–1818, 2004.

[303] C. J. Tomlin and J. D. Axelrod, "Biology by numbers: Mathematical modelling in developmental biology", *Nature reviews genetics*, vol. 8, no. 5, pp. 331–340, 2007.

[304] B. Di Ventura, C. Lemerle, K. Michalodimitrakis, and L. Serrano, "From in vivo to in silico biology and back", *Nature*, vol. 443, no. 7111, pp. 527–533, 2006.

[305] J. C. Locke, M. M. Southern, L. Kozma-Bognar, *et al.*, "Extension of a genetic network model by iterative experimentation and mathematical analysis", *Molecular systems biology*, vol. 1, no. 1, pp. 2005–0013, 2005.

[306] M.-A. Albert, J. R. Haanstra, V. Hannaert, *et al.*, "Experimental and in silico analyses of glycolytic flux control in bloodstream form trypanosoma brucei", *Journal of Biological Chemistry*, vol. 280, no. 31, pp. 28 306–28 315, 2005.

[307] E. Lee, A. Salic, R. Kruger, R. Heinrich, and M. W. Kirschner, "The roles of apc and axin derived from experimental and theoretical analysis of the wnt pathway", *PLoS Biol*, vol. 2, no. 3, pp. 405–6, 2004.

[308] J. Werfel, S. Krause, A. G. Bischof, *et al.*, "How changes in extracellular matrix mechanics and gene expression variability might combine to drive cancer progression", *PloS one*, vol. 8, no. 10, e76122, 2013.

[309] Z. Wang, J. D. Butner, R. Kerketta, V. Cristini, and T. S. Deisboeck, "Simulating cancer growth with multiscale agent-based modeling", in *Seminars in cancer biology*, Elsevier, vol. 30, 2015, pp. 70–78.

[310] L. B. Edelman, J. A. Eddy, and N. D. Price, "In silico models of cancer", *Wiley Interdisciplinary Reviews: Systems Biology and Medicine*, vol. 2, no. 4, pp. 438–459, 2010.

[311] S. Schnell, R. Grima, and P. K. Maini, "Multiscale modeling in biology: New insights into cancer illustrate how mathematical tools are enhancing the understanding of life from the smallest scale to the grandest", *American Scientist*, vol. 95, no. 2, pp. 134–142, 2007.

[312] T. S. Deisboeck, Z. Wang, P. Macklin, and V. Cristini, "Multiscale cancer modeling", *Annual review of biomedical engineering*, vol. 13, pp. 127–155, 2011.

[313] J. S. Lowengrub, H. B. Frieboes, F. Jin, *et al.*, "Nonlinear modelling of cancer: Bridging the gap between cells and tumours", *Nonlinearity*, vol. 23, no. 1, R1, 2009.

[314] L. Zhang, Z. Wang, J. A. Sagotsky, and T. S. Deisboeck, "Multiscale agent-based cancer modeling", *Journal of mathematical biology*, vol. 58, pp. 545–559, 2009.

[315] T. Loossens, F. Tuerlinckx, and S. Verdonck, "A comparison of continuous and discrete time modeling of affective processes in terms of predictive accuracy", *Scientific reports*, vol. 11, no. 1, p. 6218, 2021.

[316] S. de Haan-Rietdijk, M. C. Voelkle, L. Keijsers, and E. L. Hamaker, "Discrete- vs. continuous-time modeling of unequally spaced experience sampling method data", *Frontiers in psychology*, vol. 8, p. 1849, 2017.

[317] W. Aspray, "The origins of john von neumann's theory of automata", *Glimm et al.[GIS90]*, pp. 289–309, 1990.

[318] J. Kazil, D. Masad, and A. Crooks, "Utilizing python for agent-based modeling: The mesa framework", in *International Conference on Social Computing, Behavioral-Cultural Modeling and Prediction and Behavior Representation in Modeling and Simulation*, Springer, 2020, pp. 308–317.

[319] J. M. Epstein and R. Axtell, *Growing artificial societies: social science from the bottom up*. Brookings Institution Press, 1996.

[320] H. Byrne and D. Drasdo, "Individual-based and continuum models of growing cell populations: A comparison", *Journal of mathematical biology*, vol. 58, pp. 657–687, 2009.

[321] S. Sanga, J. P. Sinek, H. B. Frieboes, M. Ferrari, J. P. Fruehauf, and V. Cristini, "Mathematical modeling of cancer progression and response to chemotherapy", *Expert review of anticancer therapy*, vol. 6, no. 10, pp. 1361–1376, 2006.

[322] T. Vicsek, "Complexity: The bigger picture", *Nature*, vol. 418, no. 6894, pp. 131–131, 2002.

[323] D. Kahneman and A. Tversky, "On the interpretation of intuitive probability: A reply to jonathan cohen.", 1979.

[324] Å. M. Ballangrud, W.-H. Yang, A. Dnistrian, N. M. Lampen, and G. Sgouros, "Growth and characterization of lncap prostate cancer cell spheroids", *Clinical cancer research*, vol. 5, no. 10, 3171s–3176s, 1999.

[325] W. T. O'Connor, "What can the brain science of learning teach us about cybernetics?", in *2012 IEEE 11th International Conference on Cybernetic Intelligent Systems (CIS)*, IEEE, 2012, pp. 36–40.

[326] A. L. Koch, "The logarithm in biology 1. mechanisms generating the log-normal distribution exactly", *Journal of theoretical biology*, vol. 12, no. 2, pp. 276–290, 1966.

[327] M. Rice, G. Gerhardt, P. Hierl, G. Nagy, and R. Adams, "Diffusion coefficients of neurotransmitters and their metabolites in brain extracellular fluid space", *Neuroscience*, vol. 15, no. 3, pp. 891–902, 1985.

[328] M. Stroh, W. R. Zipfel, R. M. Williams, W. W. Webb, and W. M. Saltzman, "Diffusion of nerve growth factor in rat striatum as determined by multiphoton microscopy", *Biophysical Journal*, vol. 85, no. 1, pp. 581–588, 2003.

[329] M. Esler, G. Jackman, A. Bobik, *et al.*, "Determination of norepinephrine apparent release rate and clearance in humans", *Life sciences*, vol. 25, no. 17, pp. 1461–1470, 1979.

[330] G. Dachille, T. Cai, G. M. Ludovico, *et al.*, "Prognostic role of cell apoptotic rate in prostate cancer: Outcome of a long-time follow-up study", *Oncology reports*, vol. 19, no. 2, pp. 541–545, 2008.